OPTIMIZATION OF DIFFUSER FOR WATER BASED THERMAL ENERGY STORAGE SYSTEM FOR COMMERCIAL BUILDING

BRYAN WONG THIM LOONG

UNIVERSITI TUNKU ABDUL RAHMAN

OPTIMIZATION OF DIFFUSER FOR WATER BASED THERMAL ENERGY STORAGE SYSTEM FOR COMMERCIAL BUILDING

BRYAN WONG THIM LOONG

A project report submitted in partial fulfilment of the requirements for the award of Bachelor of Mechanical Engineering with Honours

Lee Kong Chian Faculty of Engineering and Science
Universiti Tunku Abdul Rahman

May 2026

DECLARATION

I hereby declare that this project report is my original work, with all sources duly acknowledged, and that it has not been submitted previously or concurrently for any degree or award at UTAR or elsewhere. I also declare the following *(check the boxes if applicable)*:

☐ Generative AI tools (e.g., ChatGPT, Gemini, Copilot, etc.) were used for language refinement, such as grammar correction and readability improvement.

☐ Vibe coding tools and/or frameworks (e.g., Replit Agent, Cursor Composer, Bolt, etc.) were used in project development.

☐ Other declaration(s), if any (*please consult your supervisor for guidance in completing this section*):

____

____

I take full responsibility for the originality, accuracy, and integrity of all content presented in this report. No Generative AI tools were used to manipulate project data and results in ways that could cause falsification or misrepresentation.

Name	:	Bryan Wong Thim Loong
ID No.	:	2201956
Date	:	2.7.2025

COPYRIGHT STATEMENT

ACKNOWLEDGEMENTS

Firstly, I would like to thank my research supervisor, Associate Professor Dr. Bernard Saw Lip Huat for his invaluable advice, guidance and patience throughout this research study. I would also like to thank my loving parents, especially my mum who supported me all the way through but is sadly not with us anymore. I would like to thank my friends as well for supporting me physically and emotionally throughout this research period. Finally, I would also like to thank the staff in the mechanical workshop for their willingness to help me with any manufacturing process that I would require.

ABSTRACT

This research attempts to analyse and optimise the performance of water diffusers in a thermal energy storage tank through computational fluid dynamic (CFD) analysis. The concept and application of thermal energy storage were detailed initially. The factors affecting the performance of a thermal energy storage tank were analysed and listed through many literature reviews from other researchers.

The performance of three different perforated plate diffuser configurations of ‘A’, ‘B’ and ‘C’ were studied under charging and discharging cycles during this research. The differences between the three diffusers are the spacing of holes between one another, total number of holes present and perforation surface area on the plate diffusers with Configuration ‘A’ having the smallest spacing between holes, greatest number of holes present and largest total perforation surface area followed by Configuration ‘B’ and finally Configuration ‘C’ with the largest spacing between holes, least number of holes present and smallest total perforation surface area. ANSYS CFX software was used to carry out the CFD simulations. A prototype tank was fabricated and tested to verify the findings.

Configuration ‘C’ with the least perforation area and number of holes produced the thinnest thermocline layer of 0.992 m and 0.549 m after eight hours of charging and discharging respectively but with the largest result deviation compared to the initial thermocline layer thickness at 4 hours as a large thermocline layer is formed after the layer passes through the first perforated plate diffuser. Configuration ‘A’ with the most perforation area and number of holes produced the most consistent results with the least deviation in thermocline thickness between partial and full charging of 0.181 m, likewise for the discharging cycle as well of 0.276 m, due to the reduction in water jet velocity through the perforations. Thus, Configuration ‘A’ was chosen as the ideal configuration of perforated plate diffuser as it is more practical in a commercial setting where it would be constantly charging and discharging.

Keywords: Sensible thermal energy storage, hybrid diffuser, computational fluid dynamic, commercial buildings, exergy efficiency, water-based TES

Subject Area: TJ260 Thermal Energy Storage

TABLE OF CONTENTS

LIST OF TABLES

LIST OF FIGURES

LIST OF SYMBOLS / ABBREVIATIONS

TES	thermal energy storage
TNB	Tenaga Nasional Berhad
CFD	computational fluid dynamic
HTF	heat transfer fluid
MIX	MIX number
r	radius, m
L	length, m
D	diameter, m
Re	Reynolds number
Gr	Grashof number
Ri	Richardson number
Fr	Froude number
ρ	density, kg/m^3
u	inlet velocity, m/s
μ	dynamic viscosity, kg/ms
c_p	specific heat capacity, J/(kg·K)
h	height, m
q	volumetric flow rate per unit diffuser length, m^2/s
g	gravitational acceleration, m/s^2
M_{str}	Moments of energy for a fully stratified simulated tank, J.m
M_{mix}	Moments of energy for a fully mixed simulated tank, J.m
M_{actual}	Moments of energy for an actual tank, J.m
β	thermal expansion coefficient, K^{-1}
T	temperature, K
k_{eff}	thermal conductivity, W/(m.K)
v	kinematic viscosity, m^2/s
Q	heat transfer rate, W
$\dot{m}$	mass flow rate, kg/s
ψ	exergy efficiency
Ex	exergy content
I	total exergy consumption

CHAPTER 1

INTRODUCTION

1.1 General introduction

In 2025, global warming has become a worldwide crisis with widespread effects on the environment. Global temperatures have been steadily rising for the past 30 years as it was reported in the Global Climate Report for 2024 that the global average surface temperature in the year 2024 is at its all-time peak at 1.29 °C above the 20^{th} century average of 13.9 °C since the global record began in 1850 (National Centers for Environmental Information, 2024). Furthermore, the number of natural disasters has been steadily at its peak at an average of 417 natural disasters annually for the past decade (Donnelly, 2025). There are several contributors to global warming such as deforestation, farming livestock and power generation that lead to excessive emission of greenhouse gases mainly carbon dioxide (CO_2), methane (CH_4) and fluorinated gases (United Nations, no date). These greenhouse gases act as a blanket layer by absorbing heat reflected from the Earth's surface from the Sun and lingers in the atmosphere, causing the "greenhouse effect", which passively raise the temperature of the Earth over time. However, the CO_2 emissions from the combustion of fossil fuels is still the largest contributor to greenhouse gas emissions as in 2019, almost two thirds of the greenhouse gas emission consist of CO_2 emissions alone from fossil fuels and industry (IPCC, 2023).

Just as recent as 2022, it was reported that about 30% of the global energy consumption is represented by the operational energy use in buildings with residential buildings contributing around 22% alone while the non-residential buildings making up the rest of the 8% (International Energy Agency, 2023). Electricity was the main energy source accounting to around 33% of the total building energy usage, increasing from 30% back in 2010. Contrary to expectations, fossil fuel usage has continued to increase annually at an average of 0.5% since 2010 despite the shift towards renewable energies. The increase in energy consumption correlates to the increase in energy demand as the energy demand in buildings have seen an average growth of just over 1% annually. Global energy demand continues to grow due to the continuous population growth, economic growth as well as the increase in energy security (Tongsopit *et al.*, 2016).

More and more countries are shifting away from fossil fuel usage in favour of renewable energies with greater investments being made into renewable energies (International Energy Agency, 2024). However, the intermittent nature of common renewable energies such as wind, tidal and solar energy poses a problem that prevents it from being able to supply a stable and readily available energy supply all day round unlike fossil fuel combustion. Therefore, more focus is being poured into research and development with an exponential increase in publications of research papers regarding energy storage systems with 3 852 publications in 2021 in India alone, comprising of over 10% of the cumulative number of publications from year 2002 to 2021 (Prakash *et al.*, 2022). These research papers focus on not only maximising the efficiency and output of both renewable and non-renewable energies but also on different types of energy storage systems. Energy storage systems will be pivotal in enabling renewable energies to potentially replace fossil fuels as the world's primary fuel source for energy generation and to help reduce the peak energy demand load by storing excess energy to be used during a higher energy demand period. Some of the known and developed forms of energy storage systems are mechanical, chemical, thermal, biological and magnetic. In order for these energy storage systems to be able to store energy, most of the primary energy sources like petroleum, wind and sunlight need to be converted through these energy storage systems into secondary energy such as electricity, power and heat energy that are directly utilisable by humans (Li and Deusen, 2025). Despite the extensive amount of research done, there are still many areas of research and improvements that can be made for all types of energy storage systems to further improve efficiency and further reduce initial costs (Dinçer and Rosen, 2011).

One of the developing types of energy storage system in the world and particularly in Malaysia to be used for commercial purposes, is the thermal energy storage (TES). A thermal energy storage system functions by storing and dispersing heat through a medium using Fourier's law of heat conduction that states according to recent research, energy in the form of heat is transferred from high energy particles to lower energy particles which can be determined through a temperature gradient in a closed system (Lobontiu, 2018). The size of the TES directly correlates with the maximum heat capacity of the TES. There are three different types of thermal energy storage systems currently known which store thermal energy in different methods (Kalaiselvam and Parameshwaran, 2014). These TES systems are the sensible TES, latent TES and thermochemical TES.

For latent TES, the heat storing medium undergoes a phase change from solid to liquid or vice versa. The phase transformation will absorb or release heat depending on heating or cooling while maintaining a constant temperature. Once the phase change is completed, the medium will absorb or release sensible heat just like in the sensible TES. However, the specific heat capacity of the medium in its new phase may be different compared to in its previous phase, leading to potentially a greater or smaller difference in temperature for equal heat supplied compared to as such in its previous state.

On the other hand, heat is stored and released through chemical reactions in thermochemical TES. The medium used for thermochemical TES is capable of reversible chemical interactions and endothermic in reaction. Thus, the medium will be broken down into simpler compounds or elements when heat is supplied as the bonds between the compounds are broken down by absorbing enough heat energy. When the reaction is reversed, the formation of bonds between atoms will release heat energy.

Finally for sensible TES, the temperature of the medium storing the thermal energy increases and decreases together with the amount of thermal energy stored without the medium changing states. The most common mediums used in sensible TES are water and gravel (Wang, 2019). However, there are other mediums used as well depending on the range of operating temperature required for the system. Mediums like oil and inorganic non-metallic materials can also be used for higher operating temperatures, while some of the other solid mediums used are molten salt and rocks. Solid mediums will not have any leakage loss or any potential of causing corrosion like how water does but has a lower thermal conductivity than of water. In the case of when high-temperature thermal storage system is required, water is not very suitable as the large increase in temperature will also cause a large increase in pressure in the storage system due to the Gay-Lussac’s Law which states that for a constant volume, the pressure is directly proportional to absolute temperature. This will lead to higher costs to modify the storage tanks as well as the pipelines to be able to withstand greater water pressure.

The operation of the TES system consists of two processes, which are the charging and discharging processes. During the charging process, the channels connecting to the load are closed off, leading to only circulation of the medium through the TES and the heat source. The medium is supplied enough heat by the heat source during the off-peak periods to partially or fully offset the critical load demand during the peak periods when the TES is discharging (Kalaiselvam and Parameshwaran, 2014). On the other hand, during the discharging process, the stored thermal energy in the TES is discharged to the desired demand load as the channels to the demand load are reopened and the channels to the heat source is closed off.

Recent research states that sensible TES is the most commonly used TES method due to its simplicity and the ease in ability to detect the amount of heat stored through the variation in temperature of the system (Patil, Prabhu P.A and Shinde N.N, 2012). In Malaysia, TES systems are being pushed as a sustainable method to drive the country's energy transformation forward by Tenaga Nasional Berhad (TNB), which is the primary electricity generation enterprise for Malaysia, as part of the country's green initiative to build a sustainable and inclusive energy system for the future (Tenaga Nasional Berhad, 2023). In conclusion, TES is a leading candidate for the future of energy storage with its many advantages in terms of energy savings and efficiency.

1.2 Importance of the study

The outcome and findings of this study may have a significant contribution towards the increase in commercial viability of water-based single tank TES systems. This study could potentially help to further reduce the energy usage by commercial buildings and in turn, running energy costs of commercial buildings through energy savings by requiring even less off-peak electrical energy for heating or cooling.

The absence of a diffuser in a TES system will cause a large mixing effect between the hot and cold water. This will cause a large increase in thermocline layer and greatly affect the heating efficiency of the TES system to the load negatively. The reduction in thickness of the thermocline layer from the optimisation of diffusers will increase the energy transfer efficiency of the TES and contribute to a more environmentally friendly TES system, complying with current environment policies. The outcome of this research can also help to predict a more accurate output on the useful energy for planning purposes.

1.3 Problem statement

During winter or cold periods in countries, heating is an important need not only for residential use to keep warm but also for commercial use, where heating is required to maintain a warm ambient temperature or for facilitating processes in certain industries. Without TES, energy usage during winter is higher as heat pumps are commonly used for long periods to directly fulfil those needs on-demand. The usage of heat pumps for long periods will incur high costs to run during peak periods.

The addition of an energy storage system to a conventional heating system will naturally reduce the heating efficiency of the system compared to just using a heat pump cycle for heating. Additionally, other factors further contribute to the reduction of energy transfer efficiency such as thermal energy losses due to imperfect heat insulation of tanks and channels. Meanwhile, TES has their own challenges to overcome. The reduction in temperature difference between the heat transfer fluid and the load from the thermocline layer will reduce the amount of heat transferred to the load and thus, reduce the energy transfer efficiency of the system.

1.4 Aim and objectives

The aims and objectives of this project are as follows:

- To design and model the water based thermal energy storage system for commercial building heating through the use of computational fluid dynamic (CFD) analysis.
- To optimise the diffuser design to produce uniform flow of water and better water stratification within the thermal energy storage tank.
- To better understand the effect of changing the total perforation surface area of the perforated plate diffuser on the performance of the thermal energy storage system.

1.5 Scope and limitation of the study

The scope of the study is as follows:

- Determining the performance of different perforated plate diffuser configurations through the data gathered from CFD simulations.
- Temperature of the heated supply water is to be at 45 °C, while the return flow of water is to be at a temperature of 35 °C.
- Dimensions of the cylindrical water storage tank used are 12 m diameter and height.

Some of the limitations of the study are stated as follows:

- Results are only based on simulation work with minimal physical experimental validation at a fixed temperature range and storage tank dimension.
- The study focuses solely on the optimization of performance of diffuser without taking in consideration the multitude aspects of the integration system required to realize the entire thermal energy storage system in a commercialized setting.

These limitations allow for further study into different aspects of the integration system required for the optimized water-based thermal energy storage tank.

1.6 Contribution of the study

This study makes a large contribution towards the thermal energy storage technology, particularly for a water-based sensible system by optimising the diffusion system for a water thermal storage tank. The findings from this study will help future research by better understanding the effects of different hole spacing and number of holes present on a perforated plate diffuser.

The improvement in performance obtained from this study will also help to contribute towards greater feasibility of thermal energy storage systems and particularly for countries that experience cold or winter weather, where thermal energy storage will help to reduce energy costs for the inhabitants.

1.7 Outline of the report

In this research study, computational fluid dynamic analysis was carried out to test the performance of different diffusers in a water-based thermal storage energy tank. The report includes five major chapters. Firstly, the basic concept as well as the need of the thermal energy storage system is introduced. The factors and indicators affecting the performance of this thermal energy storage system are further explored together with the adaptions and optimisations researched to further maximise their efficiencies. In Chapter 3, these optimisations are then implemented into the methodology for the experimental setup which is the CFD simulation. The results of the simulation will be scrutinised and analysed in Chapter 4 with the main findings and conclusion listed in Chapter 5.

CHAPTER 2

LITERATURE REVIEW

2.1 Introduction

This chapter highlights the analysis on research done on different types of diffuser configurations used in a TES along with the factors affecting thermal stratification and the thermocline thickness with their respective effects on the thermal stratification and thermocline thickness. In addition, the inadequacies and approach to the related research done for different diffuser configurations will also be analysed.

2.2 Factors affecting thermal stratification and thermocline thickness

For a water-based sensible thermal energy storage system, water is the main heat transfer liquid that will absorb heat from the heat source and expel heat to the demand load area. Once the water is heated, the heated water will then circulate back through the water storage tank and towards the demand load area for heat transfer. In a naturally stratified water storage tank, the lower density layer of hot water would lie directly above the higher density layer of cold water with a thin transitional layer in between the two layers known as a thermocline (Chung et al., 2008). Many researches have shown from simulations and experiments that stratification of water in a solar system and in extension, TES, is beneficial in improving the efficiency of those TES systems (Han, Wu and Christensen, 1978; Gutierrez et al., 1974; Wuestling, Klein and Duffie, 1985).

However, in reality, energy is lost from the heated water throughout its transport in the TES system, causing the stratification of water to weaken and thus, enlarging the thermocline layer. There are four main phenomena of energy and thermal stratification degradation cycles (Zurigat, Maloney and Ghajar, 1989; Shyu, Lin and Fang, 1989). These are: (1) Heat losses to the surroundings due to imperfect heat insulation of water storage tank or piping, (2) vertical heat conduction in the storage tank wall which will induce convective currents in the fluid, (3) heat convection in hot to cold water and (4) mixing of hot and cold water during charging and discharging. The first three sources of energy loss are the main contributing factors for the decay in stratification when the storage tank is in a static or idle state and can be managed by using good heat insulation throughout the system. However, the last phenomenon is the main cause for significant mixing losses in energy for long storage periods and is the very complex as there are many factors that can affect the magnitude of mixing of the different water temperature layers. For this study, most of the focus will be placed on analysing this phenomenon through the factors affecting it. Other than that, measures proposed by researchers to minimise this phenomenon and thermal stratification degradation within the TES such as different inlet designs, positions, flow rates as well as the introduction of diffusers will also be analysed on how they can help to promote thermal stratification in different temperature of water.

2.2.1 Effect of the length to diameter ratio

The length to diameter (L/D) ratio of the water storage tank can affect the level of thermal stratification of water in the water storage tank. In a study conducted by Nelson, Balakrishnan and Murthy (1999) on the stratification in chilled-water tanks, it was found that a reduction in L/D ratio of a cylindrical water storage tank will produce weaker stratification and increase the mixing effect between the different water temperature layers leaving a thicker thermocline layer through the increment of axial wall conduction. However, it was also found that the improvement in performance from the increment of L/D ratio is not significant beyond the ratio of 3. The results were further supported by the findings from the study done by Tipasri and Wongwuttanasatian (2019) on the effect of L/D on the temperature gradient in a chilled water storage tank during discharging. It was found that not only the thermal stratification in the water storage tank would improve, but also that the effective heating/cooling capacity would also increase together with the L/D ratio for a fixed storage tank volume. Lavan and Thompson (1977) also found from their experimental study on thermally stratified hot water storage tanks that the discharge efficiency increases with an increase in L/D ratio but eventually flattens out at higher L/D ratios.

2.2.2 Effect of the temperature difference of water

The effect of the temperature difference of water on the thermal stratification of water is widely discussed by many researchers. However, there are varying outcomes and conclusions made by researchers. In a study done on the optimisation of design for a thermal storage tank performance by Yaïci et al. (2013), it was shown that the stable thermal stratification was maintained despite the varying range of temperature differences of water from the inlet to the maintained water in the tank. Only a slight increase in mixing appeared initially during loading when increasing the temperature difference of water. The authors theorised a degradation in stratification due to enhanced axial wall conduction and thermal diffusion but an improvement in stratification from the increased difference in water density for an increase in temperature difference of water. They proposed that the nett effect from the increment of water temperature difference also depends on other operating and geometrical parameter and will not necessarily produce better stratification but potentially the opposite.

The results of the study by Yaïci et al. (2013) were also echoed by Nelson, Balakrishnan and Murthy (1999) in the results of their study when analysing the effect of water temperature difference during static, charging and discharging modes. An additional point from the results of the study of Nelson, Balakrishnan and Murthy (1999) is that the bottom layers of chilled water heat up more when the temperature difference is increased when the tank is in a static mode. Nelson, Balakrishnan and Murthy (1999) also proposed that the increase in density difference from the increase in temperature difference improves the stratification effect and reduces the mixing effect.

2.2.3 Effect of the storage tank wall & insulation thickness

In the research done by Ghaddar and Al-Marafie (1997) on the influence of finite wall thickness on stratification during charging of solar thermal tanks, they concluded from their numerical and experimental data that heat loss through the conducting storage tank walls were the main source of thermocline degradation. Their research was supported by the results from the research from Nelson, Balakrishnan and Murthy (1999) when they tested on the effect on the difference in insulation thickness. Their results showed that the temperature of both bottom and top layers of water increases over time with lesser wall and insulation thickness due to the axial conduction and heat conduction across the thermocline layer through the tank walls. They also concluded that an increase in the insulation thickness will help improve the thermal stratification in the water storage tank.

2.2.4 Effect of water flow rate throughout the system

Multiple researchers have found that an increase in flow rate of water through the TES will increase the mixing of the layers of water, leading to a degradation in stratification of water in the storage tank. One group of researchers tested the effect of varying water flow rates and found that the temperature range at a set level range decreases with the increase in water flow rate (Krafcik and Perackova, 2019). They tested using 500 to 1000 litre per hour water flow rates with results showing decreasing temperature gradients which shows a degradation in stratification of water. An interesting observation also present in the results were that the starting point of the thermocline continuously shifted further away from the inlet with increasing water flow rate. Another group of researchers also found that an increase in water flow rate will reduce the useful capacity of the TES due to an increase in degree of mixing from an increase in inlet jet velocity (Nelson, Balakrishnan and Murthy, 1999). Lavan and Thompson (1977) studied the effect of mass flow rate together with the inlet port diameter and found that the efficiency of the TES decreases with increasing water flow rate and decreasing inlet port diameter. They suggested from the results that the efficiency of the TES decreases with increasing Reynolds number of the inlet channel.

However, the study from Chung et al. (2008) had shown that through numerical simulation predictions that a decrease in water flow rate increases the energy degradation in water due to thermal diffusion. They used three different diffusers of varying Reynolds number (Re) of 400, 800 and 1200 with fixed Froude number and dimensionless diffuser diameter to examine the effects it will cause on the thermocline thickness. It was recorded that an increase in Re created an improvement in performance but in a decreasing amount from between $Re = 400$ and $Re = 800$ to $Re = 800$ and $Re = 1200$. They have suggested that the decrease in increment of performance could be due to vigorous mixing as well as an existence of an optimal Reynolds number from the compound effect of mixing and thermal diffusion.

2.2.5 Additional characteristic parameters

Despite having multiple performance parameters, it is difficult and complex to optimize theses performance parameters as they mostly affect one another when a change to a single performance characteristic is made. To simplify the analysis of these performance parameters, characteristic parameters are introduced to provide an indicator on the state of the water flow. One of these characteristic parameters is the Reynolds number, where it is the ratio of a fluid's inertial forces to its viscous forces and can be expressed as:

$$Re = \frac{\rho u L}{\mu}$$

Where,

ρ - density of inlet fluid (kg/m^3)

u - velocity of inlet fluid (m/s)

L - characteristic length of diffuser length (m)

μ - dynamic viscosity of inlet fluid (kg/m.s)

Ideally, the Reynolds number of the water flow within the water storage tank should be kept below the transition flow value to minimize the turbulence in the water flow that will cause chaotic water flow fields and increase in mixing effect. Wildin and Sohn (1993) had concluded from their study on the flow and temperature distribution in a naturally stratified thermal storage tank that both the initial thermocline thickness and the strength of mixing currents increase with increasing inlet Reynolds number. Reynolds number is not the only characteristic parameter that will affect the performance of the TES system.

Froude number is another characteristic parameter which represents the ratio of inertia forces to gravity forces present in a fluid flow (Rapp, 2017). The Froude number based on the distance from the diffuser to the opposite wall is defined by:

$$Fr = \frac{q}{\sqrt{gL^3}}$$

Where,

q - volumetric flow rate per unit diffuser length (m^2/s)

g - reduced gravitational constant (m/s^2)

L - distance from the diffuser to the opposite wall (m)

It is also an important indicator as it is believed to be directly affecting the gravity current effect, which is the horizontal flow of fluid generated by a minor difference of density (Simpson, 1999). It is desirable to maintain the thermocline thickness at a minimal thickness with a recommended range of inlet Froude number of less than 2 to ensure gravity currents are induced. Any inlet Froude number above 2 will display significant mixing effect (Dorgan and Elleson, 1993). On the other hand, Chung et al. (2008) found that the performance of the rectangular storage tank improves slightly with decreasing Froude number when fixing the conditions of Re = 800 and a dimensionless diffuser diameter of 0.0582. However, they have concluded that the contribution of the Froude number is negligible from their analysis of variance as long as it is within the recommended Froude number range stated earlier.

Moving on, the Richardson number also plays a big role on the thermal stratification in a thermal water storage tank. The Richardson number is affected by the inlet geometry and can be expressed by:

$$Ri = \frac{Gr}{Re^2}$$

Where,

Gr - Grashof number

Re - Reynolds number

Richardson number can also be related to the Froude number through the expression:

$$Fr = \frac{1}{\sqrt{Ri}}$$

Where,

Fr - Froude number

Ri - Richardson number

In a numerical study done by Ghajar and Zurigat (1991) on the effect of inlet geometry on stratification in thermal energy storage, they concluded that the inlet geometry has a significant effect when $Ri \leq 5$, moderate effect when $5 < Ri \leq 9$ and finally negligible effect when $Ri \geq 10$. Thus, a trade-off needs to be made to maximise the Richardson number of the system without overdesigning the storage tank which may inflate costs and manufacturing complexity (Ibrahim Dincer and Rosen, 2012).

Another parameter adopted by researchers in calculating the degree of mixing in a thermal storage tank is the MIX number. The MIX number characterises the total energy stored in the tank as well as the vertical temperature profile in the storage tank (Davidson, Adams and Miller, 1994). It has been derived and improved upon from previous proposed coefficients such as the Satish coefficient (McCarthy and Wood, 1990) and the stratification factor from Wu and Bannerot (1987). The MIX number is given by the following expression:

$$MIX = \frac{M_{str} - M_{actual}}{M_{str} - M_{mix}}$$

Where,

M_{str} - Moments of energy for a fully stratified simulated tank

M_{mix} - Moments of energy for a fully mixed simulated tank

M_{actual} - Moments of energy for an actual tank

A lower MIX number is ideal as a MIX number at one at specific heights represent equal amounts of energy to the fully mixed simulated tank which means an incredibly large degree of mixing has occurred at that level.

2.3 Types of inlet diffusers used in a TES system

Traditionally, water is transported through and from the thermal storage tank using a raw pipe with no diffuser present. It was observed by Baughn and Young (1981) that significant mixing of water occurred during discharge when no diffuser is present in their study on the thermal performance of a horizontal tank. Many different varieties and iterations of inlet diffusers have been designed and researched on over the past few decades. These diffusers function to reduce the mixing effects present during operation in the water storage tanks by supplying uniform water flow along with reducing the entrance velocity of the water flow. They also come in many different shapes and configurations in order to be optimised for different tank geometries.

There are two main types of water diffusers used in a water-based thermal energy storage system which are slotted diffusers and radial diffusers. Slotted diffusers are slotted pipes that are mounted horizontally above or below the tank at the tank's centre. These slotted pipes are usually formed into rings or in a concentric octagonal shape before placed in a cylindrical tank but can also be modified in shape such as the H-type diffuser for a rectangular tank in order to match the geometry of the storage tank and to provide better performance. However, the H-type diffuser suffers from maintaining self-balance due to the unbalanced forces acting upon it. Other variations of slotted diffusers include the slotted wedge diffuser, shower-type diffuser, single and branching multi-tubed diffusers. On the other hand, radial diffusers expel water at a reduced velocity in a radial direction into the thermal water tank storage. This is done by impinging the incoming water stream on a circular baffle plate to diffuse the water radially outwards through the uniform gap between the spreading and baffle plate or diffusing through a perforated baffle at a distance past the end of the main supply pipe. There can be two parallel radial plates on each vertical end of the tank or only one radial plate at the top or bottom of the tank.

2.3.1 Slotted diffusers

Single tube diffusers are a simple type of diffuser that can be used in a thermal storage tank as it only requires a single piece of tube with multiple holes in each side. Those holes act as the inlet section for the water to be jetted out into the thermal water storage tank. An iteration of this design is the multi-tubed diffuser, where multiple tubes with holes in their sides are connected to a central main tube carrying the water distributing the water to each branching tube. The tubes can be arranged linearly in an array The branching tubes increases the surface area covered of the thermal water storage tank providing a more uniformed flow across the cross-section of the tank. Al-Maraffie, Al-Kandari and Ghaddar (1991) found that the multi-tubed diffuser produced a higher range of extraction thermal efficiency of around 10% or more compared to the extraction thermal efficiency of the single tubed diffusers which produced an extraction thermal efficiency of 81-62% depending on the water flow rate used for a cylindrical thermal water storage tank.

Hegazy (2007) further explored the idea of slotted diffusers and tested the performance of three different inlet diffuser designs which are the wedged diffuser, perforated diffuser and the slotted diffuser in two different thermal storage tanks with different L/D ratios. The results showed that all three diffusers were able to promote good thermal stratification in the storage tank. However, the slotted diffuser produced the best performance in terms of discharge efficiency, extraction efficiency and fraction of heat recoverable among the three diffusers. The increase in L/D ratio significantly decreased the difference in performance among the three diffusers used while an increased water flow rate reduced the performance of all three diffusers. The author concluded that the slotted diffuser would be the best choice of diffuser in terms of performance and great energy savings, cancelling out the increased manufacturing cost due to the complexity in manufacturing compared to the perforated diffuser.

In a study done by Li et al. (2014) on the effects of different inlet structures during the discharging period of a solar water storage tank, three different configurations were tested against one another which were a slotted diffuser with three slots, a direct inlet and a shower inlet. The results showed that the slotted diffuser produced the least mixing between inlet water and hot water in the storage tank followed by the direct inlet and the shower diffuser from the thermocline thickness measured from the thermocouple sensors in the tank. The slotted diffuser also produced the greatest effective discharging efficiency and discharging time and was concluded by the author to be able to achieve greater energy savings and carbon reduction compared to the traditional direct inlet.

In a different study, Tang, Shi and OuYang (2021) studied the effects of several outlet parameters on the stratification of water in a chilled thermal storage tank. Their findings showed that the angle of the opening of the water jet outlet did not make a significant difference as the thermocline thickness profile were similar between a vertical and an inclined outlet opening. Besides that, Tang, Shi and OuYang (2021) had also tested the water distribution effect between a slot hole and a circular hole. For the same surface area, the circular hole produced the lowest thermocline thickness profile compared to two other slot holes of different length to width ratios due to the different velocity distribution of water passing through the holes. Cao et al. (2024) furthered the research on outlet parameters with their study on the effects from varying parameters of a slotted diffuser on the performance of the diffuser in a thermal storage tank. The parameters scrutinised on were the inlet distances, hole distances and the hole diameters on the diffuser at different water inlet flow rates. The results showed a wide range of performance between configurations, in terms of stratification and exergy efficiency, with the best performing configuration having a thermocline thickness three times as thin compared to the worst performing configuration.

2.3.2 Radial diffusers

A study done by Shah and Furbo (2003) on the entrance effects in solar tanks aimed to compare the performances of a direct water inlet, a small hemispherical baffle placed 1 cm above of the inlet pipe and a horizontal flat baffle plate placed 1 cm above the inlet pipe. The authors found that the horizontal flat baffle plate produced the best performance followed by the small hemispherical baffle and finally the direct inlet in their CFD simulations. However, the experimental results did not fully follow the simulation results with several conflicting results. The authors concluded that the method of data analysis applied was not robust enough with several improvements that can be made to the experimental study. However, they also mentioned that the method of analysis deployed was promising and can be of interest to further pursue development if the improvements were implemented.

An iteration of the radial diffuser was researched on by Deng et al. (2021) on a nonequal diameter radial diffuser. The effects of a reduced upper baffle diameter on the upper diffuser and vice versa were studied upon and compared to an equal diameter radial diffuser along with several different parameters related to the baffle plates such as diameter ratio and distance between plates. The results showed that the distance between baffle plates should be reduced as much as possible and an optimum diameter ratio of 1/3 between the small and large diameter baffle plates to minimise the thermocline thickness. The authors concluded that the nonequal diameter diffuser has almost equal performance to the equal diameter diffuser as the results showed similar thermocline development and thickness of 0.86 m after charging for both radial diffusers. However, the nonequal diameter diffuser has a significant reduction in cost due to lesser materials required for fabrication.

Another modification of the radial diffuser was tested by Chung et al. (2008), when the authors proposed a radial adjusted plate type that is more suited for rectangular and square tanks and was tested against a standard radial diffuser and a H-type slotted diffuser in a rectangular shaped storage tank. The radial adjusted plate produced the best performance of minimal thermocline thickness compared to the other two diffusers tested in both simulation plots and in quantitative analysis when the Reynolds and Froude number are kept equal. The H-type slotted diffuser produced the thickest thermocline layer due to the large mixing effect induced by the less uniform jet streams. The authors concluded that the Froude number was negligible to the contribution of stratification while the Reynolds number was the most dominant parameter and that the diffuser shape is also a major factor in promoting stratification in a thermal storage tank.

2.3.3 Alternative diffuser designs

In a study done by Erdemir and Altuntop (2016), different shaped obstacle plates were placed at different vertical distances to study the influence it has on the performance of a vertical mantled hot water tank. Out of the four different shaped obstacle plates that have different sections cut out and the ordinary tank, the obstacle plate with a circular hole cutout of a diameter of 100 mm at a distance of 200 mm from the bottom floor of the mantle tank produced the best stratification performance in the hot water tank with the greatest peak energy capacity and temperature gradient due to the natural convection produced from the uniform flow of water through the middle circle perforation. The height of the obstacle plate from the bottom floor affected the Richardson number of the tank with increasing height producing an increase in Richardson number up to a certain value.

An iteration of the previous authors' work was done by Lou et al. (2023) on the optimization of a flow distributor for stabilized thermal stratification in a single-medium thermal storage tank. The authors presented a new type of flow diffuser named the ring-opening plate distributors targeting to minimise the thermocline degradation caused by inlet thermal jets. In their setup, two ring-opening plate distributors of three ring-shaped openings each and 3 mm thickness were installed 30 mm away from the top and bottom of the storage tank. A variation of the ring-opening plate distributor which is the optimized design proposed by the authors were tested against the initial design and a simple port in different upper and lower tank configuration combinations (Lou, Fan and Luo, 2020). A corroboration of both simulated and experimental results showed that the proposed optimized design along with their optimization algorithm has proven to be effective and simple to implement as the increase in exergy efficiency recorded was almost 30% at 84.2% compared to the simple inlet/outlet pipes.

Another novel variation of diffuser was proposed by Parida et al. (2022) named the hemispherical diffuser in their study. Its impact on a single-tank molten salt thermal energy storage system was studied intensively and compared to three other configurations which are a diffuser free TES tank, a flat baffle plate and a coaxial ring diffuser. The novel hemispherical diffuser contains two chambers within it, the primary and secondary diffuser. The splitter-guide arrangement constraints the inlet jet flow while promoting recirculation of flow within the chambers. Despite an increase in strength of the recirculation flow near the inlet, the area of recirculation is confined to be only within the hemispherical diffuser to limit the size of recirculation. The pressure loss in the diffuser continued to increase as the HTF flow rate increased with a spike in increment at a flow rate of 27 l/min but is not a problem due to the overall operating pressures of the tank in MPa during discharging along with the presence of pumps to add pressure head into the system. The authors concluded that despite the conventional diffusers showed a 1% improvement in stratification compared to the hemispherical diffuser during an increase in HTF flow rate from 6 l/min to 12 l/min, the hemispherical diffuser produced a 6% increase in stratification at a higher flow rate of 27 l/min compared to the 4%

decrease in stratification for the conventional diffusers. The hemispherical diffuser could prove to be much more beneficial in high flow rate systems.

2.4 Summary

In conclusion, the mixing effect has many different factors that can affect the intensity of mixing effect in a TES tank during operation. These factors are interrelated to one another and have different weightage on the effect. Most of these factors can be indicated and optimized for a set geometry of storage tank using different characteristic parameters such as Reynolds number, Froude number, MIX number and Richardson number. The inlet diffuser design also plays a big role in mitigating the mixing effect in a TES tank during operation. Uniform flow distribution and lowering inlet jet velocity are the main goals of a desired diffuser design while the shape, structure, method and position of the inlet diffuser are the main design areas to be optimized to achieve the goals set.

Radial diffusers are most suitable in maintaining stratification for circular tanks while slotted diffusers are more adaptable to different tank shapes but are still able to provide decent stratification relative to radial diffusers. New and innovative diffusers designs have also shown great promise to provide great stratification performance in relative to both radial and slotted diffusers but more studies need to be done to fully verify its performance. More in-depth study is required in each area to further understand the effects it can produce on the performance of a TES system with larger tank geometries.

CHAPTER 3

METHODOLOGY AND WORK PLAN

3.1 Introduction

In this section, the process and steps to be taken to carry out the study will be explained in detail along with the parameters to be recorded in order to determine the performance of the diffusers used. This includes the setup of the computational fluid dynamics (CFD) simulation with the geometry of tank, types of diffuser configuration tested with its different variations and observed variables to be recorded during operation such as temperatures at various vertical points in the thermal storage tank and inlet flow velocity. These set parameters and observed variables will then be used in the calculation of the characteristic parameters such as Reynolds number, Richardson number, Froude number and MIX number to determine the performance of the diffusers.

CFD is the science of predicting the behaviour and characteristics of fluid flow through the usage of computers. This prediction is done through the computational part in the computer by using governing equations such as conversation of mass, momentum and energy (Ansys, 2024). The processing units present in the computer will then calculate the fluid domains using the governing equations to analyse the fluid flow. CFD is an ever-improving experimental method that has and is still being adopted by various researchers in different fields, particularly in studies focusing in complex liquid and gas flows. One of the upsides of using a CFD simulation to analyse fluid flow behaviour is the cost and time savings from not having to fabricate a physical prototype to test (Yaïci et al., 2013). Besides that, CFD is able to analyse many different data variables such as pressure, temperature, heat transfer and so on which can be incredibly difficult physically for specific data variables. Optimisation and visualisation of fluid flow will also be made much easier through the visualisation tools made available through CFD such as the contour, graph and vector plots.

The main downside of using CFD is that it is computationally very intensive, meaning that powerful processing units are required to carry out more complex three-dimensional flows and larger analysis for better accuracy of data.

CFD simulations may not always be able to provide the most accurate results as the mathematical models used for the simulations are only an approximation of the actual physics happening in real life. The meshing of the fluid flow domain can also affect the accuracy of simulation with the quality of mesh through skewness, orthogonality and aspect ratio of the mesh playing a part in the calculation. CFD simulation times can also vary based on the complexity and scale of fluid flow domain analysed with more complex and larger domains potentially increasing the computational time and resources required exponentially. In conclusion, despite the downsides of potential inaccuracy and large computational cost, CFD is still a great tool for researchers to analyse fluid flow cases. CFD results is a great supporting tool to identify and proof the physics happening in a physical experiment that has been done.

3.2 Methodology flowchart

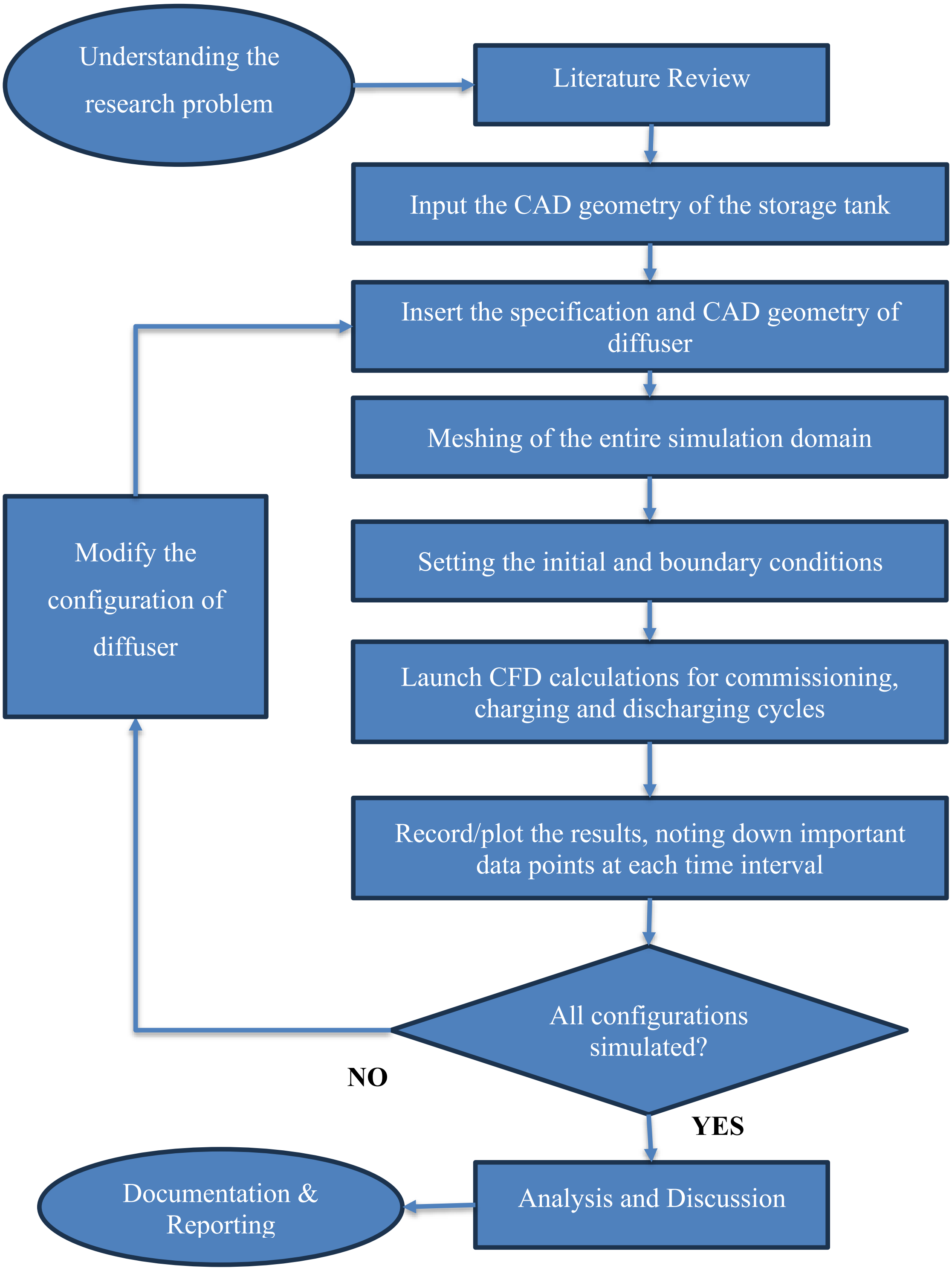

Figure 3.1: Flow Chart of Simulation Process

The main methodology that will be used for this study is through CFD simulations, with multiple iterations and simulations of diffusers across multiple time intervals. Once the geometry and configuration of the diffusers used are set and modelled, preparation for CFD simulation will then begin through the meshing of diffusers and tank, setting up CFD parameters to be run at and finally running the CFD solver. After the results are recorded, the next configuration of diffuser will then be inserted into the project file to be used and analysed. This process is repeated until all configurations of diffusers have been simulated with their results recorded. Once completed, those results will then be analysed and discussed upon.

3.3 Mathematical model

There are several governing equations that will be required to determine the temperature gradient in the thermal storage tank. These governing equations will be used by the CFD solver in its computation for fluid flow through the storage tank. These are the continuity equation (conservation of mass), conservation of momentum and the conversation of energy which are the following (Tipasri and Wongwuttanasatian, 2019):

Continuity equation:

$$\frac{\partial p}{\partial t}+\frac{1}{r}\frac{\partial(r\rho u_r)}{\partial r}+\frac{1}{r}\frac{\partial(r\rho u_z)}{\partial z}=0$$

Conservation of momentum (radial direction):

$$\frac{\partial(\rho u_r)}{\partial t}+\frac{1}{r}\frac{\partial(r\rho u_r u_r)}{\partial r}+\frac{\partial(\rho u_z u_z)}{\partial z} = -\frac{\partial p}{\partial r}+\mu_{eff}\left[\frac{\partial}{\partial r}\left(\frac{1}{r}\frac{\partial(ru_r)}{\partial r}\right)+\frac{\partial^2 u_r}{\partial z^2}\right]+\rho g_r\beta\Delta T$$

Conservation of momentum (axial direction):

$$\frac{\partial(\rho u_z)}{\partial t}+\frac{1}{r}\frac{\partial(r\rho u_r u_z)}{\partial r}+\frac{\partial(\rho u_z u_z)}{\partial z} = -\frac{\partial p}{\partial z}+\mu_{eff}\left[\frac{\partial}{\partial r}\left(\frac{1}{r}\frac{\partial(ru_z)}{\partial r}\right)+\frac{\partial^2 u_r}{\partial z^2}\right]+\rho g_z\beta\Delta T$$

Conservation of energy:

$$\frac{\partial(\rho c_p T)}{\partial t}+u_r\frac{\partial(\rho c_p T)}{\partial r}+u_z\frac{\partial(\rho c_p T)}{\partial z}=k_{eff}\left[\frac{1}{r}\frac{\partial}{\partial r}\left(r\frac{\partial T}{\partial r}\right)+\frac{\partial^2 T}{\partial z^2}\right]$$

Where,

u_r - Radial velocity

u_z - Axial velocity

r - Radial coordinates

z - Axial coordinates

ρ - Density of water

μ_{eff} - Effective viscosity of water

β - Thermal expansion coefficient of water

ΔT - Temperature difference between hot and cold water

C_p - Specific heat capacity of water

k_{eff} - Effective thermal conductivity of water

Besides that, dimensionless number analysis is also required in determining the flow and heat transfer phases present in the thermal storage tank. The dimensionless numbers that will be calculated are the Reynolds, Grashof and Richardson numbers (Bergman and Al, 2011). They can be calculated with the following formulas:

Reynolds number, *Re*

$$Re = \frac{\rho u_{inlet} D}{\mu}$$

Grashof number, *Gr*

$$Gr = \frac{g\beta(T_S - T_\infty)L^3}{v^2}$$

Richardson number, *Ri*

$$Ri = \frac{Gr}{Re^2}$$

Where,

ρ - Density of water

u_{inlet} - Velocity of flow at the inlet

D - Diameter of the inlet

μ - Dynamic viscosity of water

v - Kinematic viscosity of water

g - Gravitational acceleration

β - Coefficient of thermal expansion of water

L - Vertical length of water layer

The heat transfer rate through a control volume occurring in the thermal storage tank can be calculated theoretically using the following formula (Bejan, 2013):

$$Q = \dot{m}_{in} c_p (T_{out} - T_{in})$$

Where,

Q - Heat transfer rate

$\dot{m}_{in}$ - Inlet mass flow rate of water

c_p - Specific heat capacity of water

T_{out} - Outlet temperature of water

T_{in} - Inlet temperature of water

These equations will be used to predict the performance of the diffusers through theoretical and simulation means.

3.3.1 Performance indicators

The performance indicator for the thermocline thickness during charging and discharging can be determined using a dimensionless temperature unit of θ. This dimensionless temperature unit can be calculated using the following formula:

$$\theta(x) = \frac{T(x) - T_C}{T_h - T_C}$$

Where,

$T(x)$ - Temperature of water at x^{th} level in the storage tank

T_h - Temperature of hot inlet water

T_c - Temperature of initial cold water

The denominator represents the temperature difference of charging, and the numerator represents the difference value between the temperature at any point in the storage tank and the cold water. As the thermocline thickness is defined as the region in tank height with a large variation of temperature of water, data points in the range of $0.1 \leq \theta(x) \leq 0.9$ will be taken as the thermocline thickness with a balanced 10% truncation to ensure that no outlier data points will be taken for a overly large range due to slight fluctuations in temperature and also that not a significant amount of data is omitted due to an overly small range.

Another performance indicator that will be used is the exergy efficiency of the TES system. Exergy is a quantity of potential useful energy in a system that can be utilized for work (Ibrahim Dincer and Rosen, 2012). A greater exergy efficiency results in more useful potential energy stored as thermal energy that can be utilised during discharging. The overall exergy efficiencies of a TES system can be calculated using the following formula (Ibrahim Dincer and Rosen, 2012):

Exergy efficiency, ψ

$$\psi = \frac{Exergy\ recovered\ from\ TES\ during\ discharging}{Exergy\ input\ to\ TES\ during\ charging} = \frac{Ex_{d,h} - Ex_{d,c}}{Ex_{c,h} - Ex_{c,c}}$$

However, as the storage tank is modelled as an adiabatic storage tank which means there is zero loss of energy to the surroundings, the exergy efficiency can be simplified into the following formula:

$$\psi = 1 - \frac{I}{Ex_{c,h} - Ex_{c,c}}$$

Where,

$Ex_{c,h}$ - Exergy content of hot water during charging

$Ex_{c,c}$ - Exergy content of cold water during charging

I - Exergy consumption during charging, storing and discharging cycles

3.4 Storage tank geometry setup

The geometry of the simulated thermal storage tank prototype is a cylindrical storage tank. Table 3.1 shows the specification of the cylindrical storage tank used for this study.

Table 3.1: Storage Tank Specification

Specifications	Value
Shape	Cylindrical
Diameter	12 m
Height	15 m
Effective Storage Height	12 m
Effective Storage Volume	1357.17 m^3
Height to Diameter Ratio (H/D)	1:1
Inlet Water Flow Velocity	0.2 m/s
Inlet Water Flow Rate	93.4 m^3/h

Figure 3.2 shows the storage tank model used for simulation.

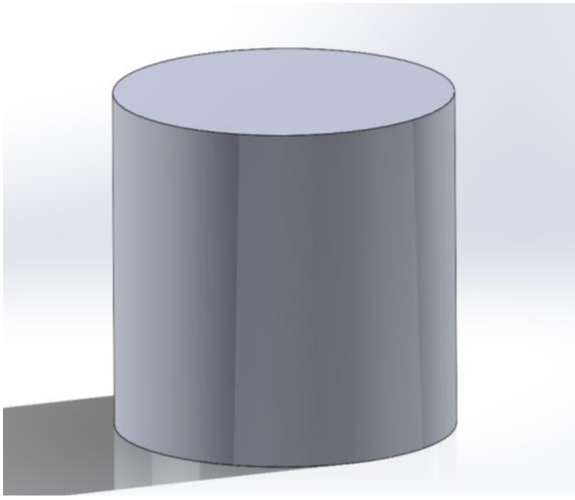

Figure 3.2: Visualisation of storage tank model

The storage tank will be simulated as well-insulated which means negligible loss of heat to the surroundings of the storage tank. The tank will be initially fully filled uniformly with 35 °C water during commissioning. Heated water of 45 °C will then be supplied to the thermal storage tank through the inlet during charging.

3.5 Diffuser setup

For this study, three different configurations of 12 m diameter perforated diffusers will be tested and compared against one another. These diffusers will be placed 1.5 m from the bottom of the storage tank with a slotted pipe with perforated plate diffuser placed 1.5 m from the top of the storage tank that has been optimised from previous research. Figure 3.3 shows the optimised slotted pipe with perforated plate diffuser that will be used at the top section of the storage tank.

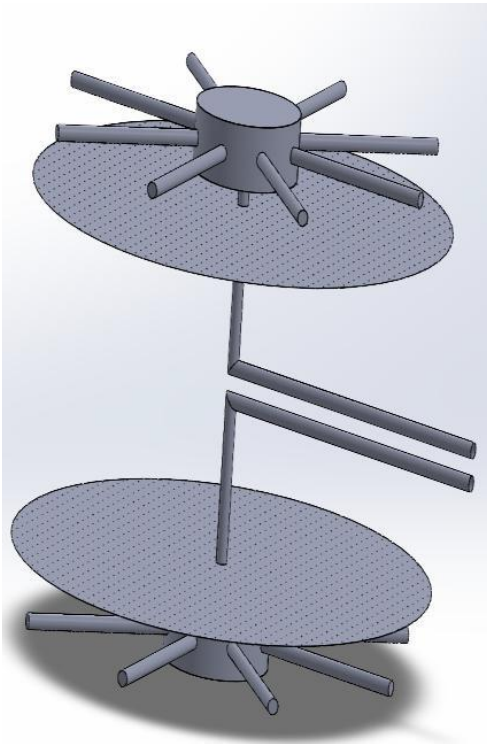

Figure 3.3: Optimised Slotted Pipe with Perforated Plate Diffuser

Table 3.2: Optimised Slotted Pipe with Perforated Plate Diffuser Parameters

Parameter	Value
Main pipe diameter	0.40640 m
Branch pipe diameter	0.33834 m
Outlet holes present	592
Perforated plate holes present	2280

Figure 3.4, 3.5 and 3.6 shows the three different diffuser configurations that will be used for testing. These configurations have varying spacing between holes, opening ratios, number of holes present and total perforation surface area ranging from highest total perforation surface area for Configuration ‘A’ to the least for Configuration ‘C’.

Configuration 'A' Perforated Plate Diffuser

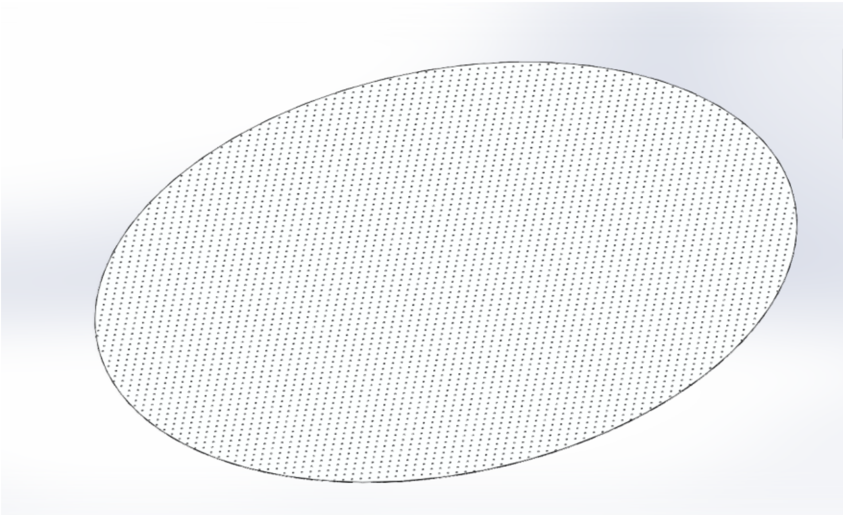

Figure 3.4: Configuration 'A' Perforated Plate Diffuser

Table 3.3: Configuration 'A' Perforated Plate Diffuser Parameters

Parameter	Value
Hole diameter	0.02605 m
Spacing between holes	0.15 m
Opening ratio	0.02347
Perforated plate holes present	4981
Total hole surface area	2.6547 m^2

Configuration 'B' Perforated Plate Diffuser

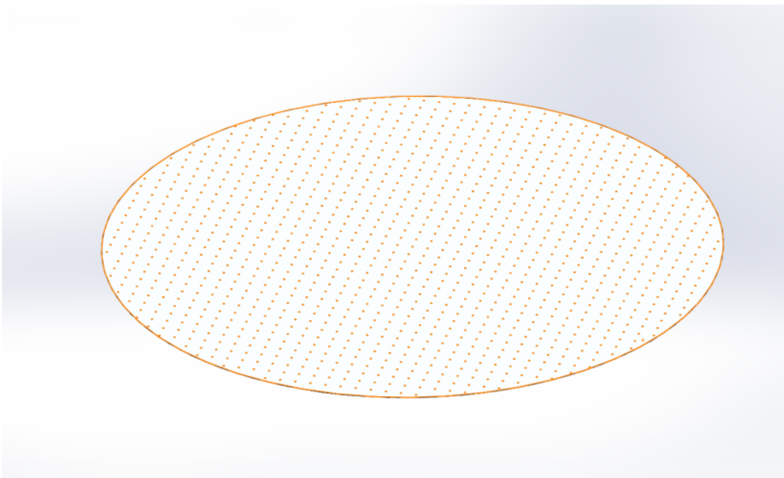

Figure 3.5: Configuration 'B' Perforated Plate Diffuser

Table 3.4: Configuration ‘B’ Perforated Plate Diffuser Parameters

Parameter	Value
Hole diameter	0.02605 m
Spacing between holes	0.3 m
Opening ratio	0.00583
Perforated plate holes present	1237
Total hole surface area	0.6593 m^2

Configuration ‘C’ Perforated Plate Diffuser

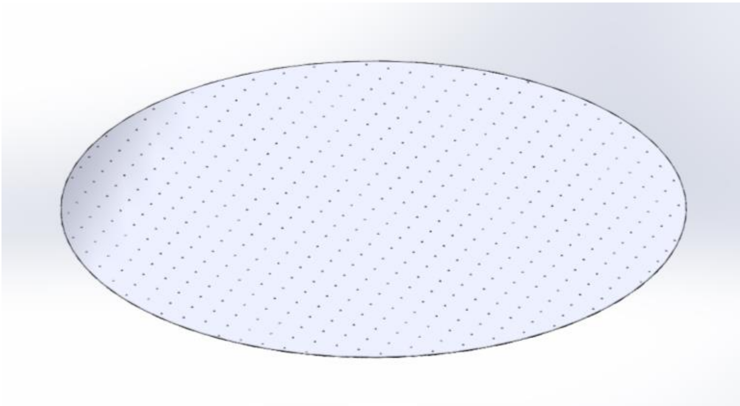

Figure 3.6: Configuration ‘C’ Perforated Plate Diffuser

Table 3.5: Configuration ‘C’ Perforated Plate Diffuser Parameters

Parameter	Value
Hole diameter	0.02605 m
Spacing between holes	0.45 m
Opening ratio	0.00263
Perforated plate holes present	557
Total hole surface area	0.2969 m^2

3.6 CFD simulation setup

For this study, ANSYS CFX software will be used to carry out the CFD simulations. ANSYS Workbench version 2025 R1 will be used to prepare and run these simulations. A transient analysis simulation model will be used to track the required data points that changes state over a period of time. Both the charging and discharging cycles will be simulated and analysed. The entire setup sequence to prepare the setup and operating parameters of the solver will be detailed in this section.

3.6.1 Geometry Setup

Firstly, a new Fluid Flow (CFX) project is created in ANSYS Workbench. The storage tank CAD model is then imported into the project as a Parasolid file (.x_t). Figure 3.7 shows the storage tank model used.

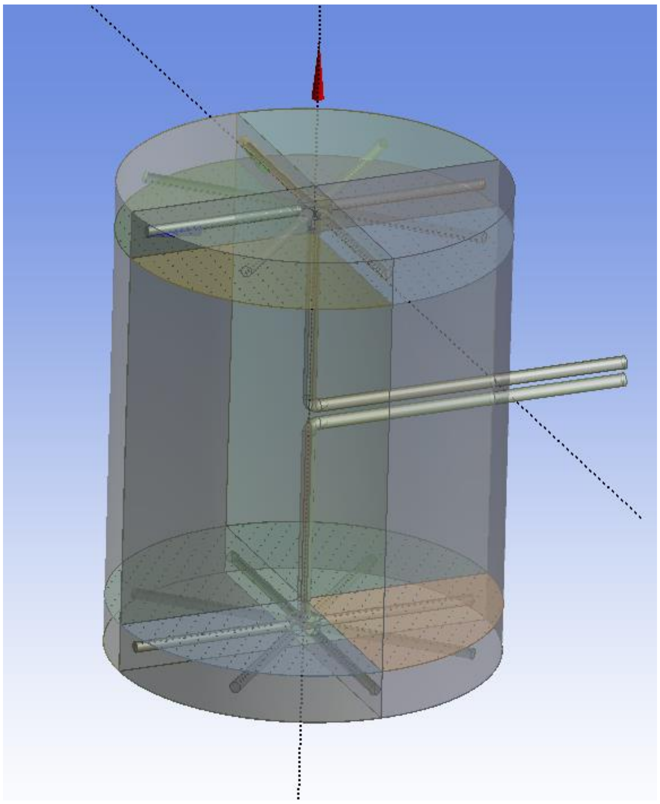

Figure 3.7: Modelled Storage Tank

Inside the 'Design Modeler' application, apply a 'Fill' command to fill the internal fluid region of the storage tank by setting 'Extraction Type' to 'By Cavity'. Next, three quarters of the cylinder geometry will be deleted as only one quarter is required for simulation to reduce the computational cost and time. This can be done using the 'Slice' function. The 'Slice' function is applied along the XY and YZ plane respectively to split the storage tank into four quarters. Figure 3.8 shows the sliced body to be used for simulation.

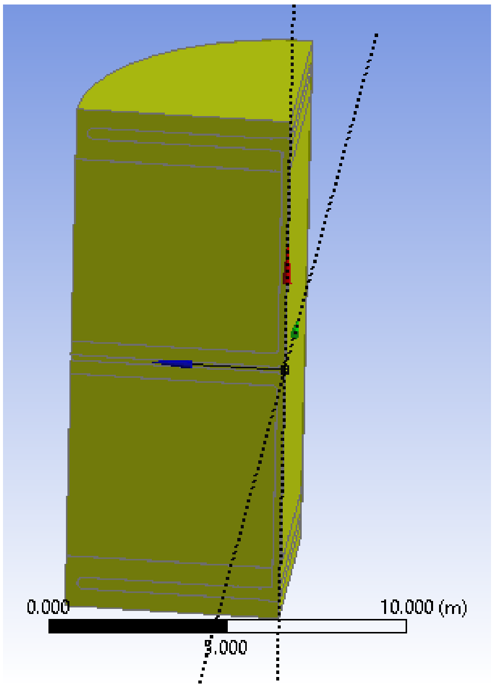

Figure 3.8: Sliced Storage Tank

3.6.2 Meshing setup

Once completing the geometry setup, the geometry will be sent for meshing. This step is required to partition the solid bodies of the geometry into smaller domains to allow the solver to accurately calculate and predict the fluid flow behaviour. Figure 3.9 shows the meshing parameters:

Details of "Mesh"	
Display	
Display Style	Use Geometry Setting
Defaults	
Physics Preference	CFD
Solver Preference	CFX
Element Size	1.0 m
Sizing	
Use Adaptive Sizing	No
Growth Rate	Default (1.2)
Max Size	Default (2.0 m)
Mesh Defeaturing	Yes
Defeature Size	Default (5.e-003 m)
Capture Curvature	Yes
Curvature Min Size	Default (1.e-002 m)
Curvature Normal An...	Default (18.0°)

Figure 3.9: Meshing Parameters

Figure 3.10 shows the meshed fluid domain that will be used for the simulation.

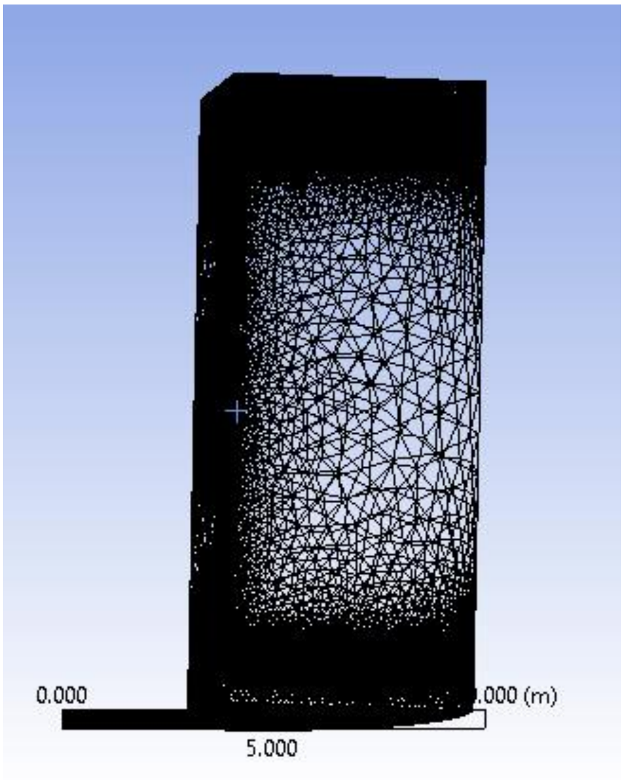

Figure 3.10: Meshed Fluid Domain

After that, specific named selections are created to specify the boundary and initial conditions for the setup part later. Figures 3.11 to 3.14 shows the “Outlet”, “Inlet”, “Symmetry” and “Body” named selections that were created along with the respective faces selected to be used for the location setting in the CFX-Setup.

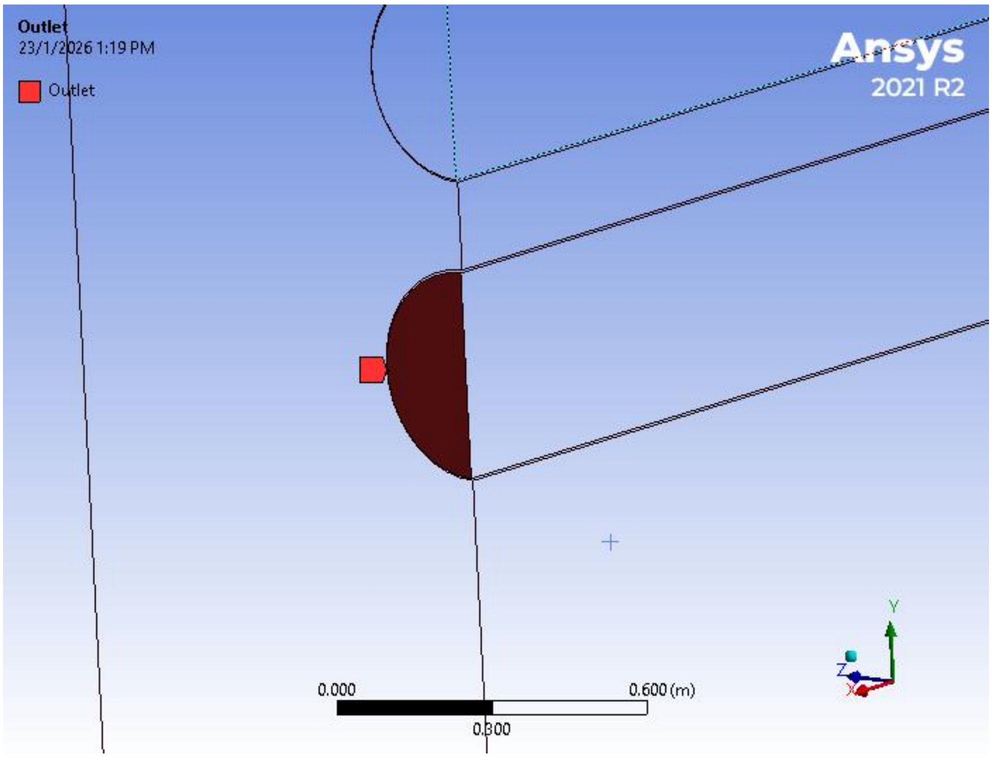

Figure 3.11: “Outlet” Location on the Model

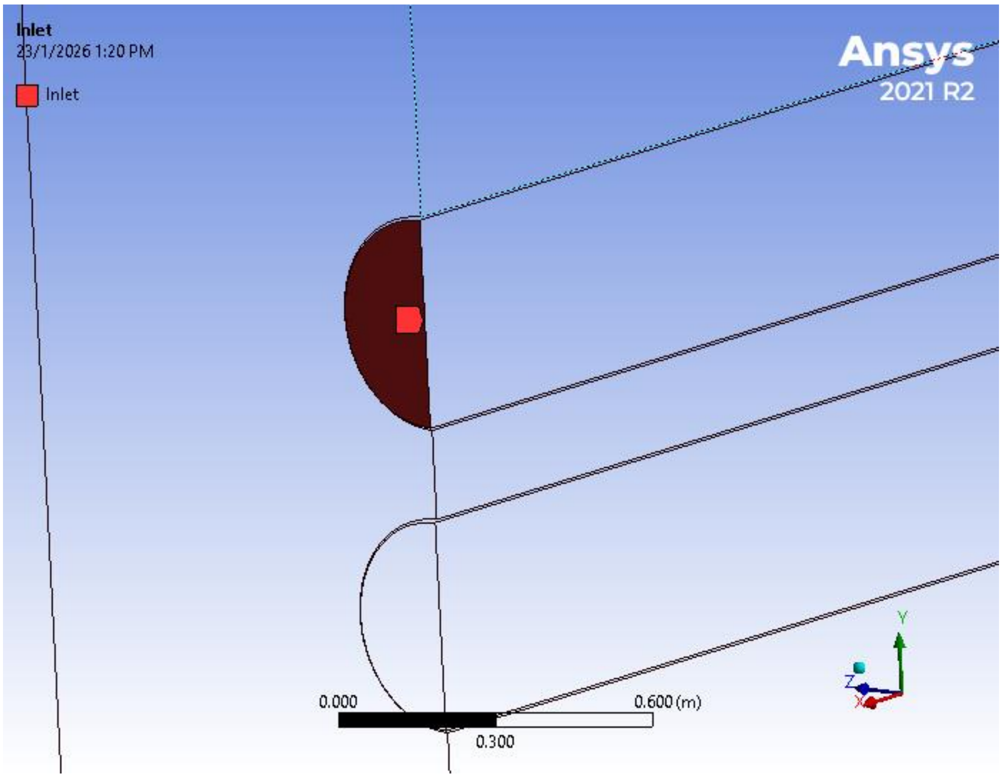

Figure 3.12: “Inlet” Location on the Model

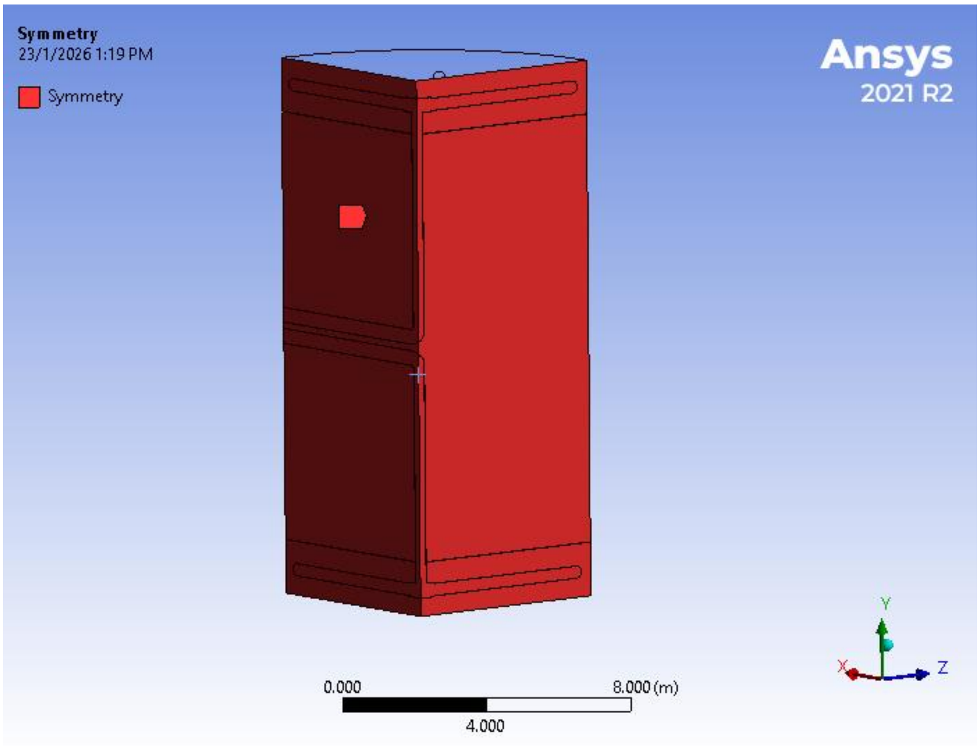

Figure 3.13: “Symmetry” Location on the Model

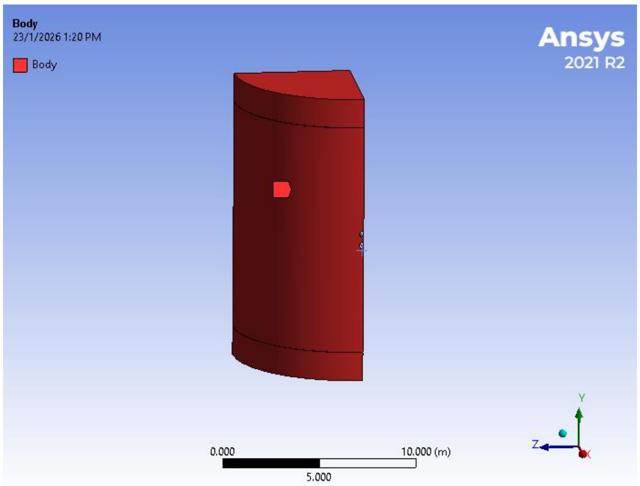

Figure 3.14: “Body” Location on the Model

3.6.3 CFX-Pre setup

Once meshing is done, the main operating parameters of the simulation is setup in CFX-Pre application. Figure 3.15 shows the parameters of the analysis type for the simulation.

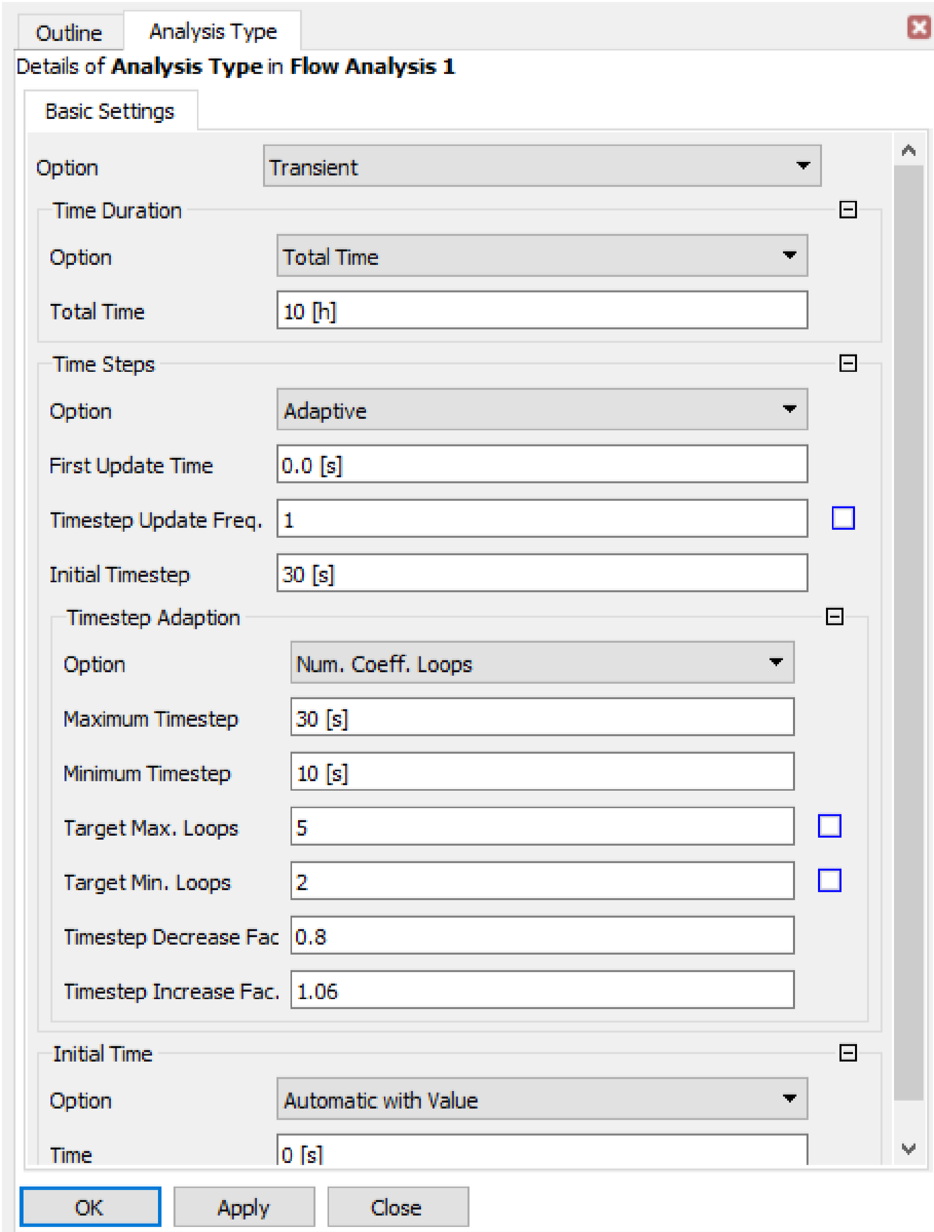

Figure 3.15: Analysis Type Parameters

Figure 3.16 and 3.17 show the default domain settings for transient discharging to be used for the simulation.

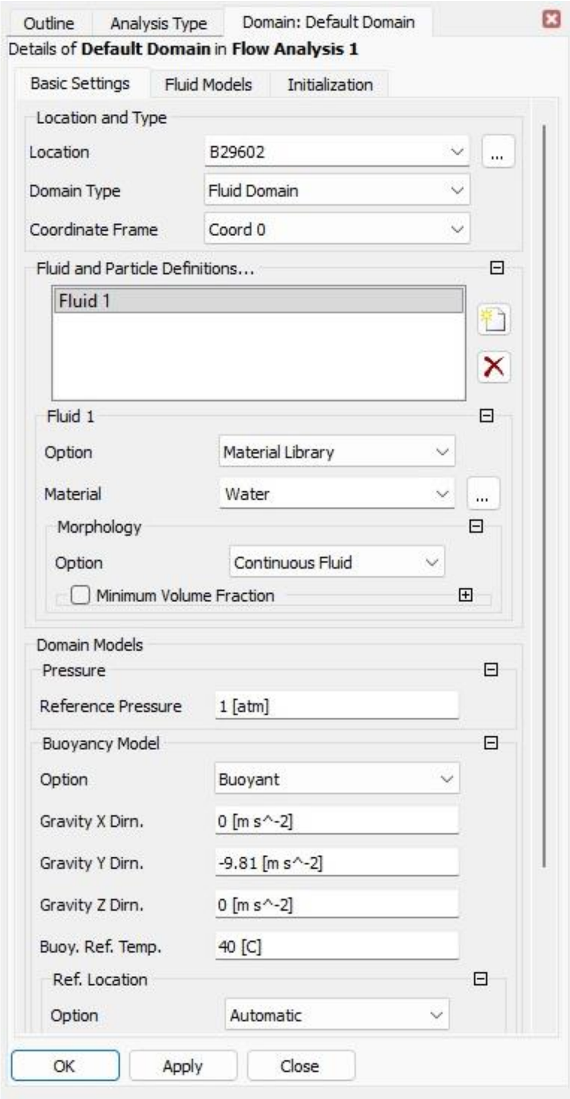

Figure 3.16: Default Domain Basic Settings For Discharging Cycle

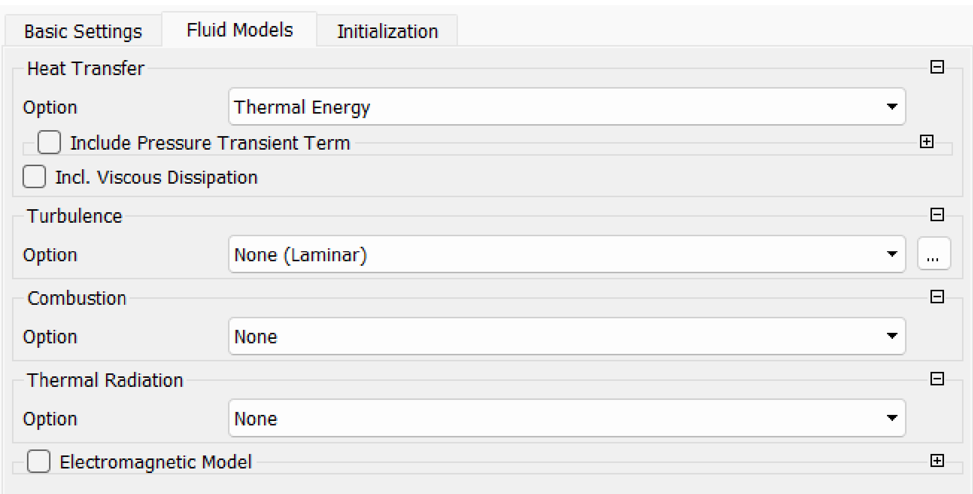

Figure 3.17: Default Domain Fluid Model For Discharging Cycle

Figure 3.18 shows the global initialization settings for the discharging cycle.

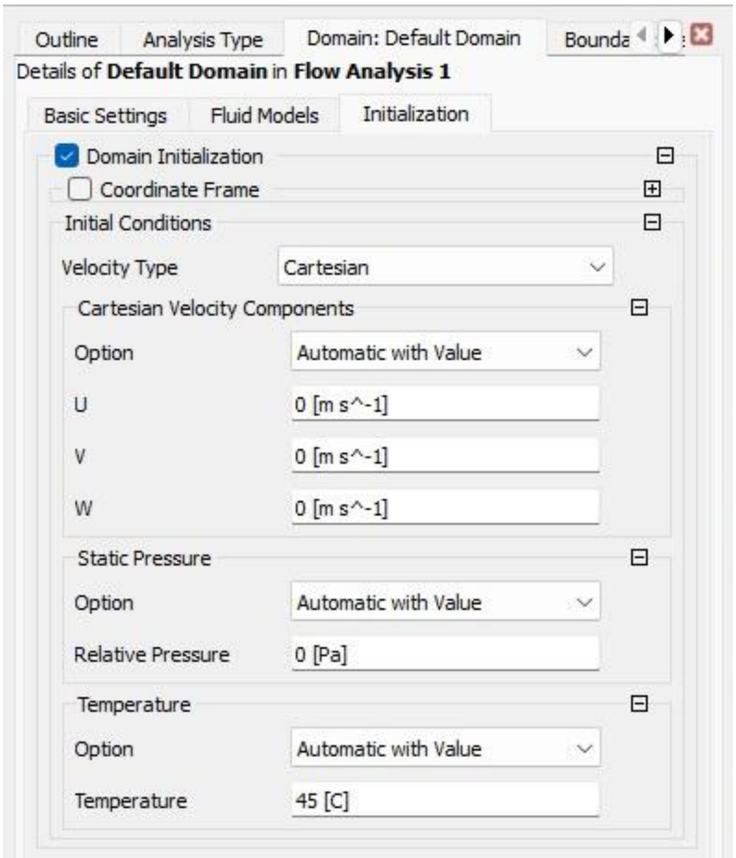

Figure 3.18: Global Initialization Parameters For Discharging Cycle

Figure 3.19 shows the location chosen for the simulated 'Inlet'

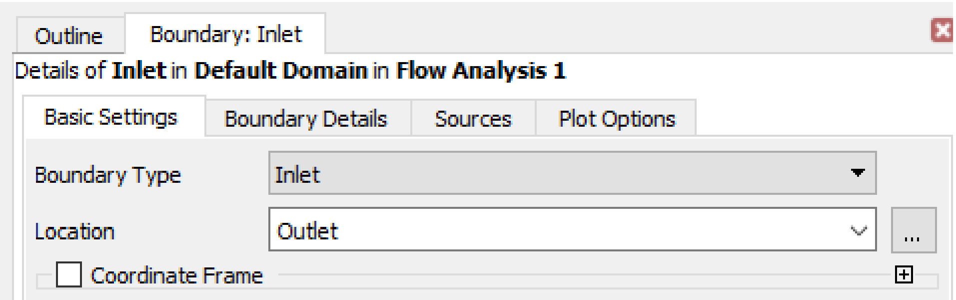

Figure 3.19: Location set in simulation for Boundary Type 'Inlet' for Discharging Cycle

Figure 3.20 shows the boundary condition settings of the simulation 'Inlet' for discharging.

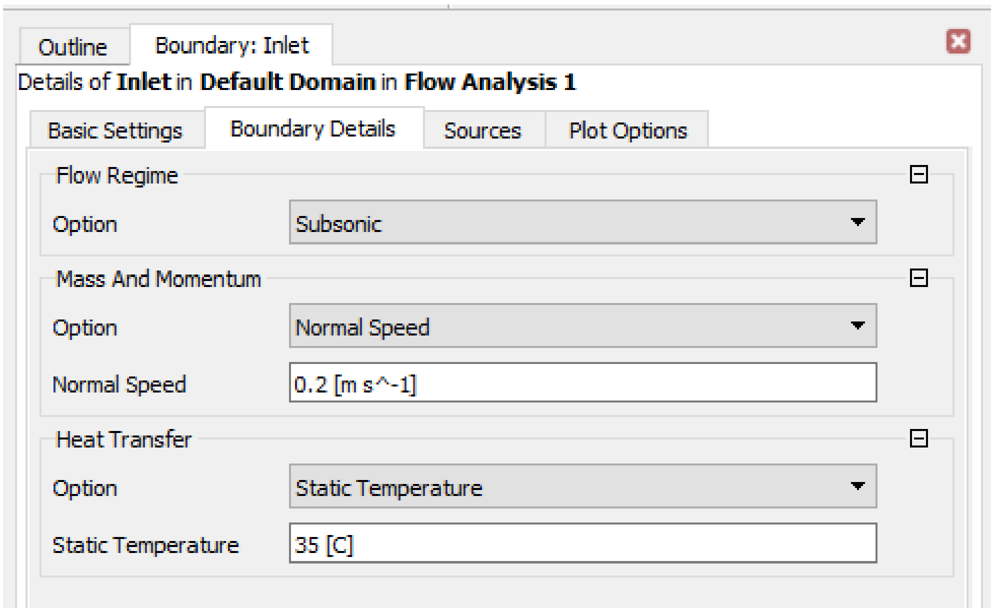

Figure 3.20: Boundary Conditions at 'Inlet' for Discharging Cycle

Figure 3.21 shows the location chosen for the simulated 'Outlet'

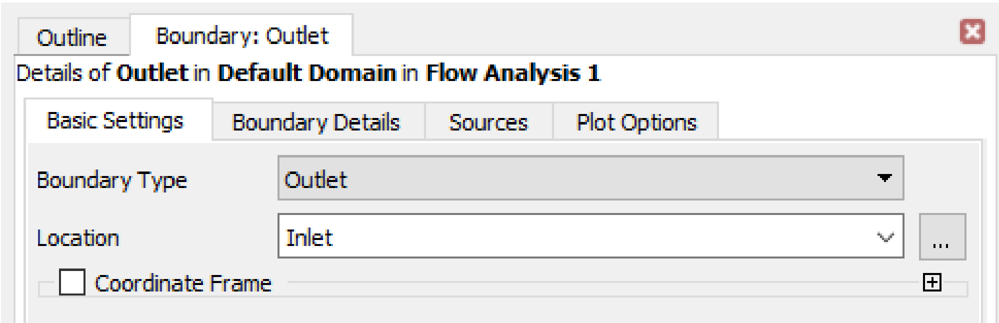

Figure 3.21: Location set in simulation for Boundary Type 'Outlet' for Discharging Cycle

Figure 3.22 shows the boundary condition settings of the 'Outlet' for discharging.

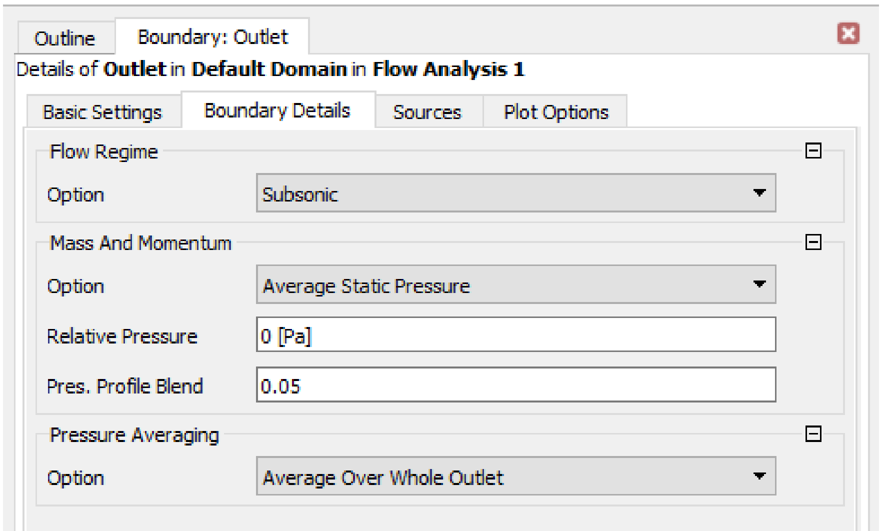

Figure 3.22: Boundary Conditions at 'Outlet' for Discharging Cycle

Figure 3.23 shows the solver control settings used.

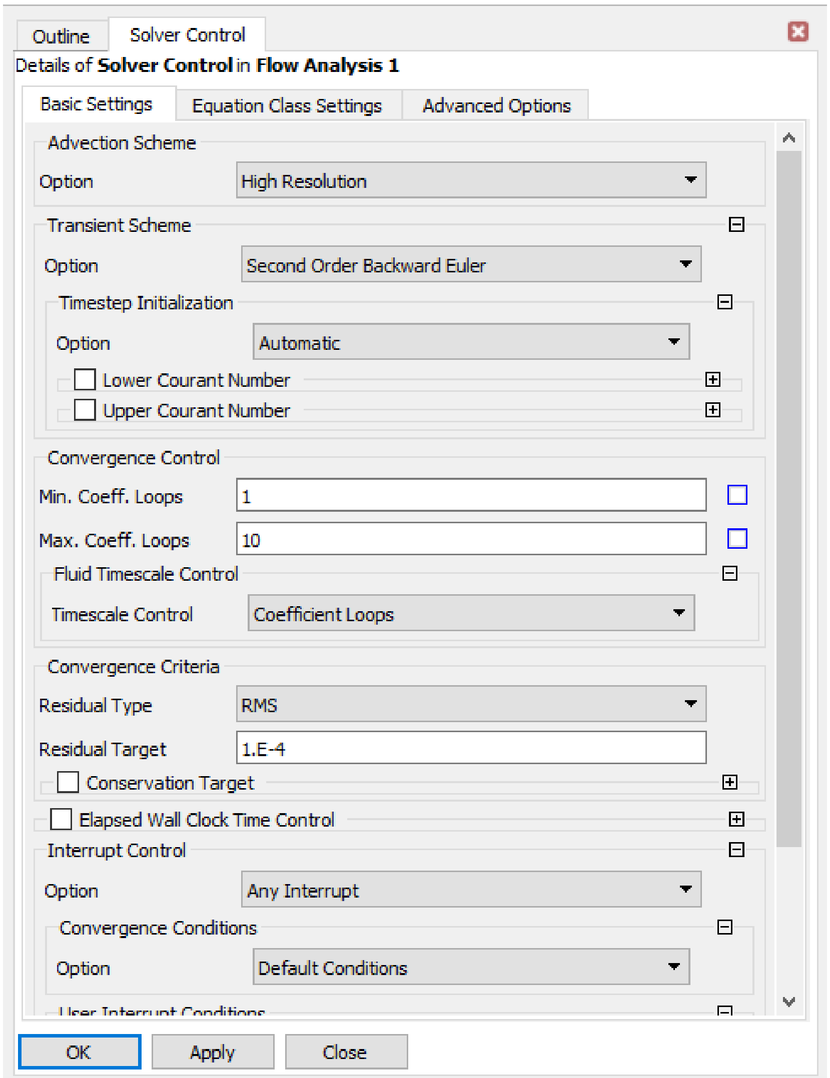

Figure 3.23: Solver Control Settings Used

Figure 3.24 shows the output control settings used. The output frequency can be changed from every timestep to time interval instead at every 30 seconds or so to reduce the number of transient result files generated as the generated transient result files will occupy a large amount of storage space. Changing the output frequency will not affect the calculation of the results but just the time points of the simulation where the results can be displayed.

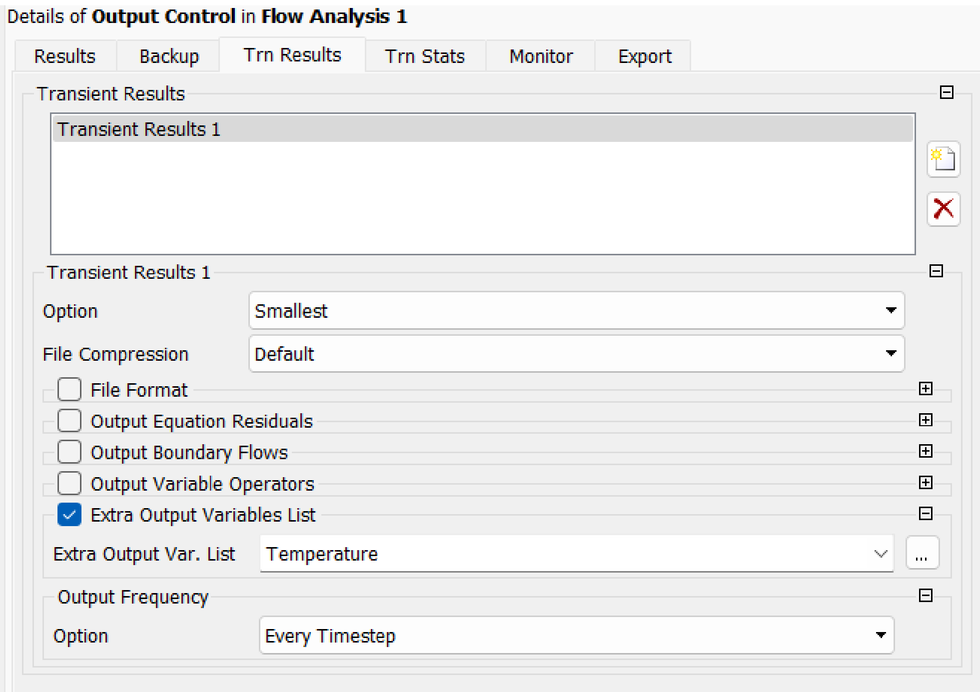

Figure 3.24: Output Control Settings Used

The setups used for the transient charging cycle simulations are almost identical to the setup used for the transient discharging cycle simulations. The main difference in setup is only in the boundary conditions for both 'Inlet' and 'Outlet' as well as for the global initialization settings. Figure 3.18 and 3.19 displays the boundary condition changes required when changing to charging cycle simulations while Figure 3.20 displays the modifications made for the global initialization parameters for charging cycle.

Figure 3.19 shows the location chosen for the simulated 'Inlet' for Charging Cycle.

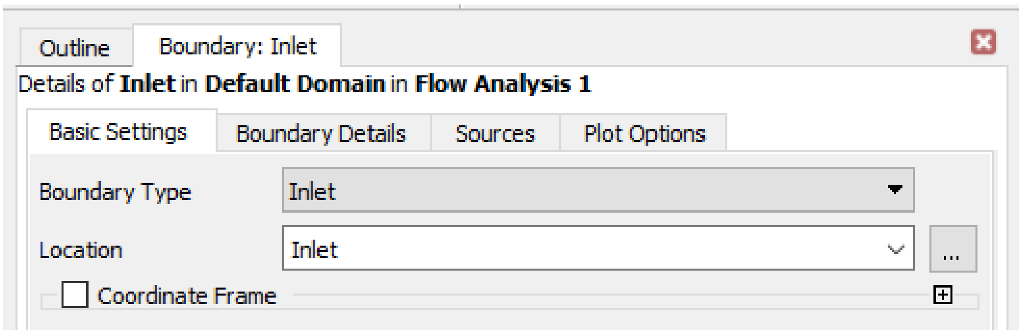

Figure 3.25: Location set for simulation 'Inlet' for Charging Cycle

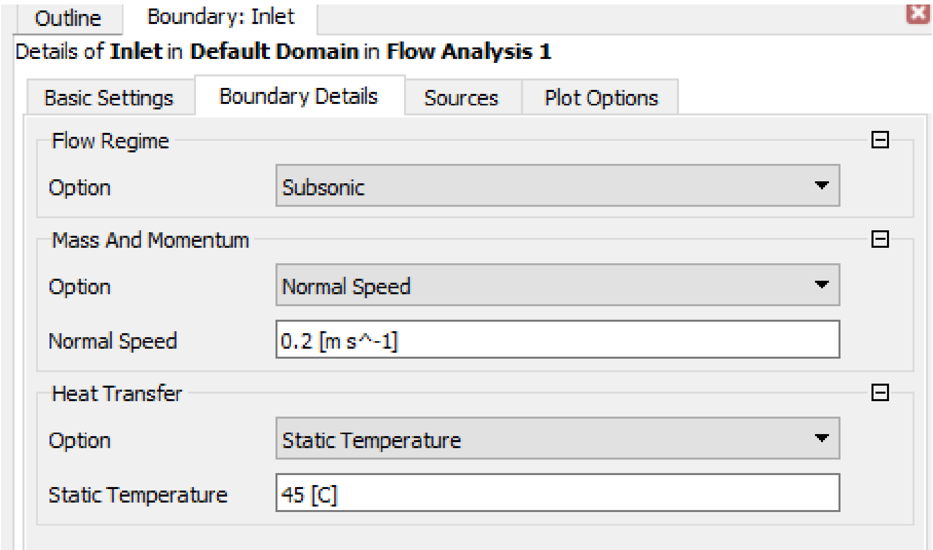

Figure 3.26: Boundary Conditions at 'Inlet' for Charging Cycle

Figure 3.19 shows the location chosen for the simulated 'Outlet' for Charging Cycle.

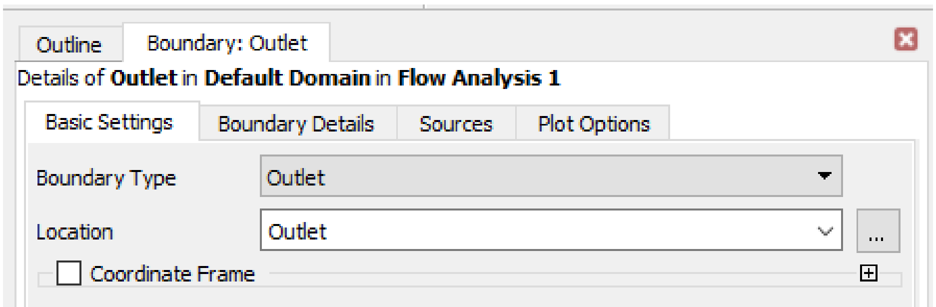

Figure 3.27: Location set for simulation 'Outlet' for Charging Cycle

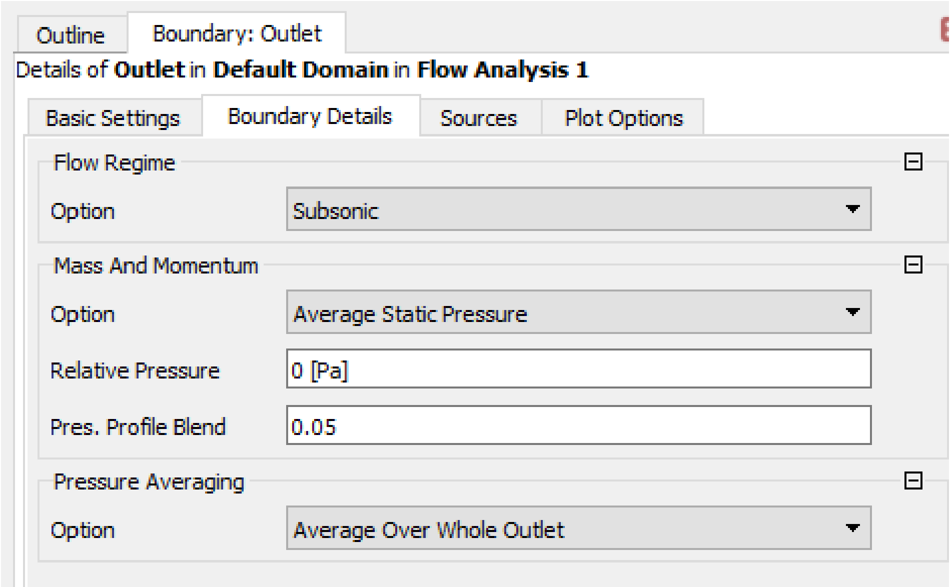

Figure 3.28: Boundary Conditions at ‘Outlet’ for Charging Cycle

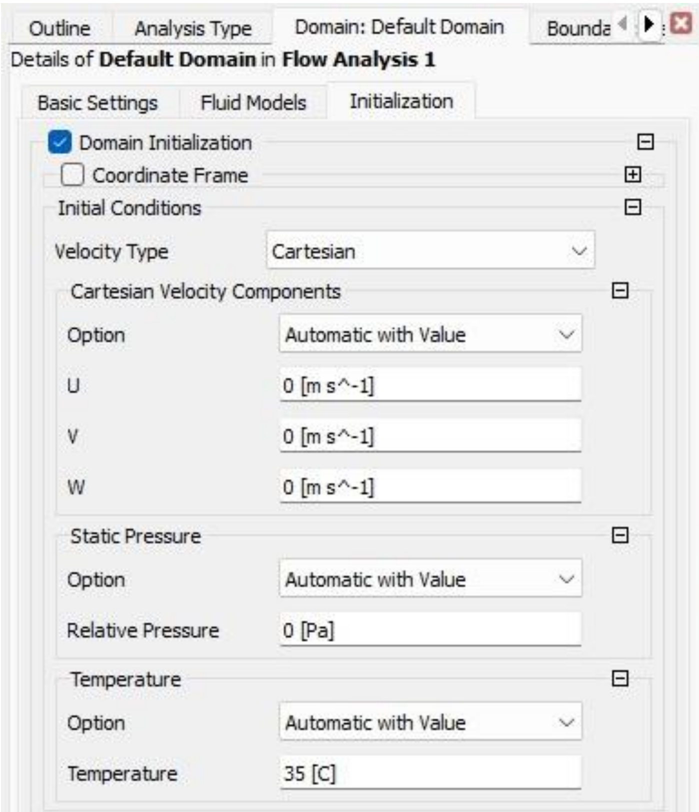

Figure 3.29: Global Initialization Parameters For Charging Cycle

3.6.4 CFX-Solver Setup

Once all of the parameters have been set, the CFX-Solver is run under double precision and under a local parallel run mode to utilise the multiple processor cores present. Under the solver tab, the memory allocation can be increased to utilise any extra memory present in the computer for faster computation.

3.6.5 Prototype Tank

A scaled down prototype tank is built alongside to verify the findings from the large commercial tank simulation. The testing results of the prototype tank were also simulated just like for the main TES commercial tank. Table 3.6 shows the specifications of the tank prototype.

Table 3.6: Prototype Tank Parameters

Parameter	Value
Material	Polypropylene (PP)
Shape	Cylindrical
Diameter	0.2850 m
Height	0.3840 m
Volume	0.0205 m^3
Effective Storage Height	0.2000 m
Effective Storage Volume	0.0128 m^3
Height to Diameter Ratio (H/D)	0.7:1
Inlet Water Flow Velocity	0.15 m/s
Inlet Water Flow Rate	0.0954 m^3/h

Table 3.7 shows the parameters for the inlet and outlet radial slotted pipe diffusers.

Table 3.7: Radial Slotted Pipe Diffuser Parameters

Parameter	Value
Material	• Polyvinyl Chloride (pipes) • Polyactic Acid (pipe adapters)
Slotted Hole Diameter	0.004 m
Inlet/Outlet Pipe Diameter	0.015 m
Number of Branches	6
Number of Slotted Holes per Branch	11

Table 3.8 and 3.9 shows the general and specific parameters for the perforated plate configurations to be used in the prototype. These parameters are chosen to try to match the parameters used by the large TES commercial tank parameters as close as possible by aligning the opening ratios.

Table 3.8: Perforated Plate Diffuser General Parameters

Parameter	**Value**
Material	Acrylic Plastic
Hole Diameter	0.004 m
Thickness	0.005 m

Table 3.9: Perforated Plate Diffuser Specific Parameters

Configuration	Spacing Between Holes (m)	Number of Holes	Total Perforation Surface Area (m^2)	Opening Ratio
A	0.02	129	0.00162	0.02539
C	0.06	13	0.00016	0.00251

As for the simulation side of the testing prototype, the boundary conditions and setup parameters for this prototype tank simulation are the same as for the large TES commercial tank except for the inlet water flow speed of 0.15 m/s.

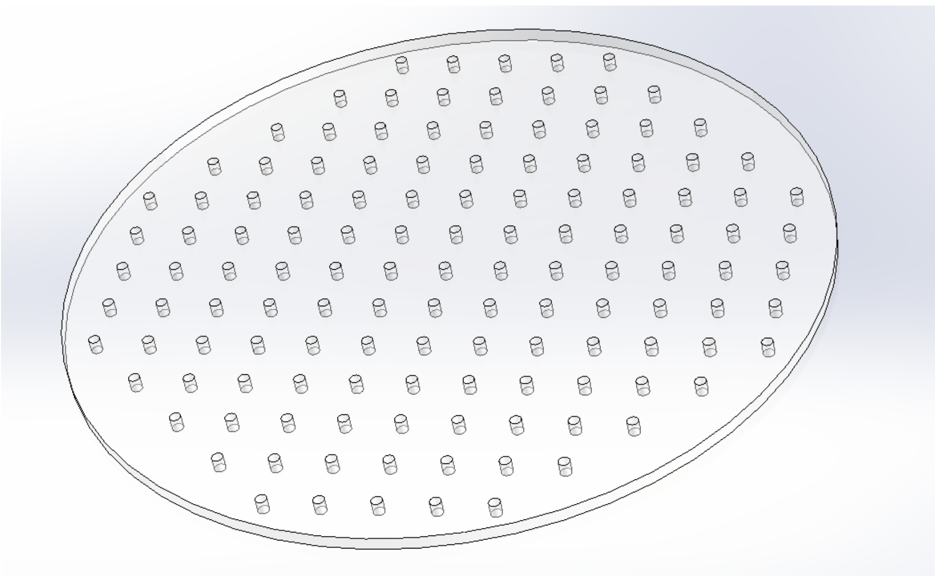

Figure 3.30: Configuration ‘A’ Plate

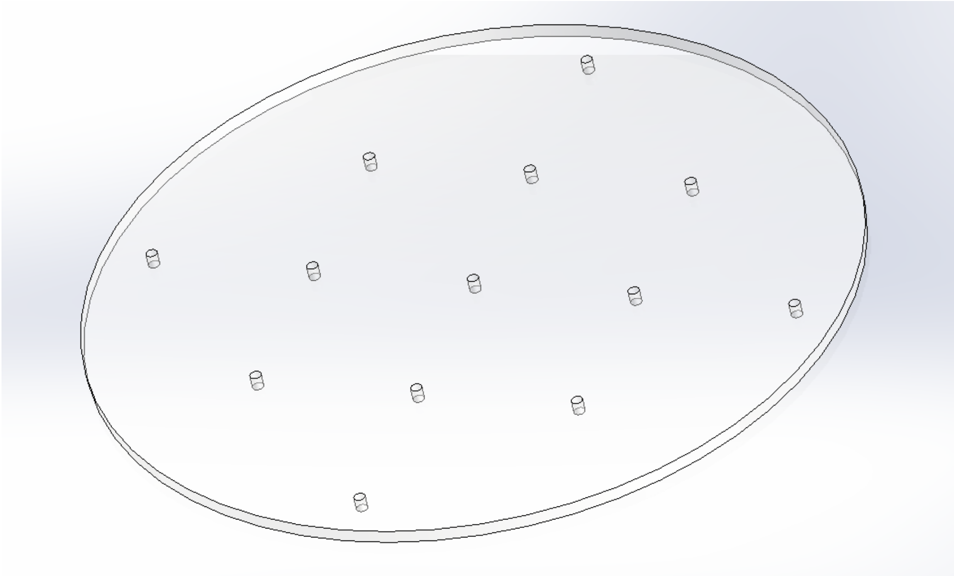

Figure 3.31: Configuration ‘C’ Plate

The thermocouple system used in the prototype is controlled by a programmed Arduino Uno R3 that records the temperature of the water within the tank every second. 10 type-K thermocouples were used in the system with each thermocouple spaced out 3.2 cm vertically from each other. The thermocouples are labelled from T1 to T10 respectively according to their position in the tank with T1 and T2 positioned at the top buffer of the tank, T3 to T7 positioned in the effective storage volume and T8 to T10 positioned at the bottom buffer of the tank.

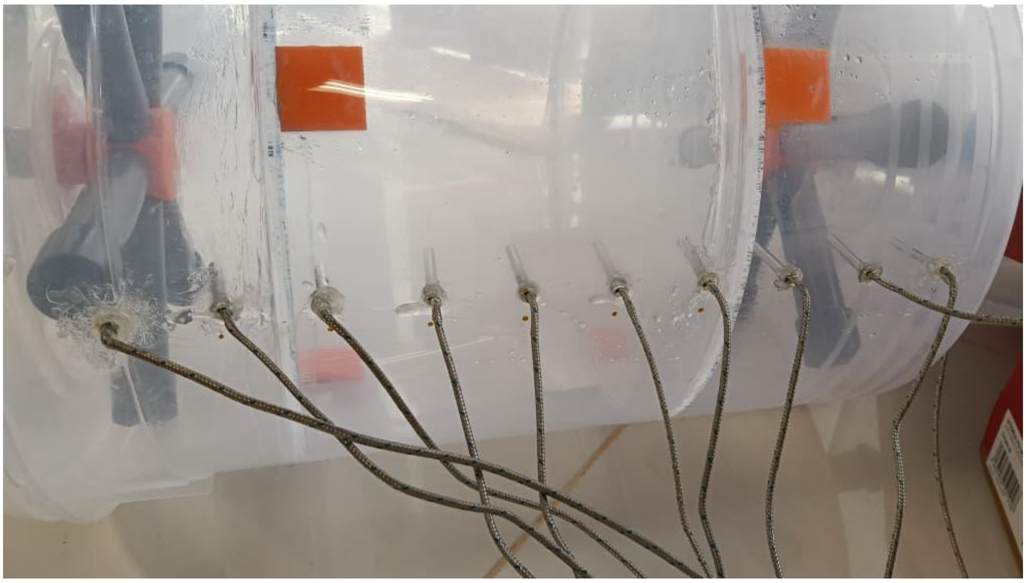

Figure 3.32: Thermocouple System and Position of Probes

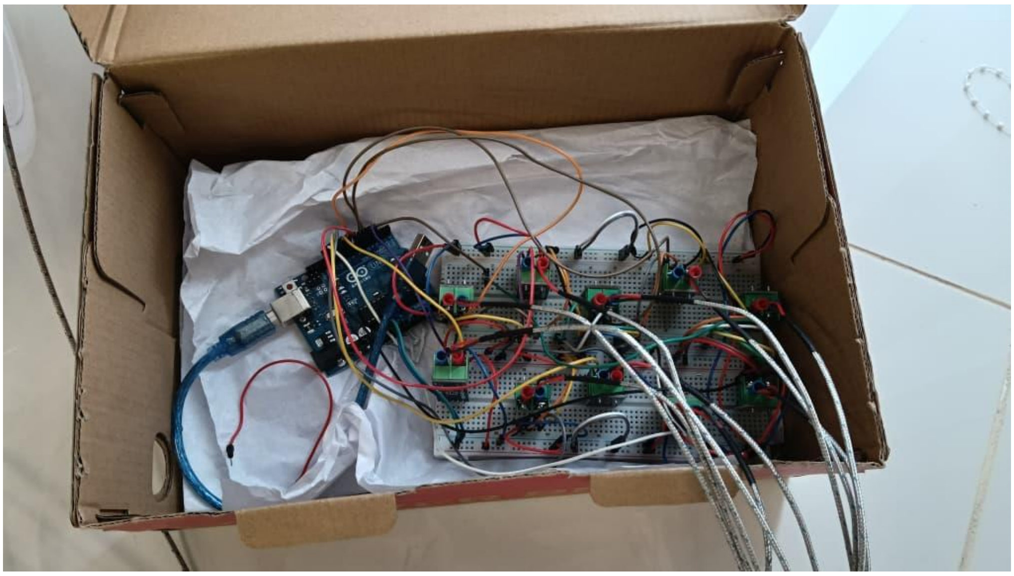

Figure 3.33: Thermocouple System Circuitry

The edges of the perforated plate diffusers inside the tank were sealed using silicon sealant while any other gap present were sealed using two-part epoxy mix. Figure 3.34 shows the prototype tank used for testing.

Figure 3.34: Prototype Tank Used For Testing

For the charging cycle testing, the prototype tank is firstly filled up with cold water from the water bath at 35°C. After that, the water bath is then heated up to 50°C and pumped into the tank. The data stream from the thermocouple system is then recorded through a data logging add-on in Microsoft Excel. 14 minutes of data will be recorded and analysed. This testing is then repeated with the other configuration of perforated plate diffuser. Figure 3.35 shows the testing setup used.

Figure 3.35: Testing Setup With The Water Bath (right), Prototype Tank (center) and Computer (left) For Data Logging

CHAPTER 4

RESULTS AND DISCUSSION

4.1 Introduction

In this section, the CFD results from the simulation for both the charging and discharging cycles using all three different perforated plate diffuser configurations will be displayed and analysed. The results from the physical tank prototype testing will also be analysed and compared to the results obtained for the commercial TES tank simulations.

The CFD results for the charging and discharging cycle of the large TES commercial tank using the three different configurations of perforated plate diffusers are presented through the temperature profile contour visualization at the X-Y plane of the model (+Z view) at every two-hour interval up to the 10^{th} hour of simulation. A measured temperature distribution plot at the 4^{th} and 8^{th} hour of simulation using PlotDigitizer and simulation data is also presented.

On the other hand, CFD results for the charging cycle using the two different perforated plate diffusers are presented through the temperature profile contour visualization at the X-Y plane of the model (+Z view) at every two-minute interval up to the 14^{th} minute of simulation. A measured temperature distribution plot at the 10^{th} minute of simulation using PlotDigitizer and simulation data is also presented.

4.2 Charging Cycle CFD Results

4.2.1 CFD Results For Configuration A

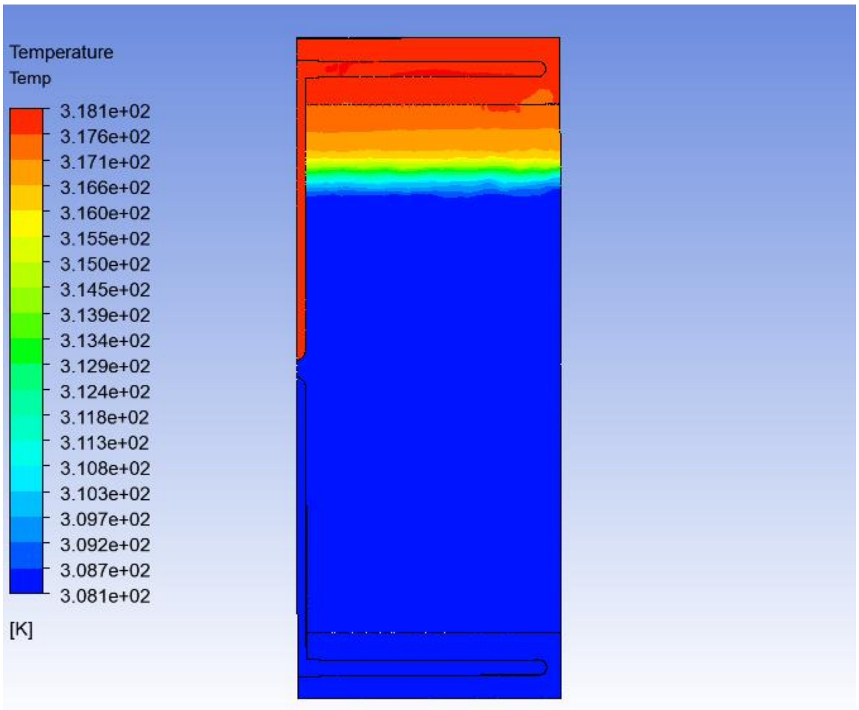

Figure 4.1: 2nd Hour Temperature Profile of the Charging Cycle Simulation For Configuration A

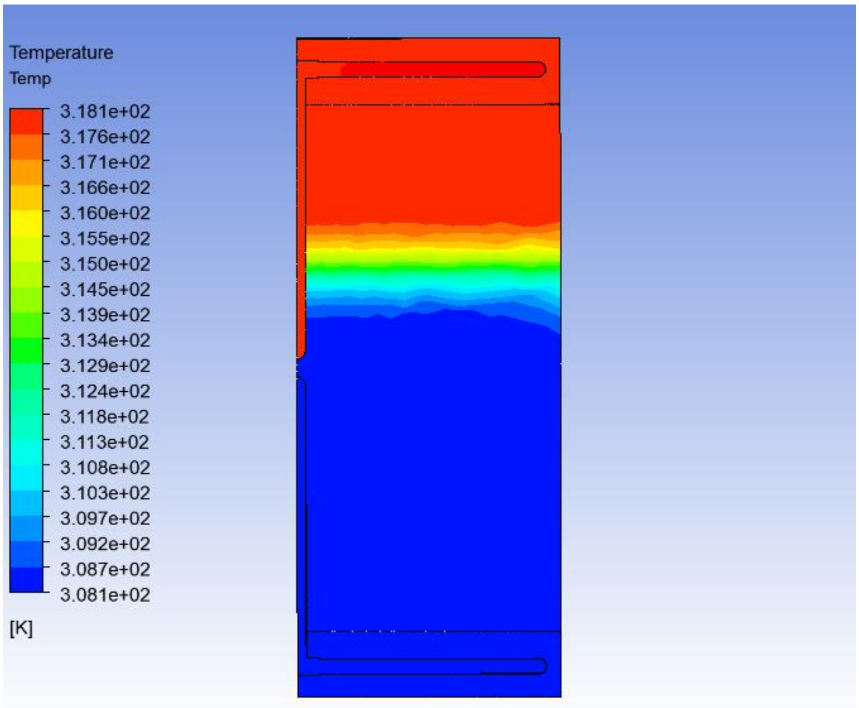

Figure 4.2: 4th Hour Temperature Profile of the Charging Cycle Simulation For Configuration A

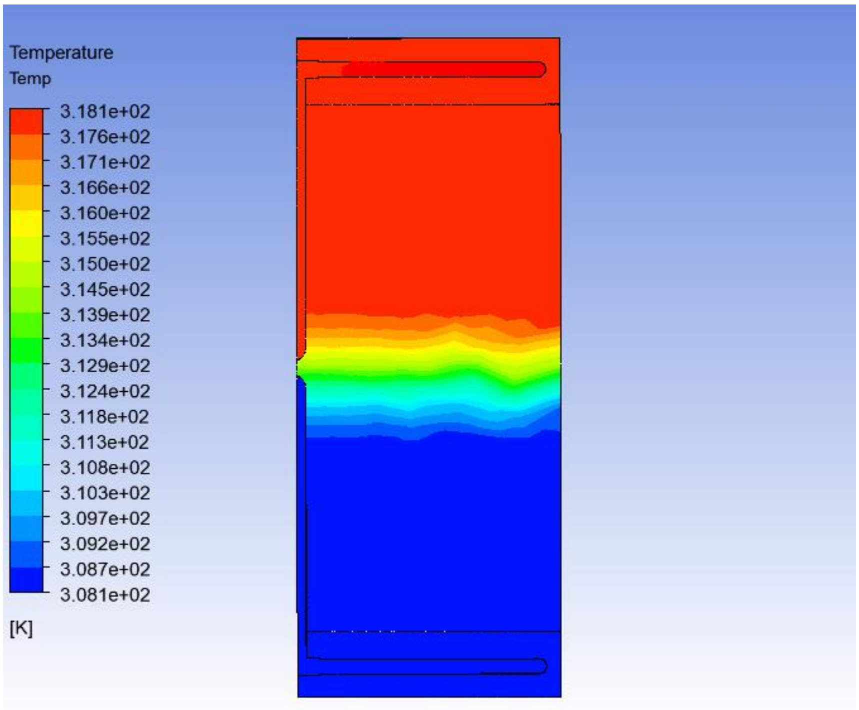

Figure 4.3: 6th Hour Temperature Profile of the Charging Cycle Simulation For Configuration A

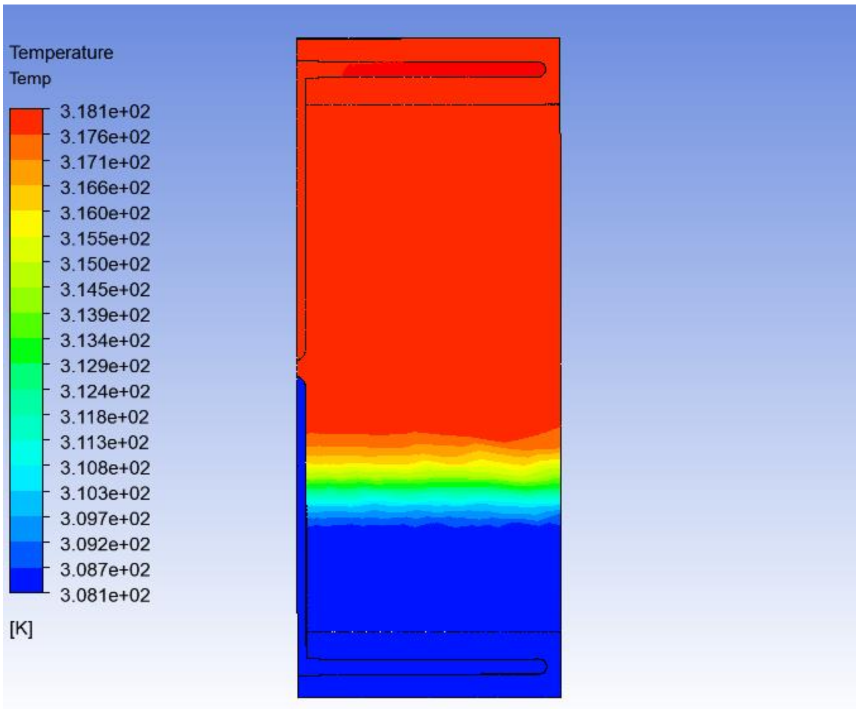

Figure 4.4: 8th Hour Temperature Profile of the Charging Cycle Simulation For Configuration A

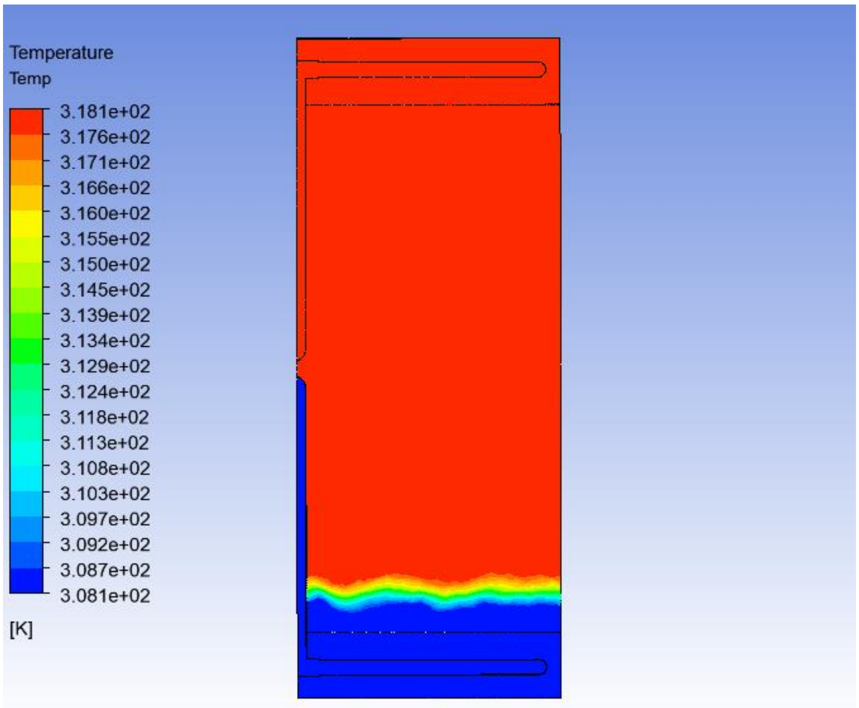

Figure 4.5: 10th Hour Temperature Profile of the Charging Cycle Simulation For Configuration A

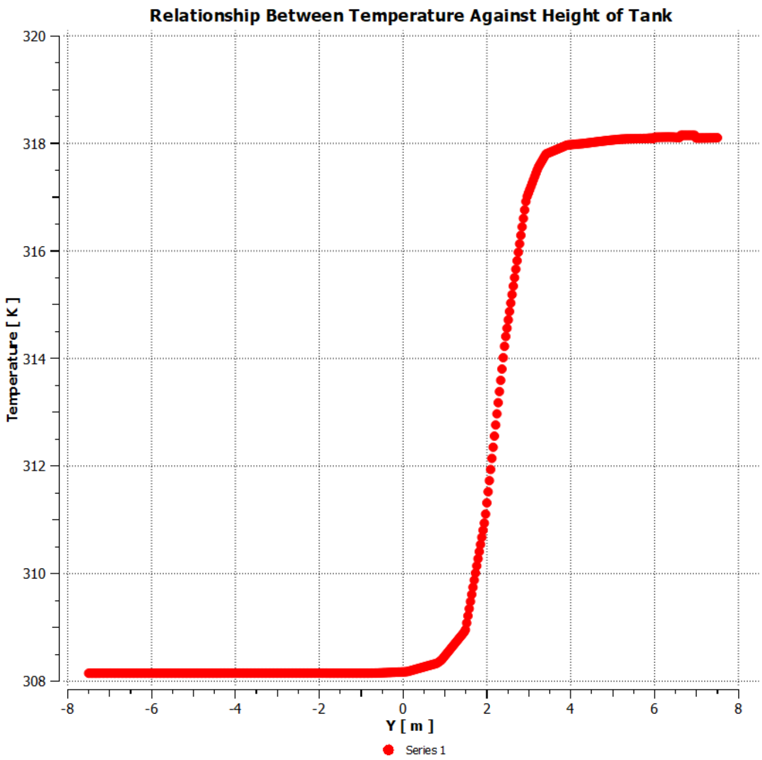

Figure 4.6: 4th Hour Temperature Distribution Plot of the Charging Cycle Simulation For Configuration A

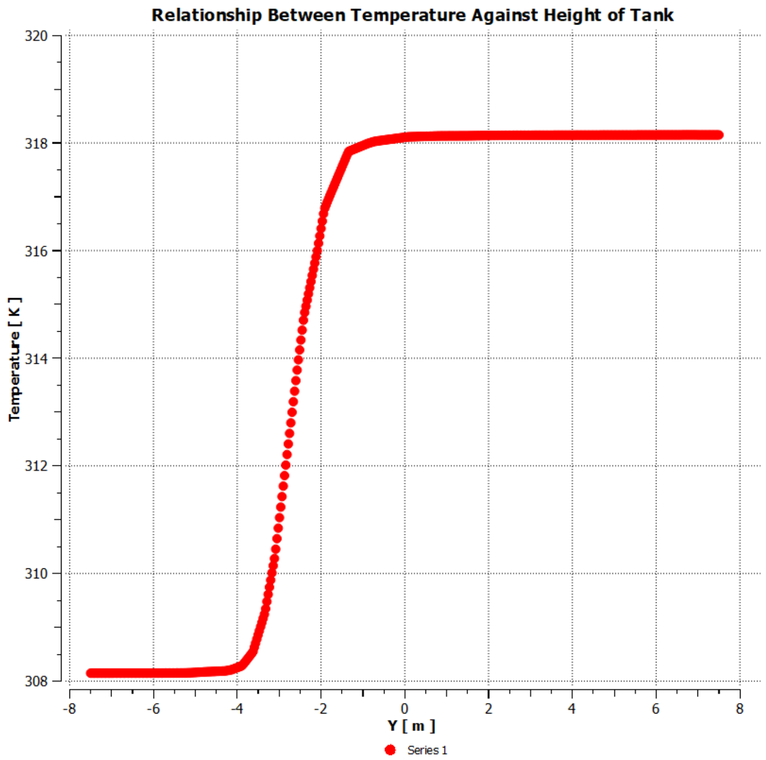

Figure 4.7: 8th Hour Temperature Distribution Plot of the Charging Cycle Simulation For Configuration A

Table 4.1: Position of Performance Indicators at 4th Hour of Charging Cycle for Configuration A

Performance Indicator, θ	Height of Tank, X (m)	Temperature, Y (K)	Thermocline Layer (m)
0.1	1.544	309.15	**1.464**
0.9	3.008	317.15	

Table 4.2: Position of Performance Indicators at 8th Hour of Charging Cycle for Configuration A

Performance Indicator, θ	Height of Tank, X (m)	Temperature, Y (K)	Thermocline Layer (m)
0.1	-3.373	309.15	**1.645**
0.9	-1.728	317.15	

4.2.2 CFD Results For Configuration B

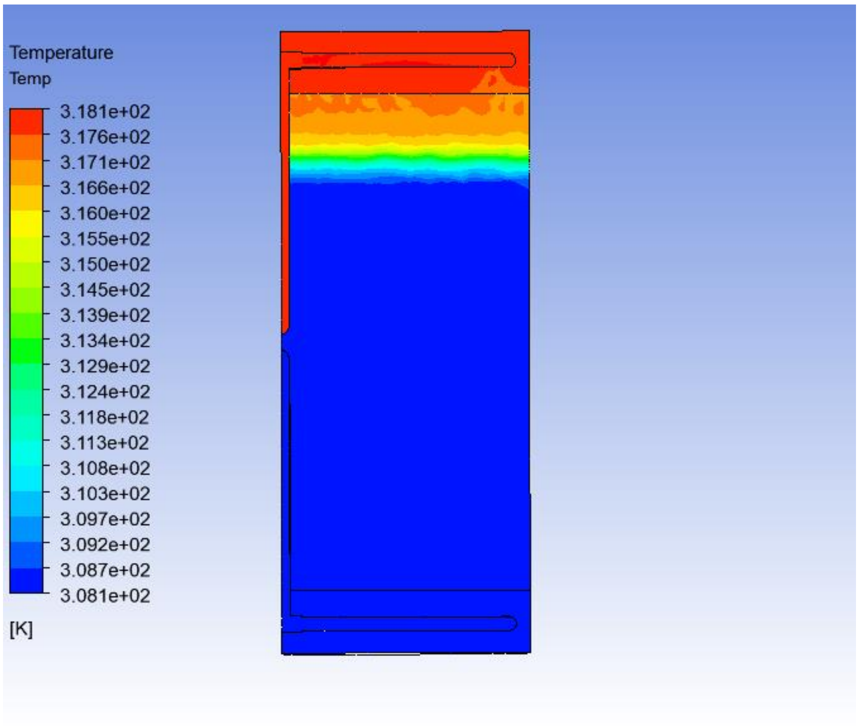

Figure 4.8: 2nd Hour Temperature Profile of the Charging Cycle Simulation For Configuration B

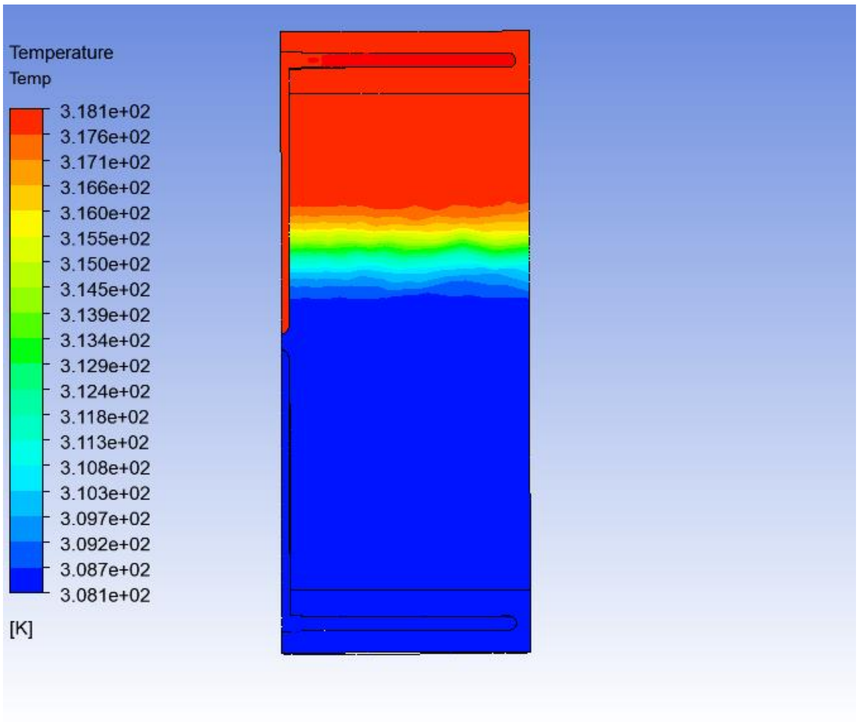

Figure 4.9: 4th Hour Temperature Profile of the Charging Cycle Simulation For Configuration B

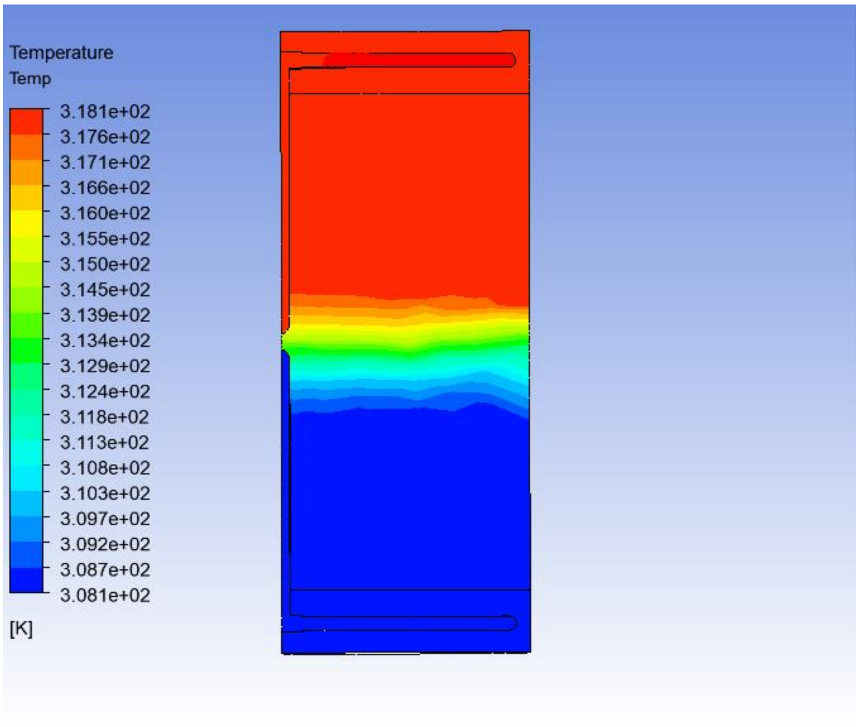

Figure 4.10: 6th Hour Temperature Profile of the Charging Cycle Simulation For Configuration B

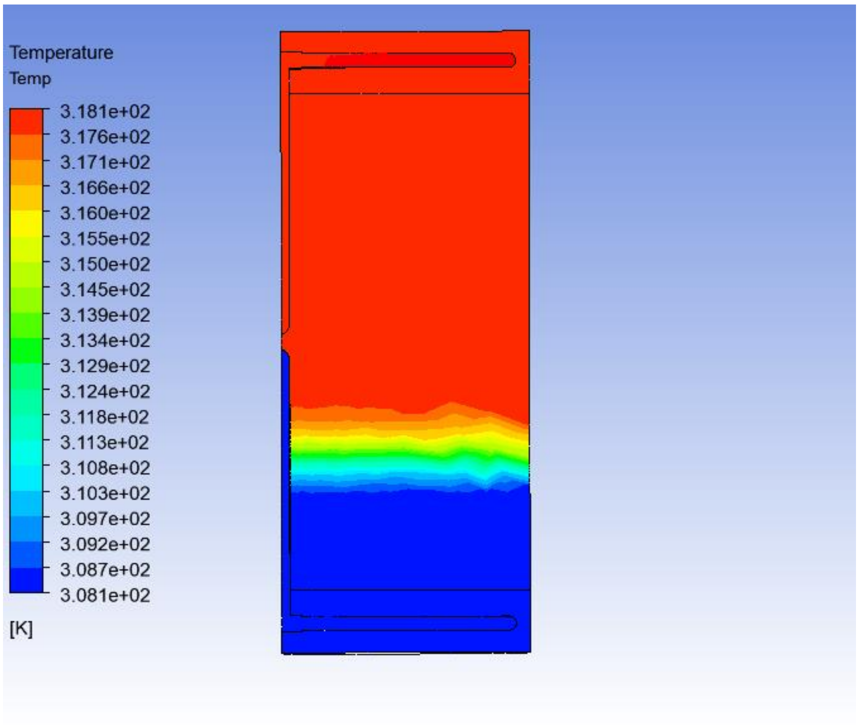

Figure 4.11: 8th Hour Temperature Profile of the Charging Cycle Simulation For Configuration B

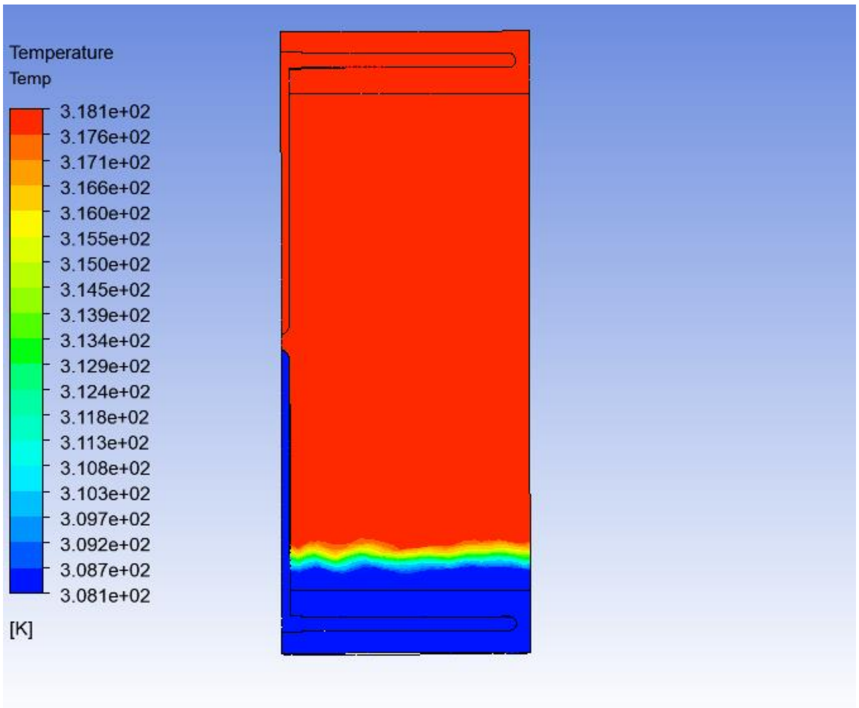

Figure 4.12: 10th Hour Temperature Profile of the Charging Cycle Simulation For Configuration B

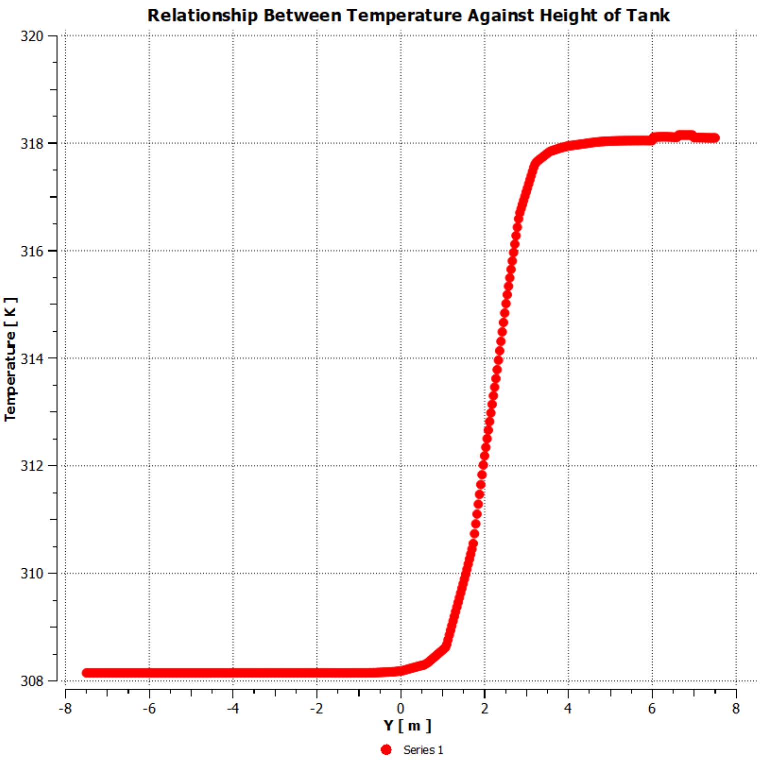

Figure 4.13: 4th Hour Temperature Distribution Plot of the Charging Cycle Simulation For Configuration B

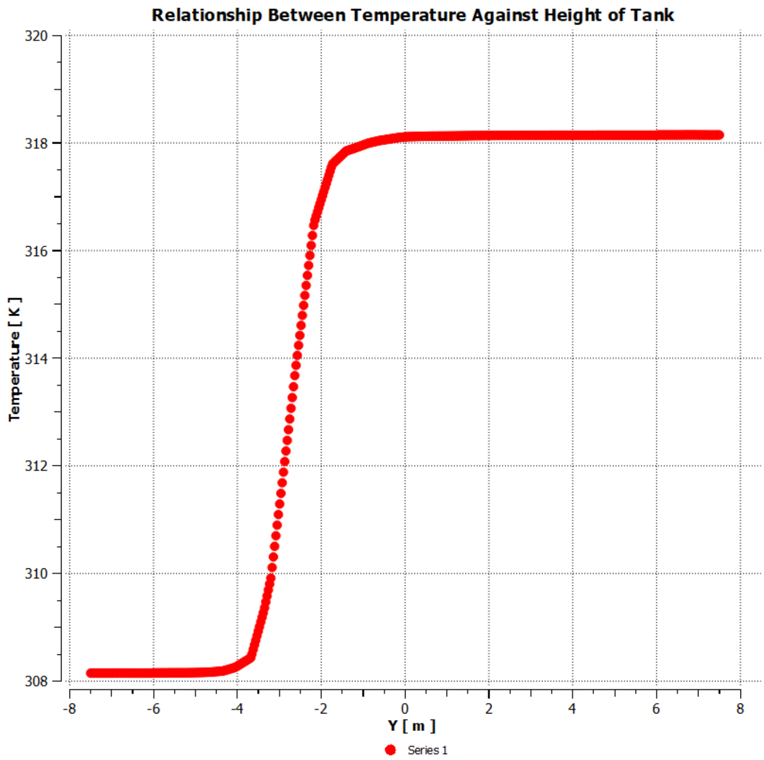

Figure 4.14: 8th Hour Temperature Distribution Plot of the Charging Cycle Simulation For Configuration B

Table 4.3: Position of Performance Indicators at 4th Hour of Charging Cycle for Configuration B

Performance Indicator, θ	Height of Tank, X (m)	Temperature, Y (K)	Thermocline Layer (m)
0.1	1.260	309.15	**1.727**
0.9	2.987	317.15	

Table 4.4: Position of Performance Indicators at 8th Hour of Charging Cycle for Configuration B

Performance Indicator, θ	Height of Tank, X (m)	Temperature, Y (K)	Thermocline Layer (m)
0.1	-3.382	309.15	**1.383**
0.9	-1.999	317.15	

4.2.3 CFD Results For Configuration C

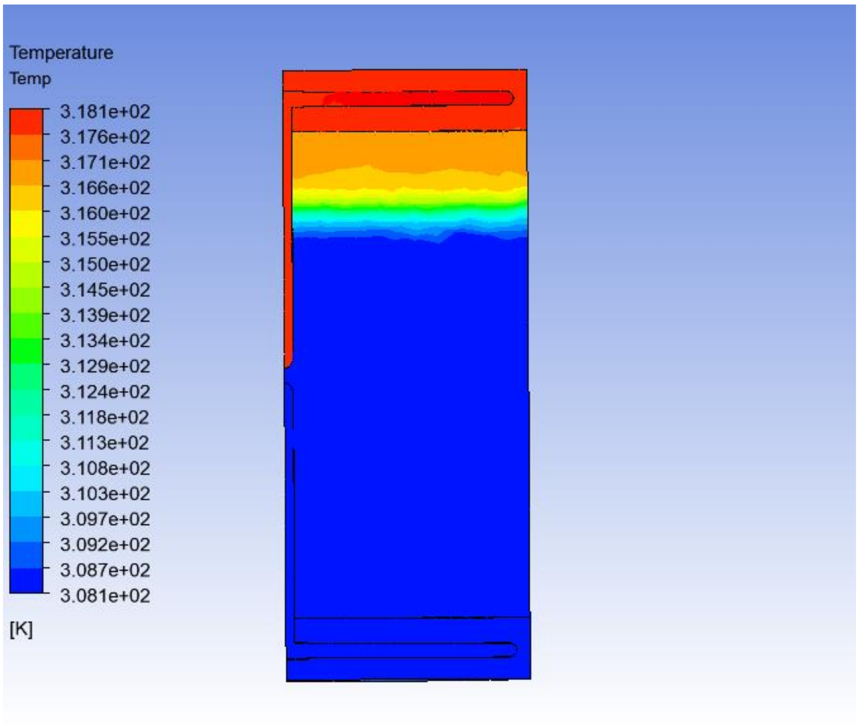

Figure 4.15: 2nd Hour Temperature Profile of the Charging Cycle Simulation For Configuration C

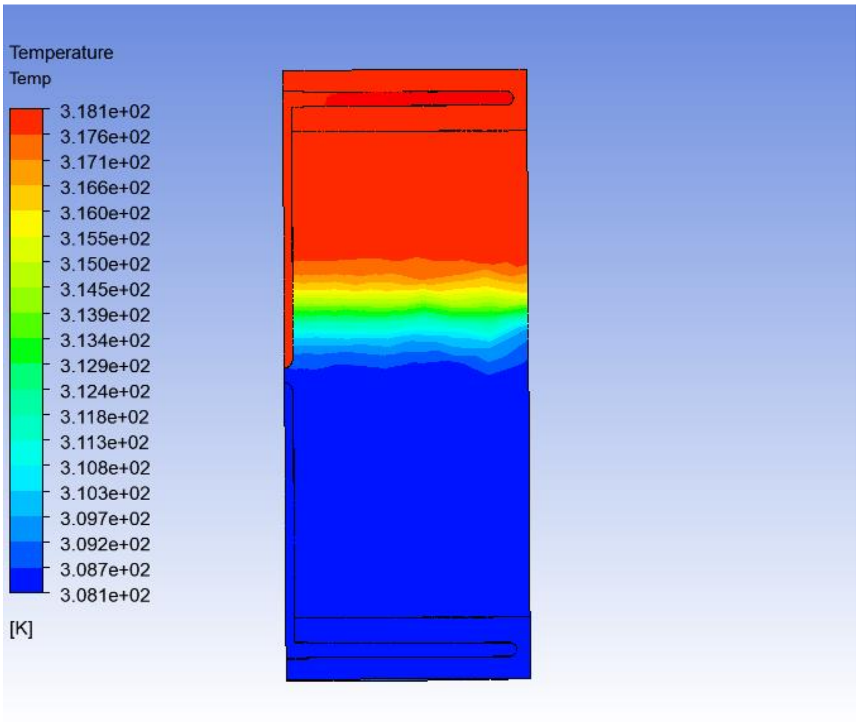

Figure 4.16: 4th Hour Temperature Profile of the Charging Cycle Simulation For Configuration C

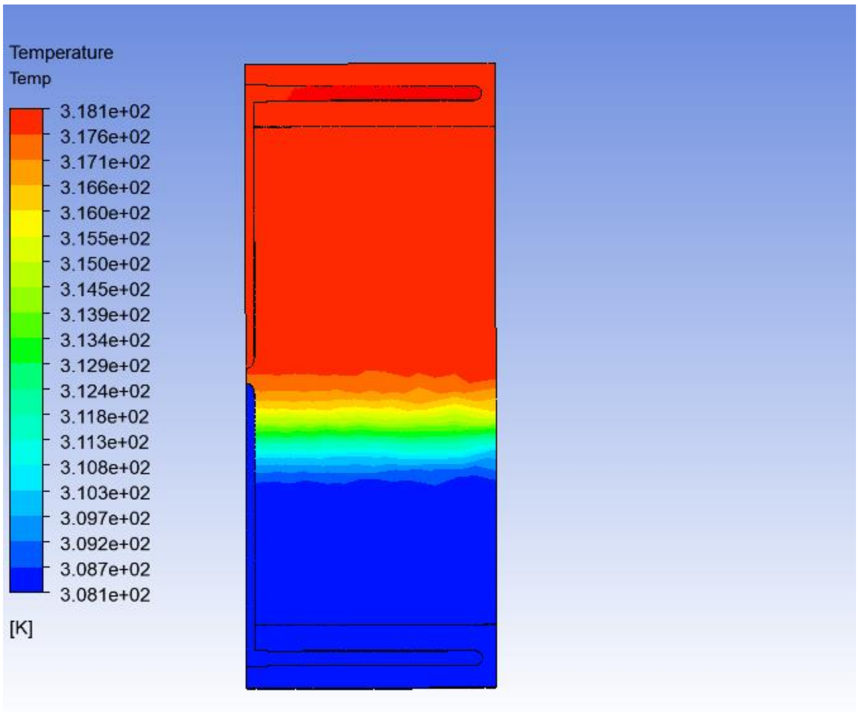

Figure 4.17: 6th Hour Temperature Profile of the Charging Cycle Simulation For Configuration C

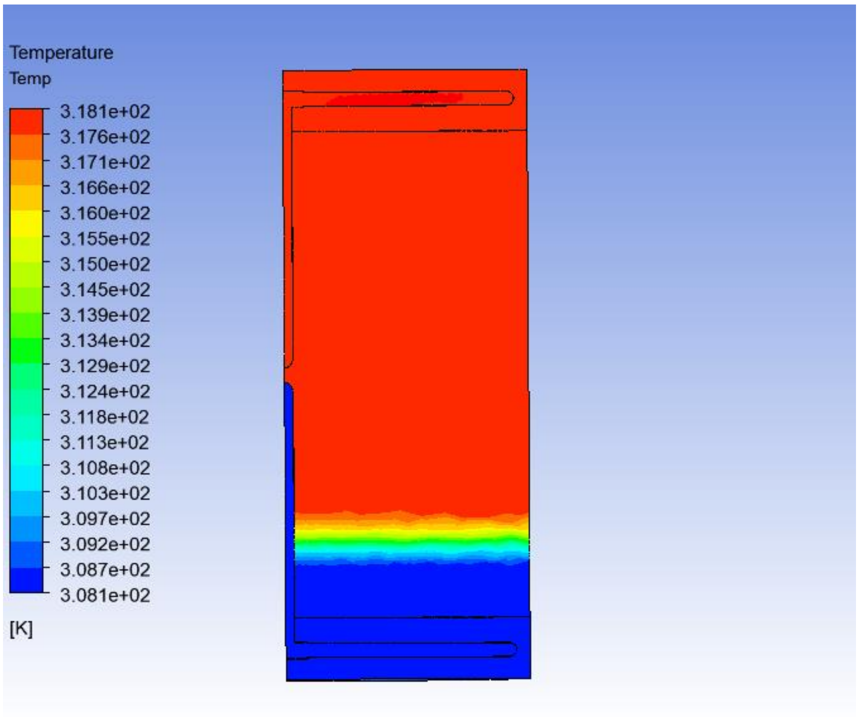

Figure 4.18: 8th Hour Temperature Profile of the Charging Cycle Simulation For Configuration C

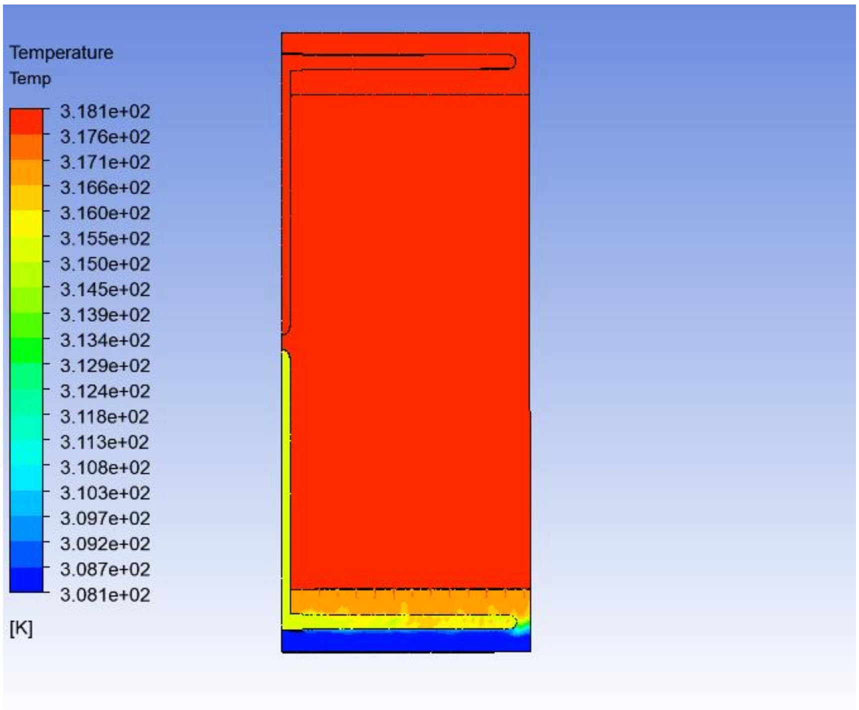

Figure 4.19: 10th Hour Temperature Profile of the Charging Cycle Simulation For Configuration C

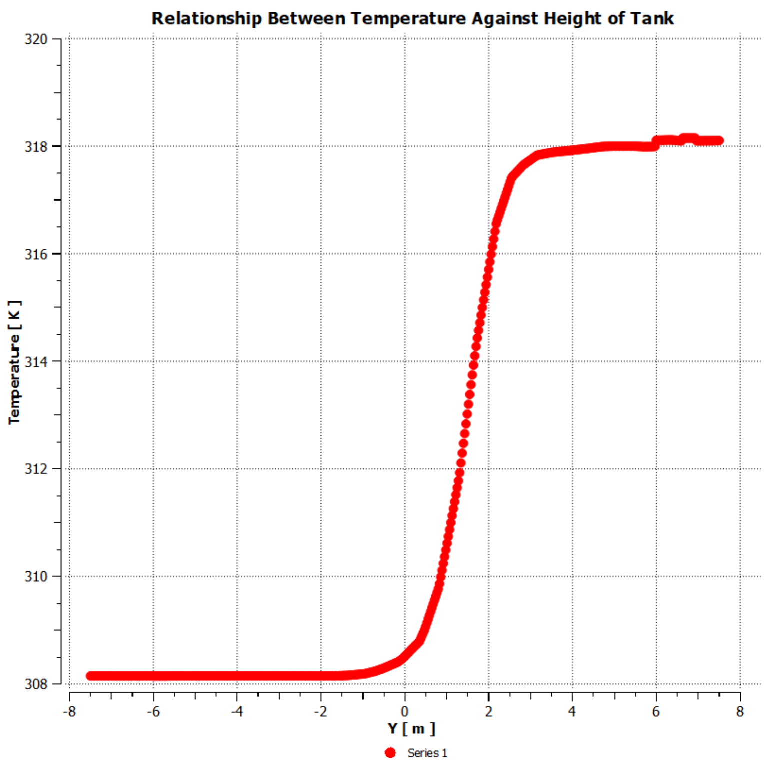

Figure 4.20: 4th Hour Temperature Distribution Plot of the Charging Cycle Simulation For Configuration C

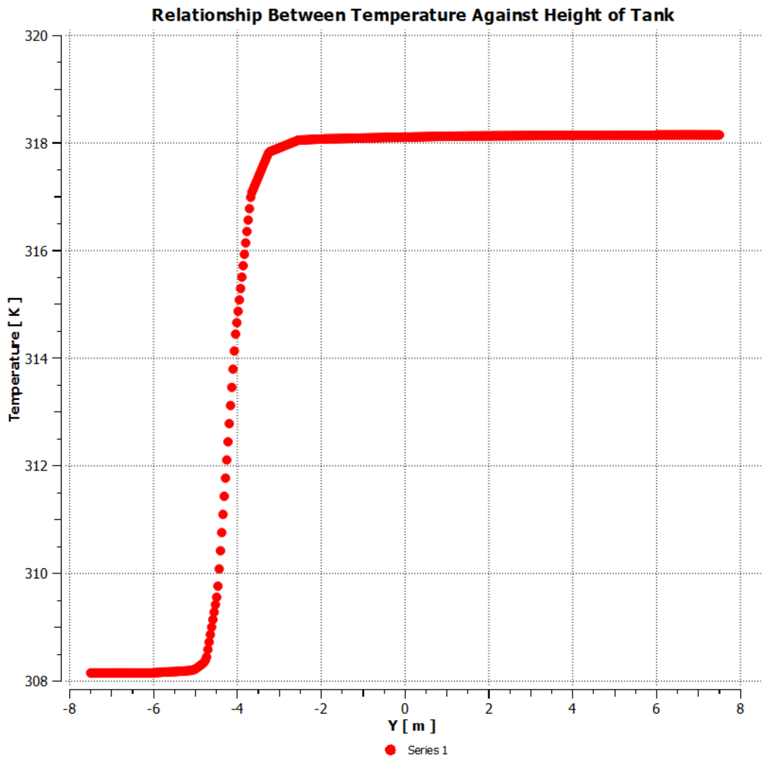

Figure 4.21: 8th Hour Temperature Distribution Plot of the Charging Cycle Simulation For Configuration C

Table 4.5: Position of Performance Indicators at 4th Hour of Charging Cycle for Configuration C

Performance Indicator, θ	Height of Tank, X (m)	Temperature, Y (K)	Thermocline Layer (m)
0.1	0.539	309.15	**1.873**
0.9	2.412	317.15	

Table 4.6: Position of Performance Indicators at 8th Hour of Charging Cycle for Configuration C

Performance Indicator, θ	Height of Tank, X (m)	Temperature, Y (K)	Thermocline Layer (m)
0.1	-4.584	309.15	**0.992**
0.9	-3.592	317.15	

4.3 Discharging Cycle CFD Results

4.3.1 CFD Results For Configuration A

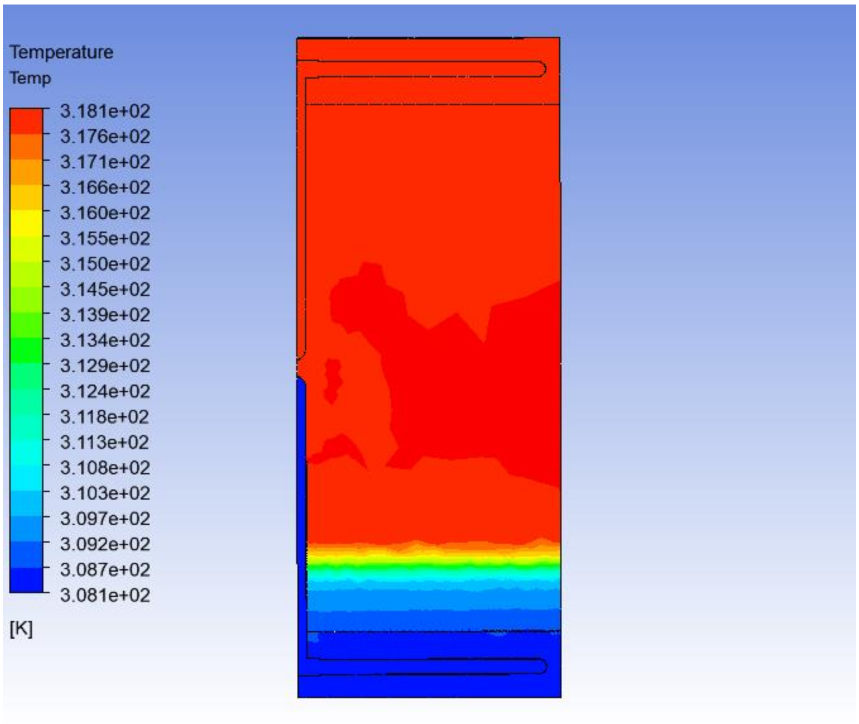

Figure 4.22: 2nd Hour Temperature Profile of the Discharging Cycle Simulation For Configuration A

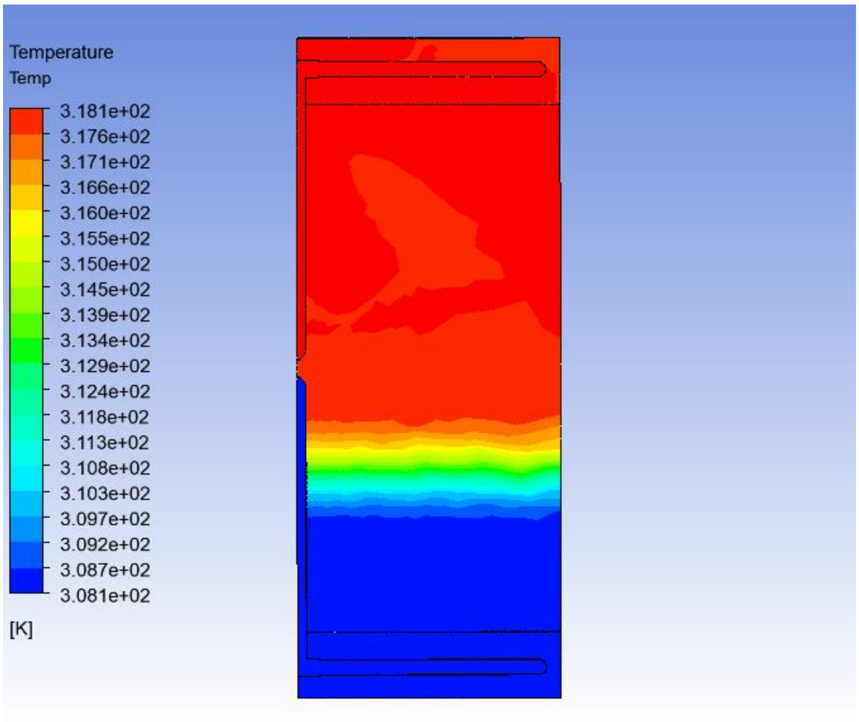

Figure 4.23: 4th Hour Temperature Profile of the Discharging Cycle Simulation For Configuration A

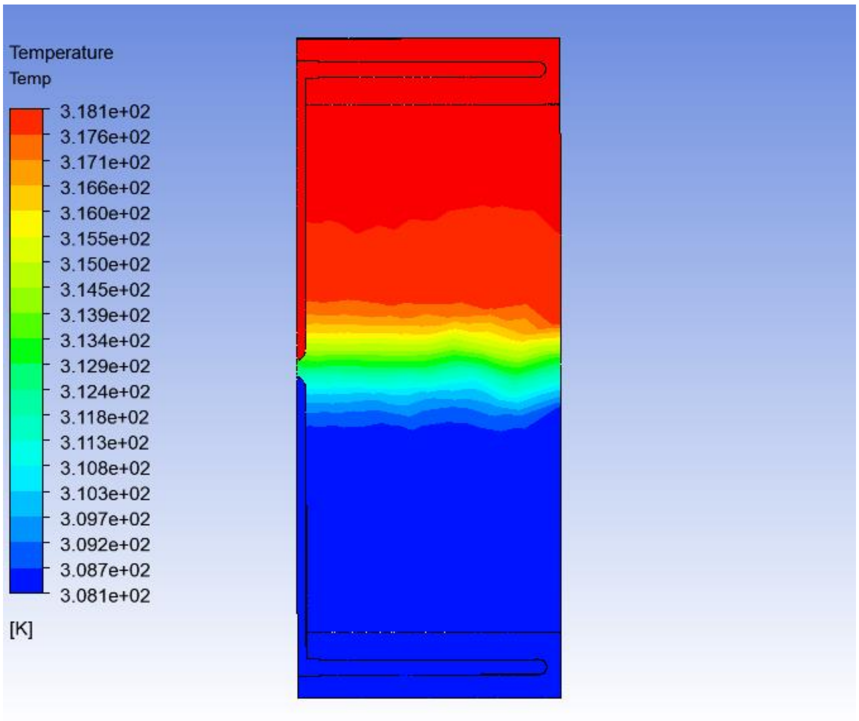

Figure 4.24: 6th Hour Temperature Profile of the Discharging Cycle Simulation For Configuration A

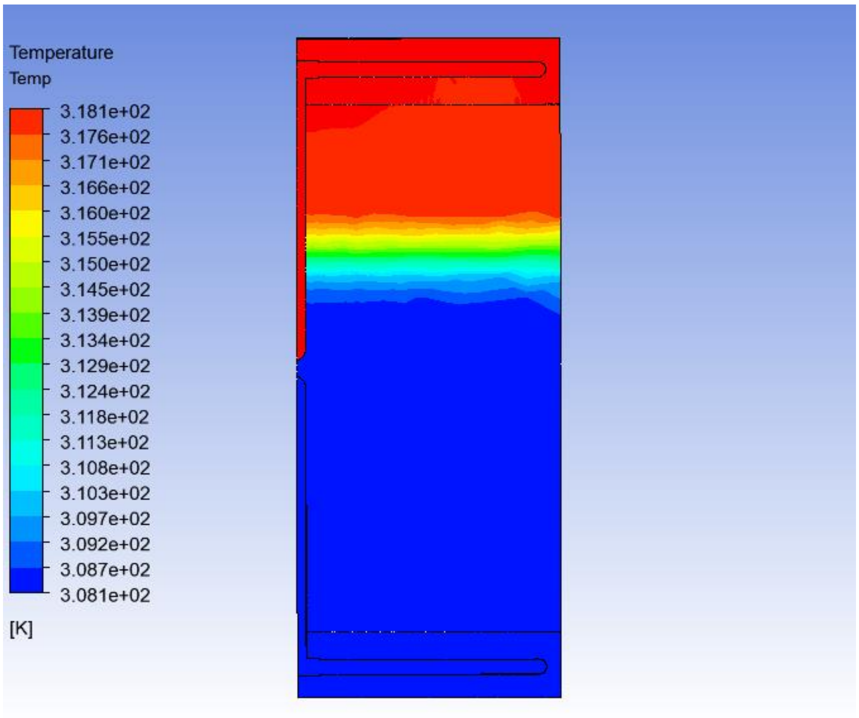

Figure 4.25: 8th Hour Temperature Profile of the Discharging Cycle Simulation For Configuration A

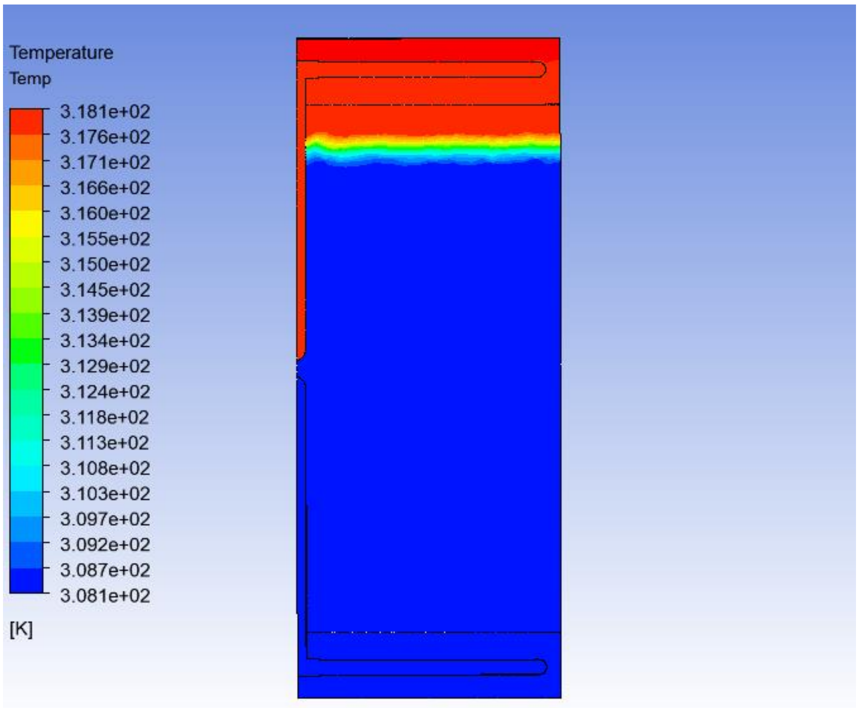

Figure 4.26: 10th Hour Temperature Profile of the Discharging Cycle Simulation For Configuration A

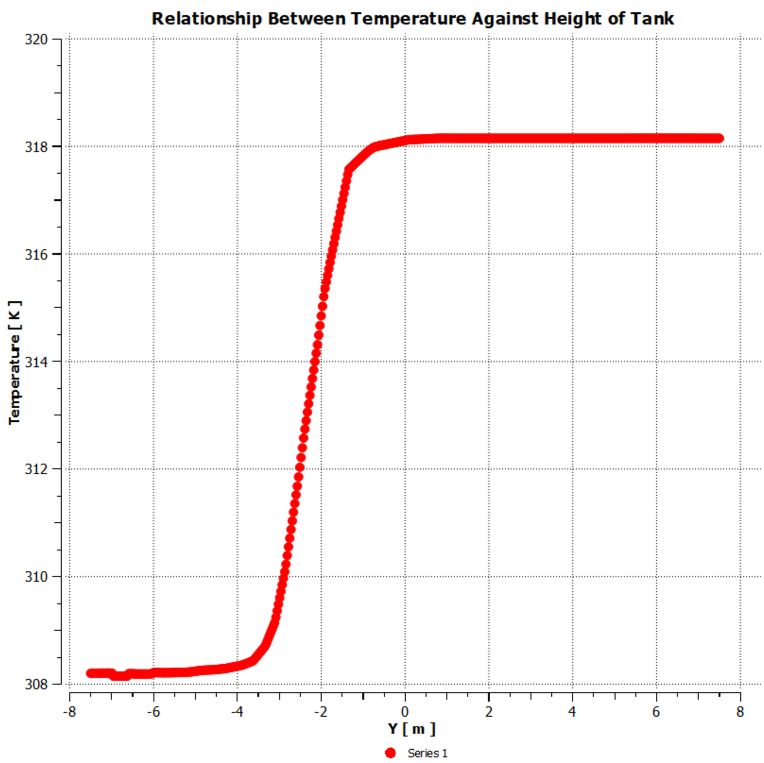

Figure 4.27: 4th Hour Temperature Distribution Plot of the Discharging Cycle Simulation For Configuration A

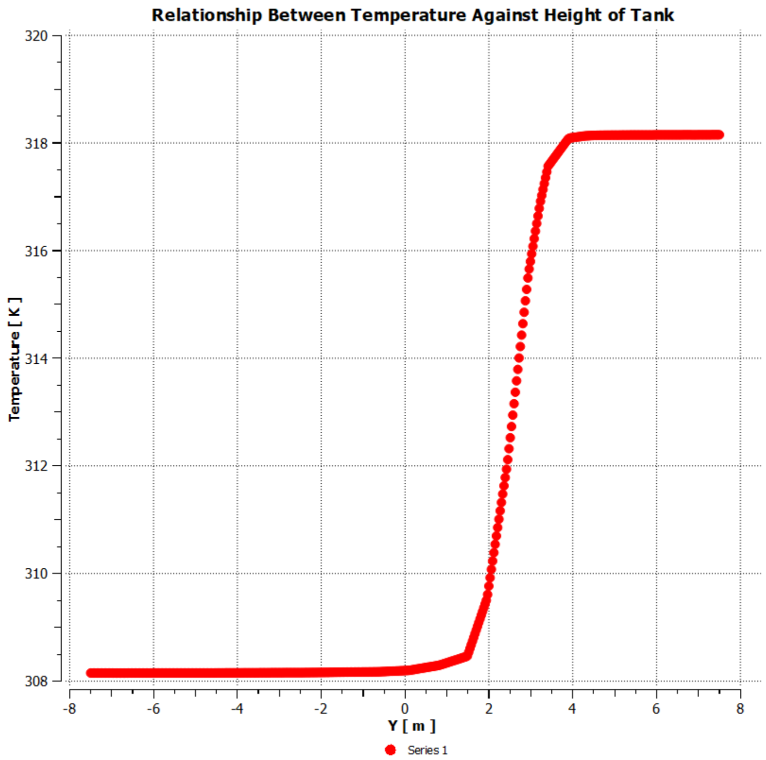

Figure 4.28: 8th Hour Temperature Distribution Plot of the Discharging Cycle Simulation For Configuration A

Table 4.7: Position of Performance Indicators at 4th Hour of Discharging Cycle for Configuration A

Performance Indicator, θ	Height of Tank, X (m)	Temperature, Y (K)	Thermocline Layer (m)
0.1	-3.083	309.15	**1.628**
0.9	-1.455	317.15	

Table 4.8: Position of Performance Indicators at 8th Hour of Discharging Cycle for Configuration A

Performance Indicator, θ	Height of Tank, X (m)	Temperature, Y (K)	Thermocline Layer (m)
0.1	1.864	309.15	**1.352**
0.9	3.216	317.15	

4.3.2 CFD Results For Configuration B

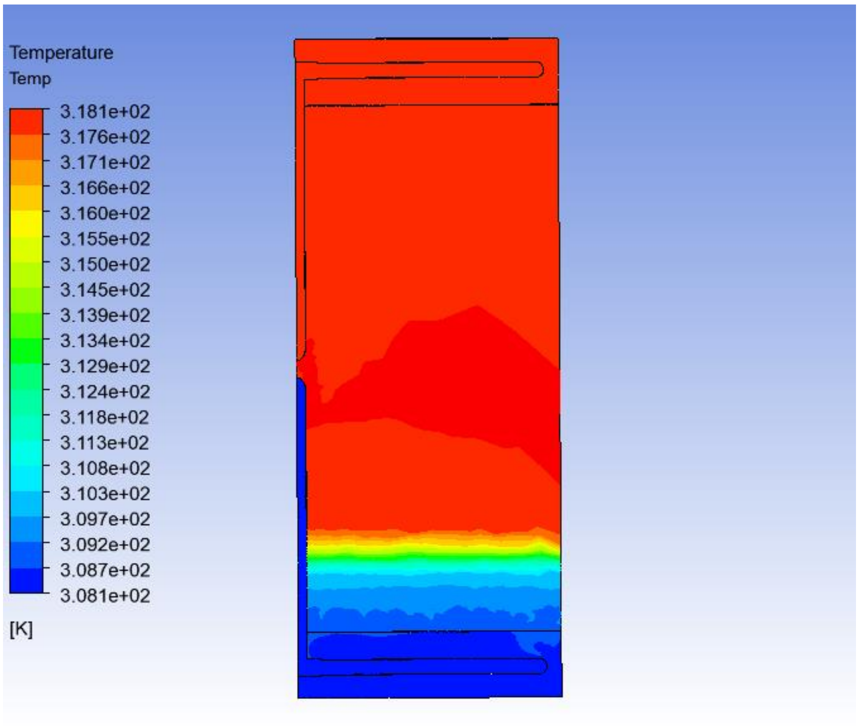

Figure 4.29: 2nd Hour Temperature Profile of the Discharging Cycle Simulation For Configuration B

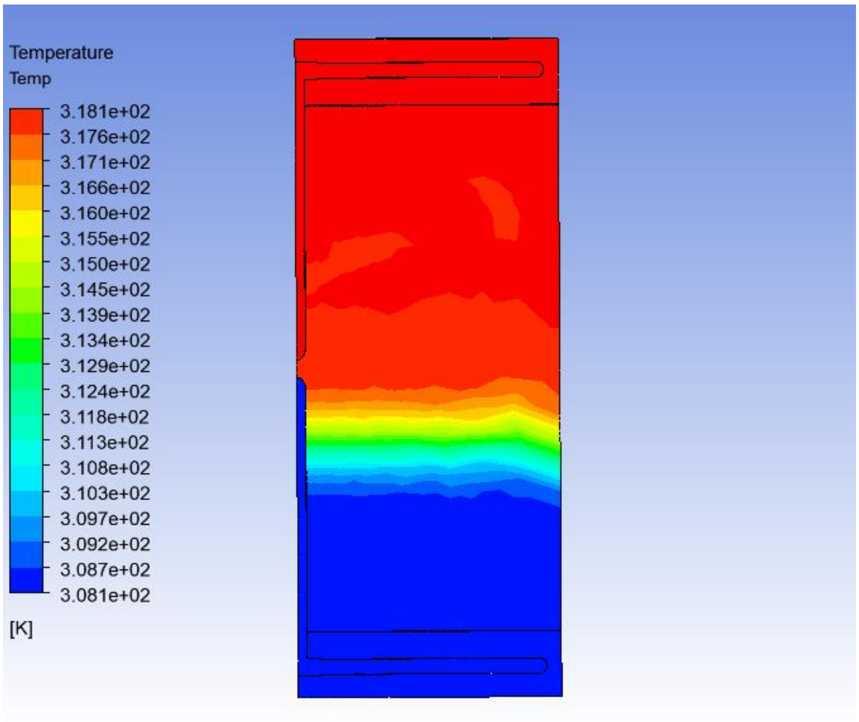

Figure 4.30: 4th Hour Temperature Profile of the Discharging Cycle Simulation For Configuration B

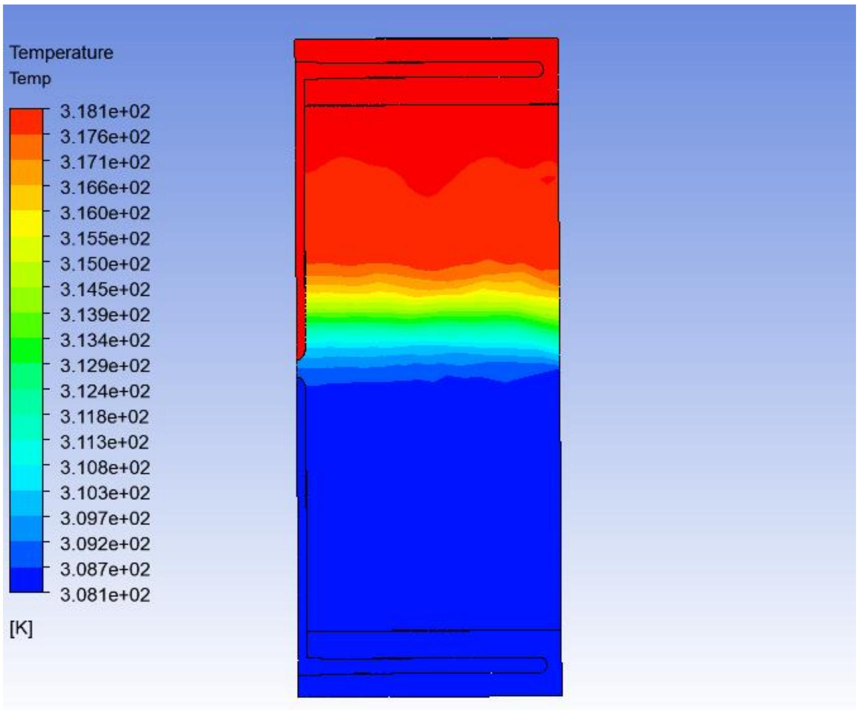

Figure 4.31: 6^{th} Hour Temperature Profile of the Discharging Cycle Simulation For Configuration B

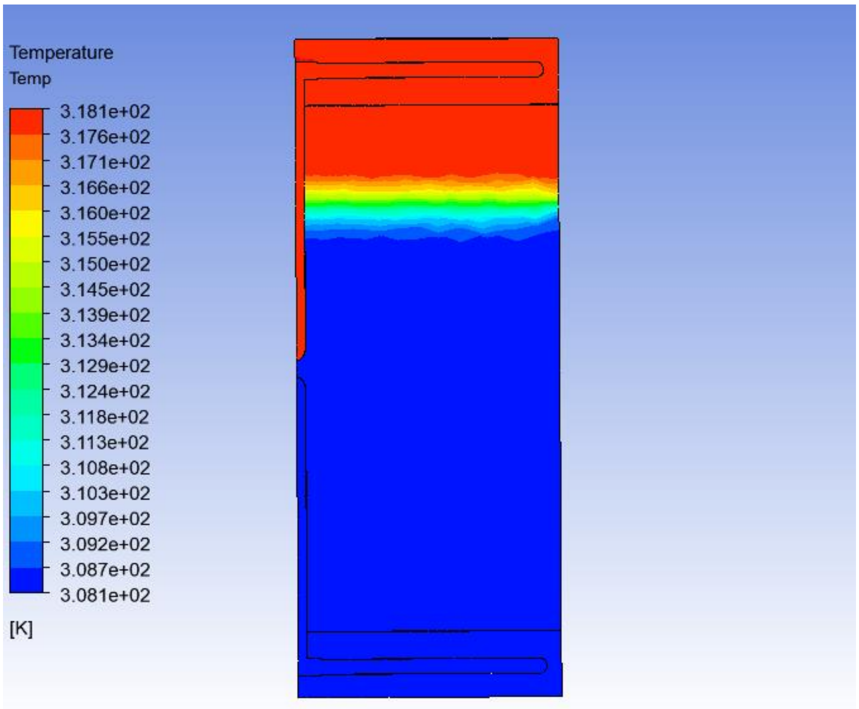

Figure 4.32: 8^{th} Hour Temperature Profile of the Discharging Cycle Simulation For Configuration B

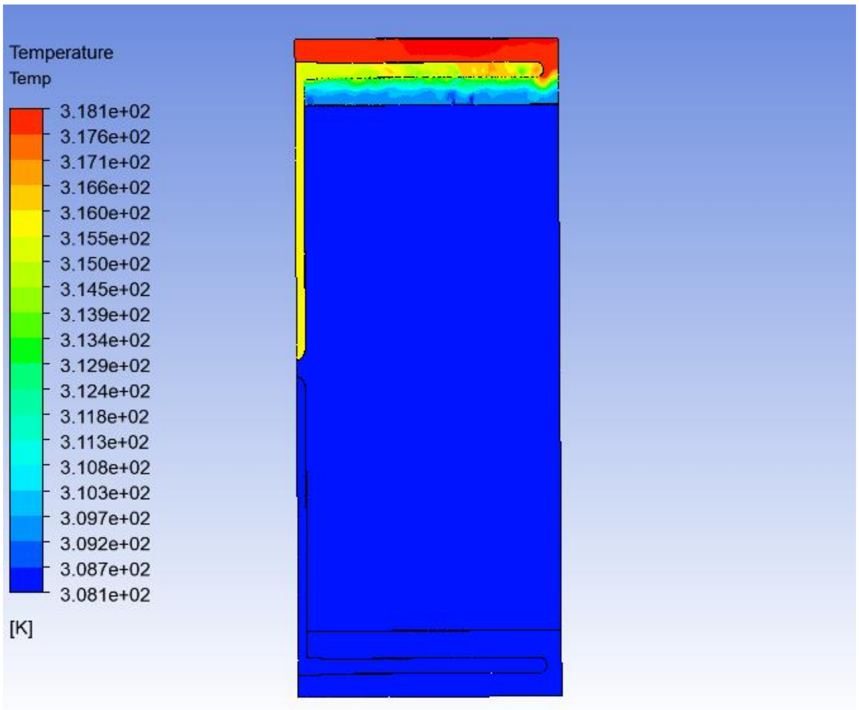

Figure 4.33: 10th Hour Temperature Profile of the Discharging Cycle Simulation For Configuration B

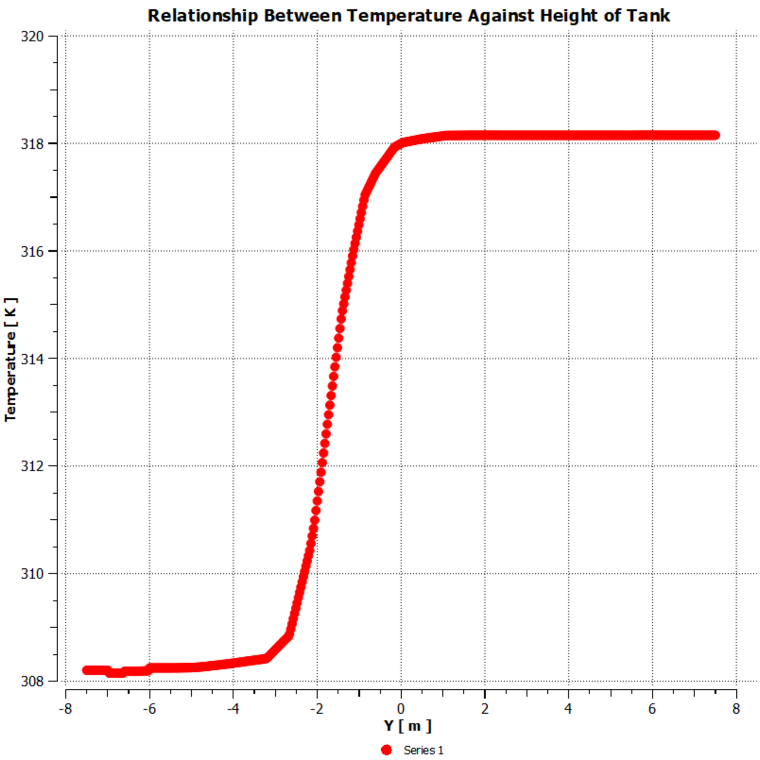

Figure 4.34: 4th Hour Temperature Distribution Plot of the Discharging Cycle Simulation For Configuration B

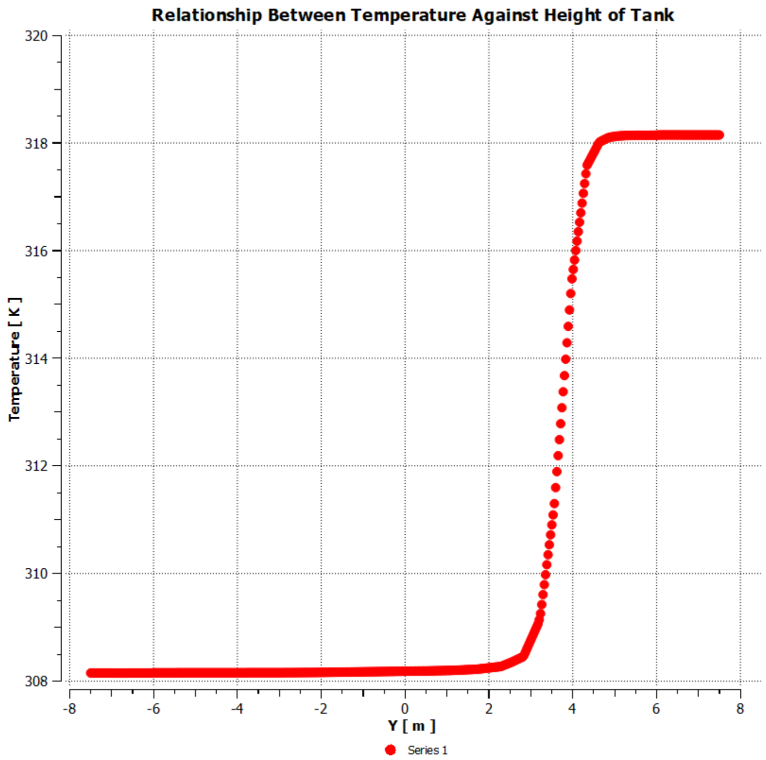

Figure 4.35: 8th Hour Temperature Distribution Plot of the Discharging Cycle Simulation For Configuration B

Table 4.9: Position of Performance Indicators at 4th Hour of Discharging Cycle for Configuration B

Performance Indicator, θ	Height of Tank, X (m)	Temperature, Y (K)	Thermocline Layer (m)
0.1	-2.554	309.15	**1.770**
0.9	-0.784	317.15	

Table 4.10: Position of Performance Indicators at 8th Hour of Discharging Cycle for Configuration B

Performance Indicator, θ	Height of Tank, X (m)	Temperature, Y (K)	Thermocline Layer (m)
0.1	3.216	309.15	**1.053**
0.9	4.269	317.15	

4.3.3 CFD Results For Configuration C

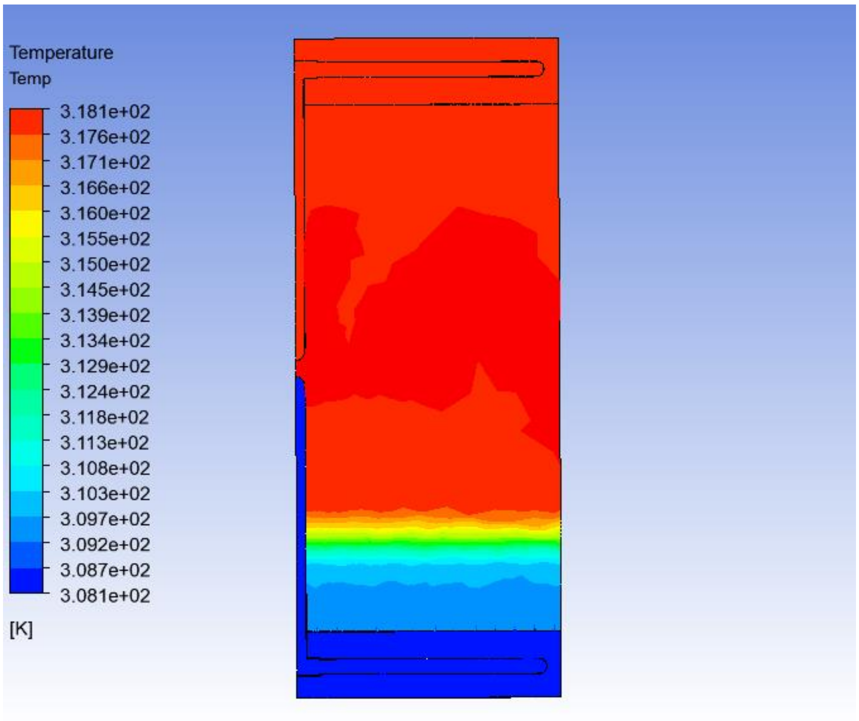

Figure 4.36: 2nd Hour Temperature Profile of the Discharging Cycle Simulation For Configuration C

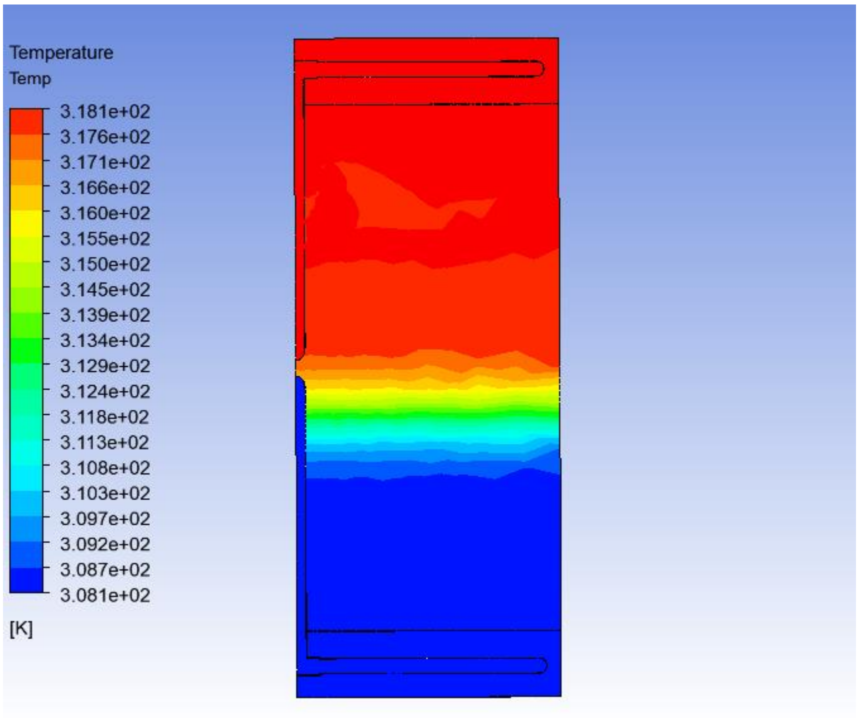

Figure 4.37: 4th Hour Temperature Profile of the Discharging Cycle Simulation For Configuration C

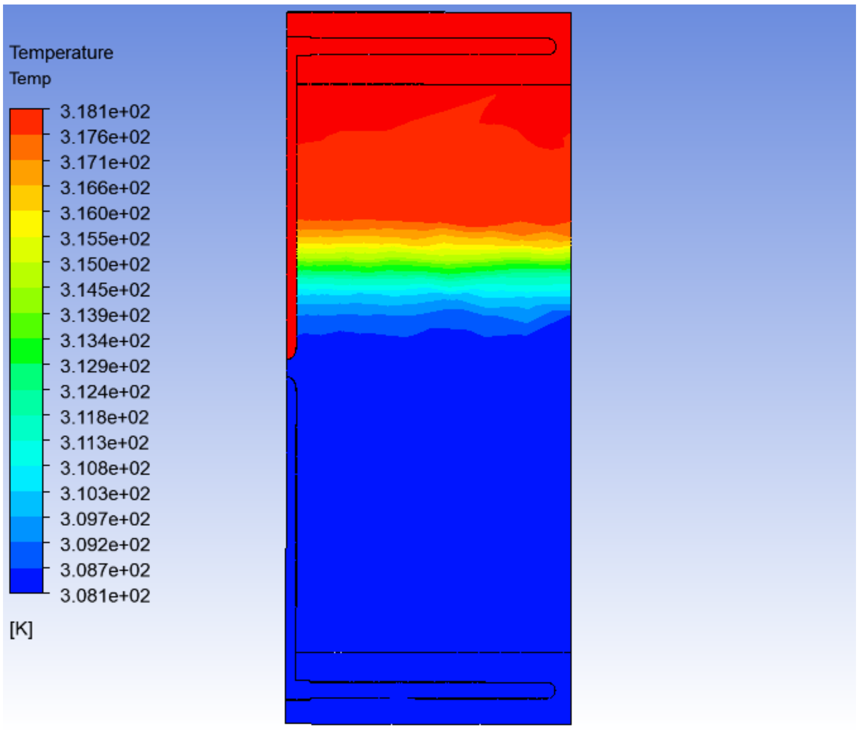

Figure 4.38: 6th Hour Temperature Profile of the Discharging Cycle Simulation For Configuration C

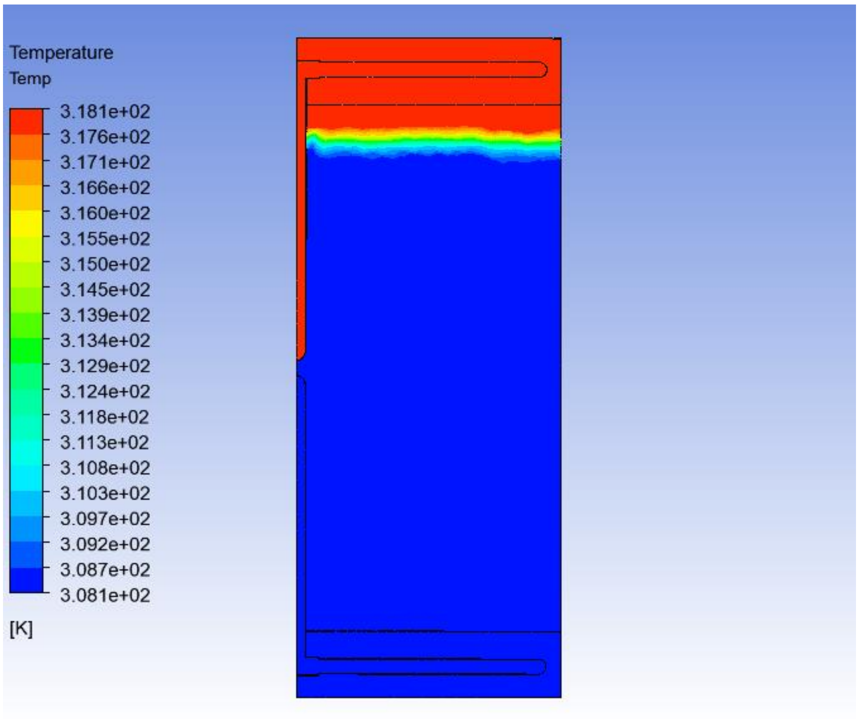

Figure 4.39: 8th Hour Temperature Profile of the Discharging Cycle Simulation For Configuration C

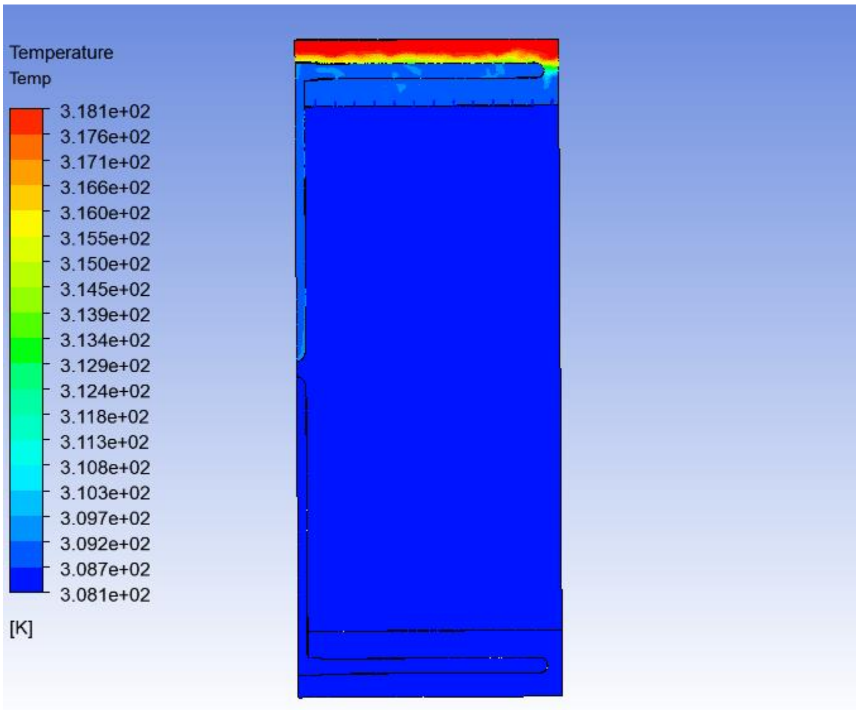

Figure 4.40: 10th Hour Temperature Profile of the Discharging Cycle Simulation For Configuration C

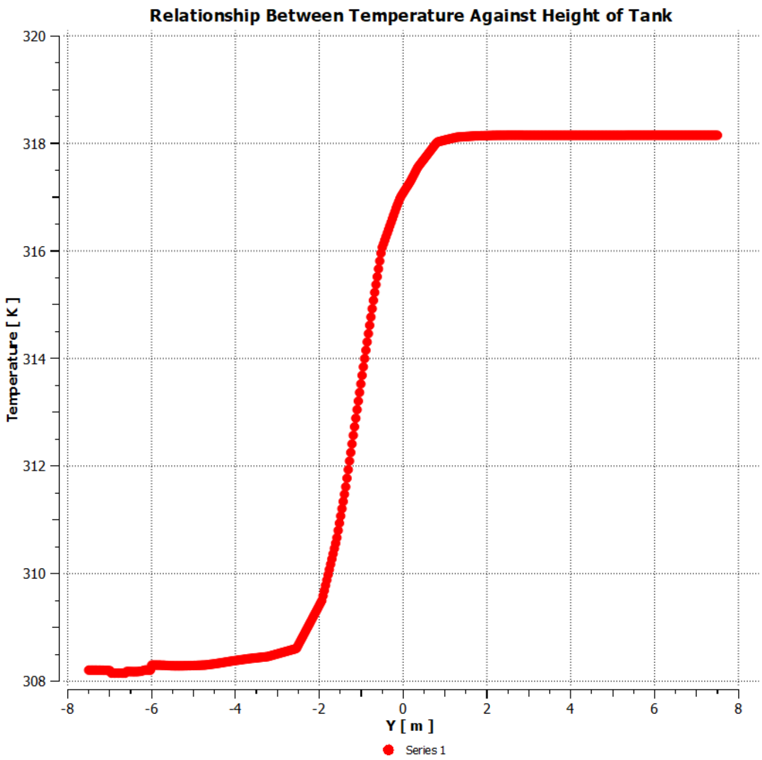

Figure 4.41: 4th Hour Temperature Distribution Plot of the Discharging Cycle Simulation For Configuration C

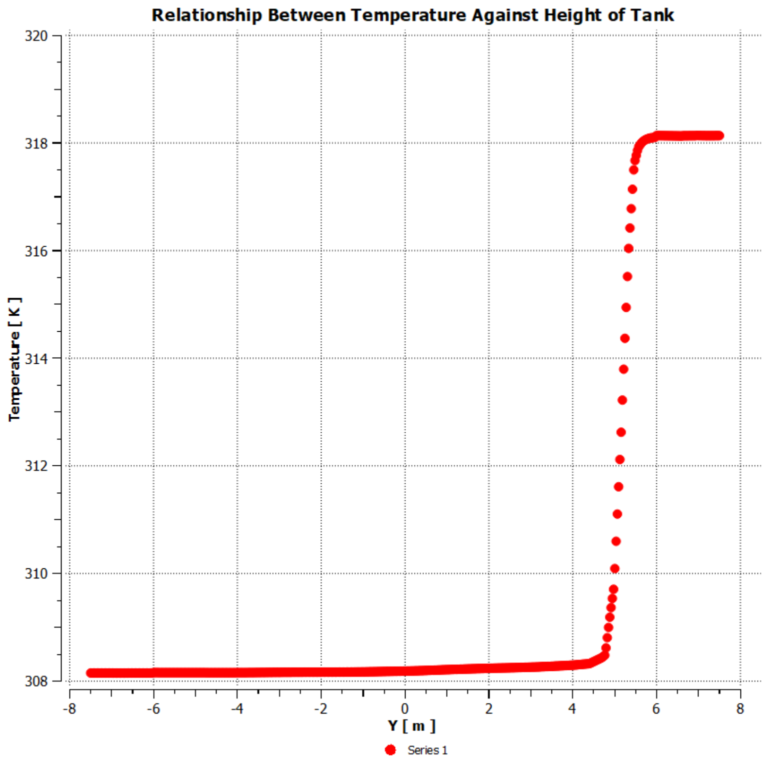

Figure 4.42: 8th Hour Temperature Distribution Plot of the Discharging Cycle Simulation For Configuration C

Table 4.11: Position of Performance Indicators at 4th Hour of Discharging Cycle for Configuration C

Performance Indicator, θ	**Height of Tank, X (m)**	**Temperature, Y (K)**	**Thermocline Layer (m)**
0.1	-2.154	309.15	**2.195**
0.9	0.041	317.15	

Table 4.12: Position of Performance Indicators at 8th Hour of Discharging Cycle for Configuration C

Performance Indicator, θ	**Height of Tank, X (m)**	**Temperature, Y (K)**	**Thermocline Layer (m)**
0.1	4.877	309.15	**0.549**
0.9	5.426	317.15	

4.4 Results For Prototype Testing

4.4.1 CFD Results For Configuration A

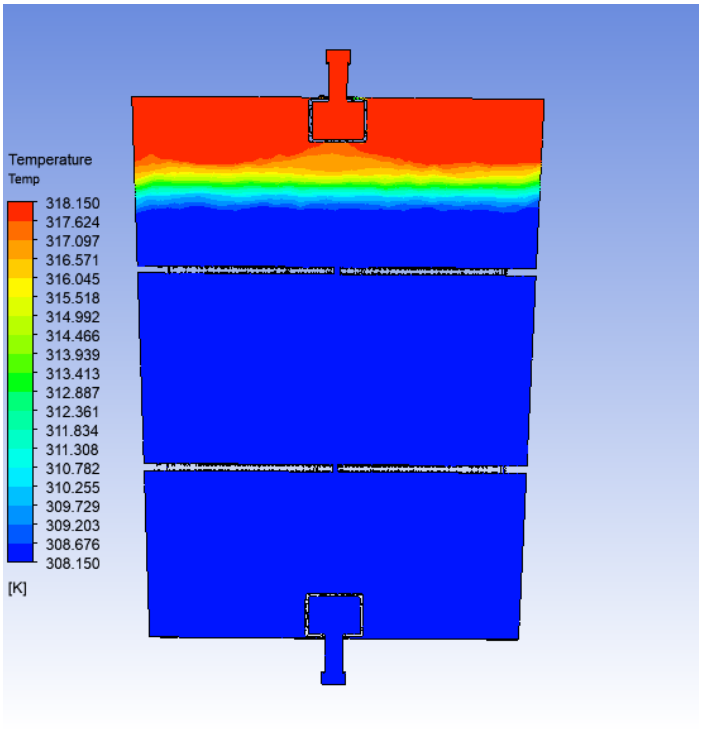

Figure 4.43: 2nd Minute Temperature Profile of the Charging Cycle Simulation For Configuration A

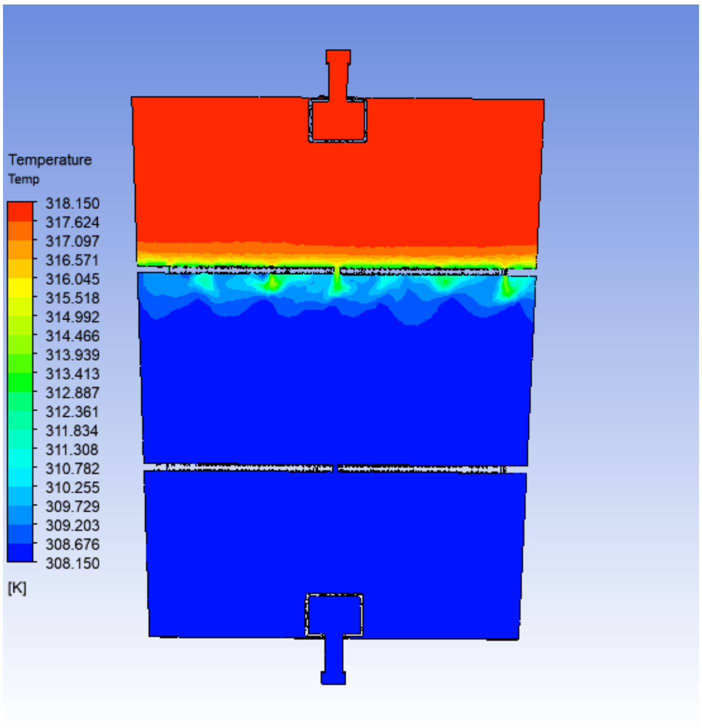

Figure 4.44: 4th Minute Temperature Profile of the Charging Cycle Simulation For Configuration A

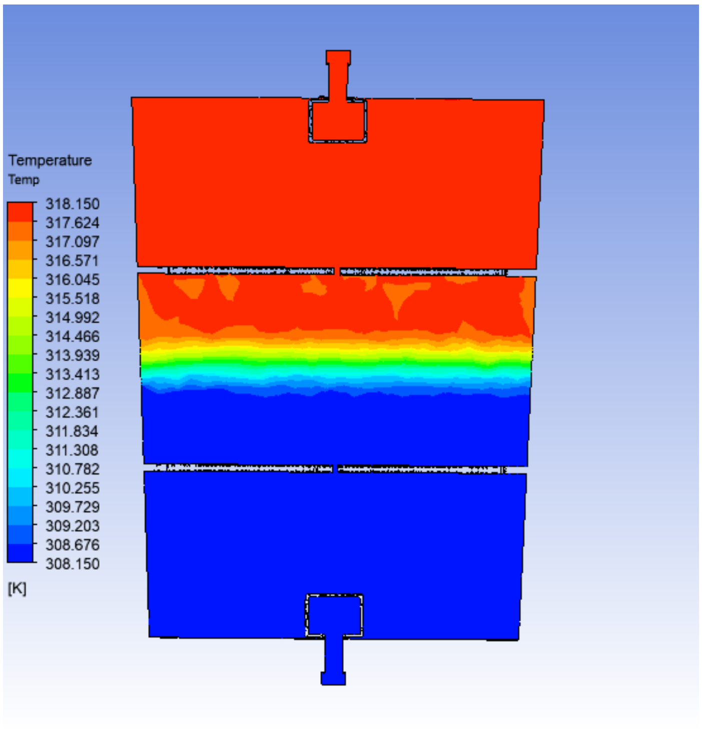

Figure 4.45: 6th Minute Temperature Profile of the Charging Cycle Simulation For Configuration A

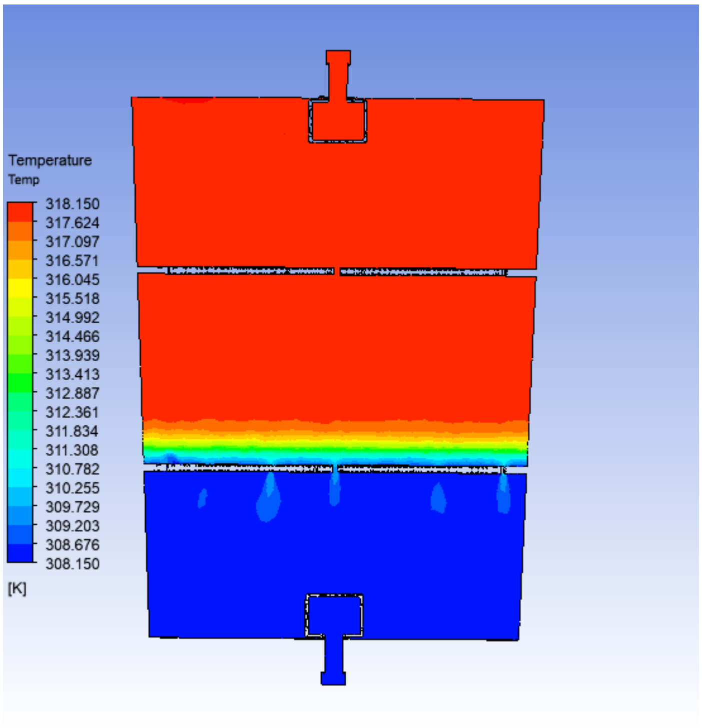

Figure 4.46: 8th Minute Temperature Profile of the Charging Cycle Simulation For Configuration A

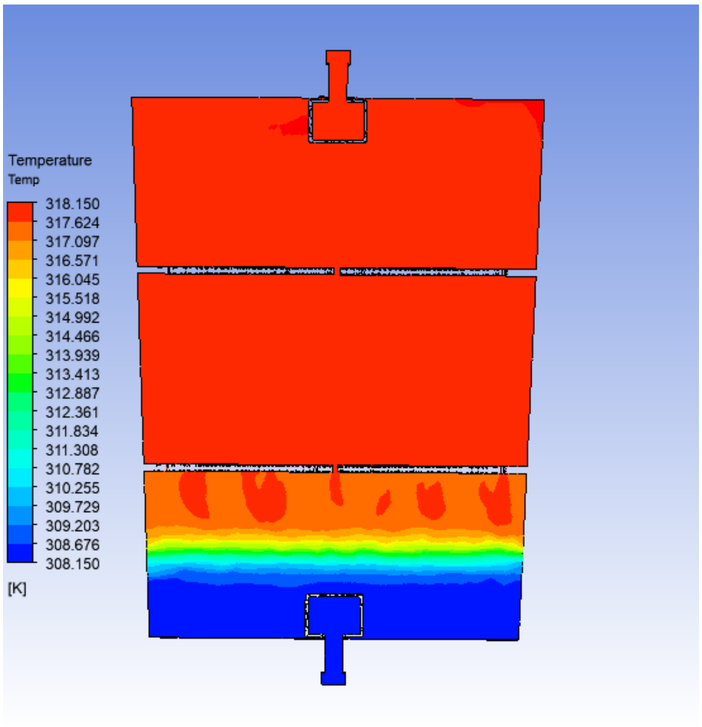

Figure 4.47: 10th Minute Temperature Profile of the Charging Cycle Simulation For Configuration A

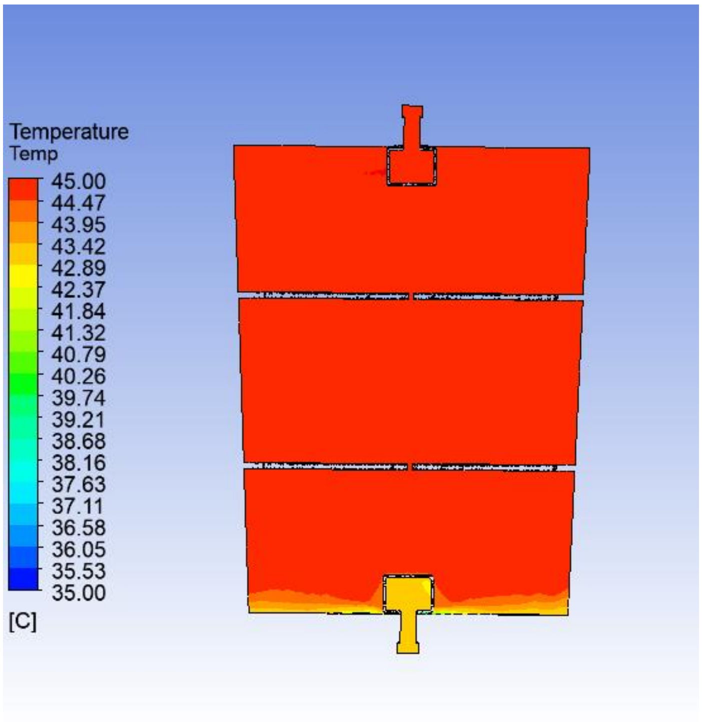

Figure 4.48: 12th Minute Temperature Profile of the Charging Cycle Simulation For Configuration A

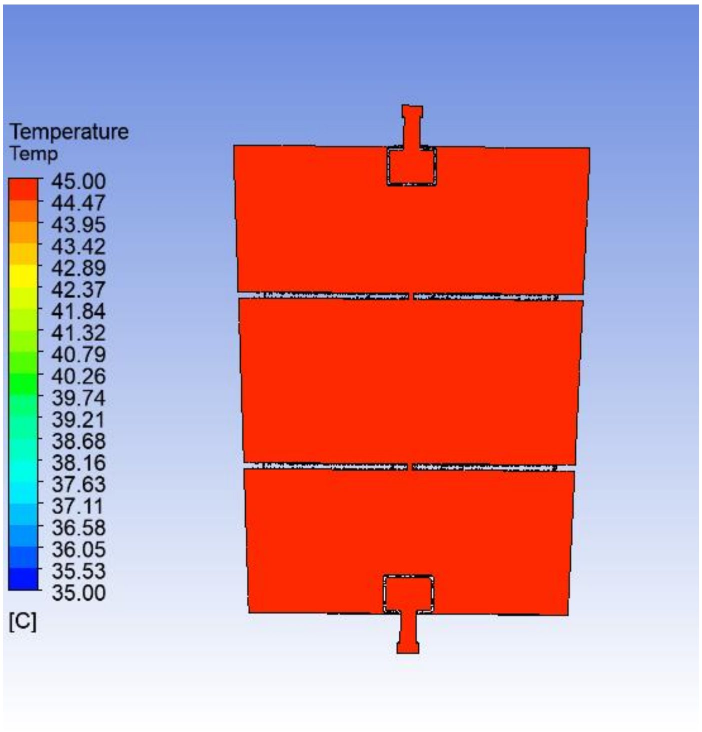

Figure 4.49: 14th Minute Temperature Profile of the Charging Cycle Simulation For Configuration A

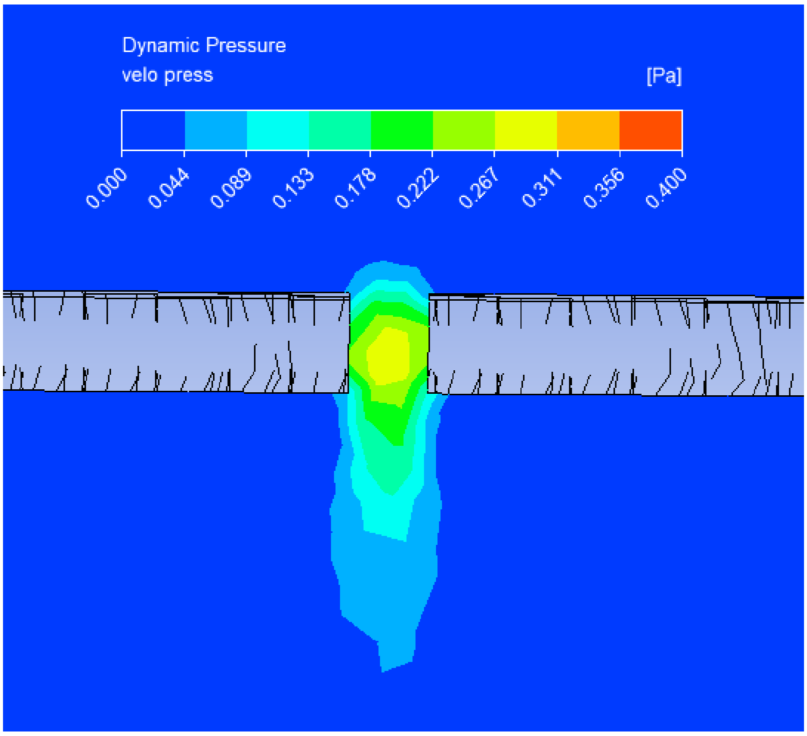

Figure 4.50: Dynamic Pressure Profile of the Charging Cycle Simulation For Configuration A

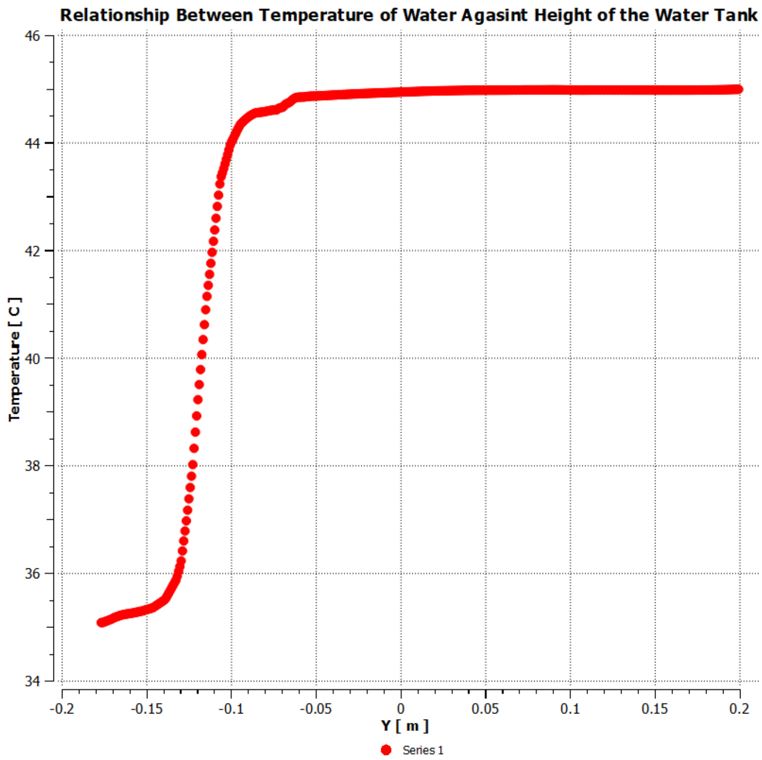

Figure 4.51: 10th Minute Temperature Distribution Plot of the Charging Cycle Simulation for Configuration A

Table 4.13: Position of Performance Indicators at 10th Minute of Charging Cycle CFD Simulation for Configuration A

Performance Indicator, θ	**Height of Tank, X (m)**	**Temperature, Y (K)**	**Thermocline Layer (m)**
0.1	-0.130	309.15	**0.031**
0.9	-0.099	317.15	

4.4.2 Experimental Results For Configuration A

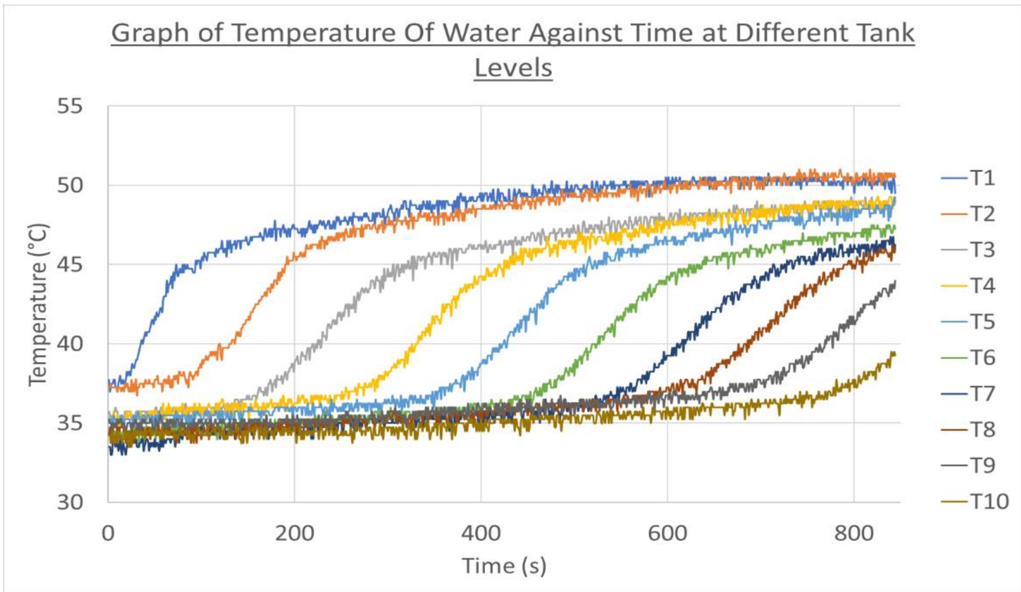

Figure 4.52: Full Charging Cycle Testing Results For Configuration A

4.4.3 CFD Results For Configuration C

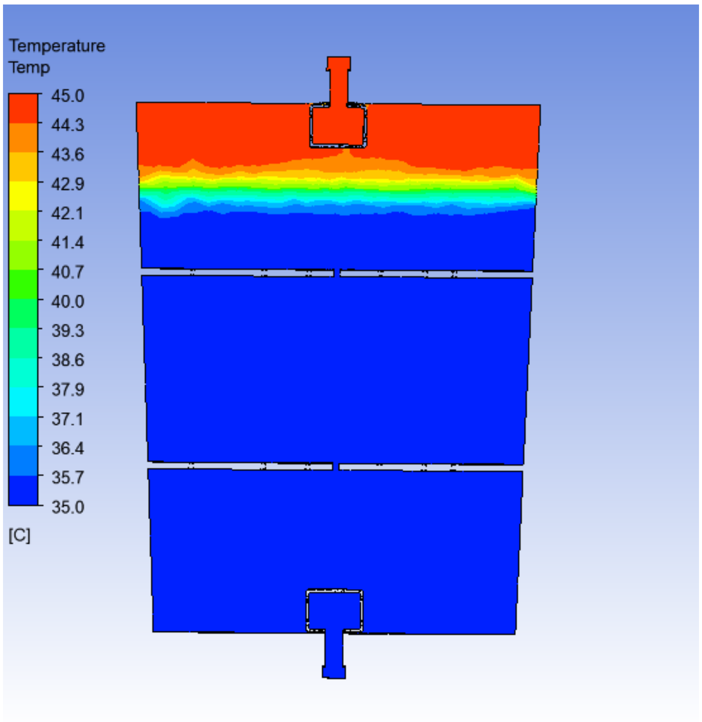

Figure 4.53: 2nd Minute Temperature Profile of the Charging Cycle Simulation For Configuration C

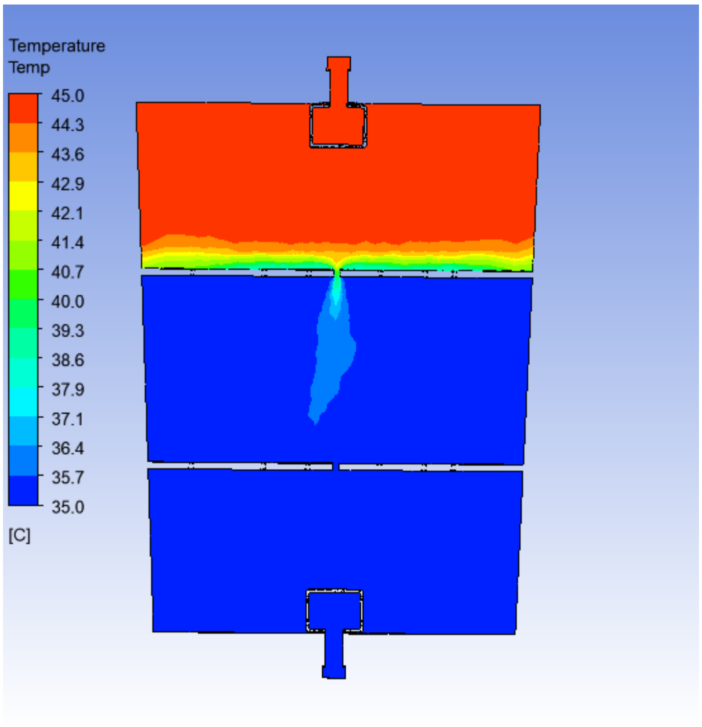

Figure 4.54: 4th Minute Temperature Profile of the Charging Cycle Simulation For Configuration C

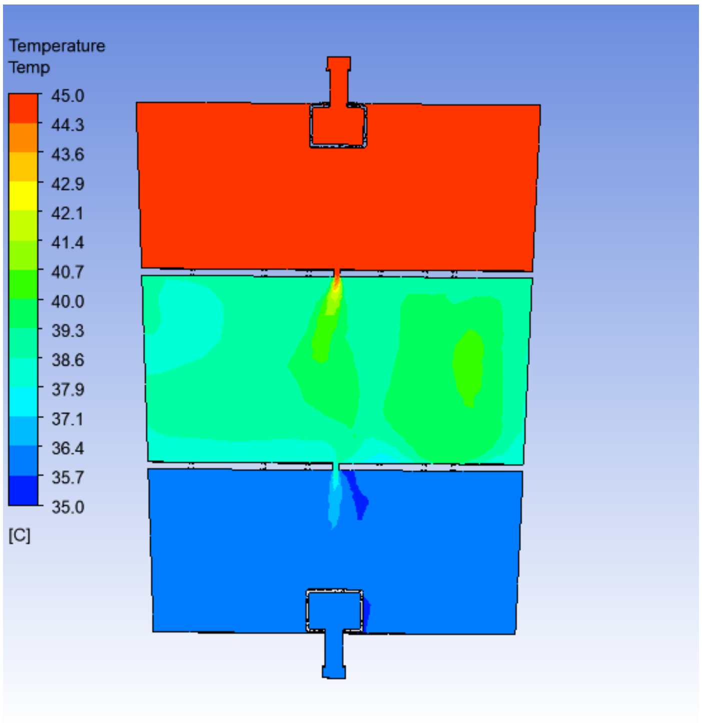

Figure 4.55: 6th Minute Temperature Profile of the Charging Cycle Simulation For Configuration C

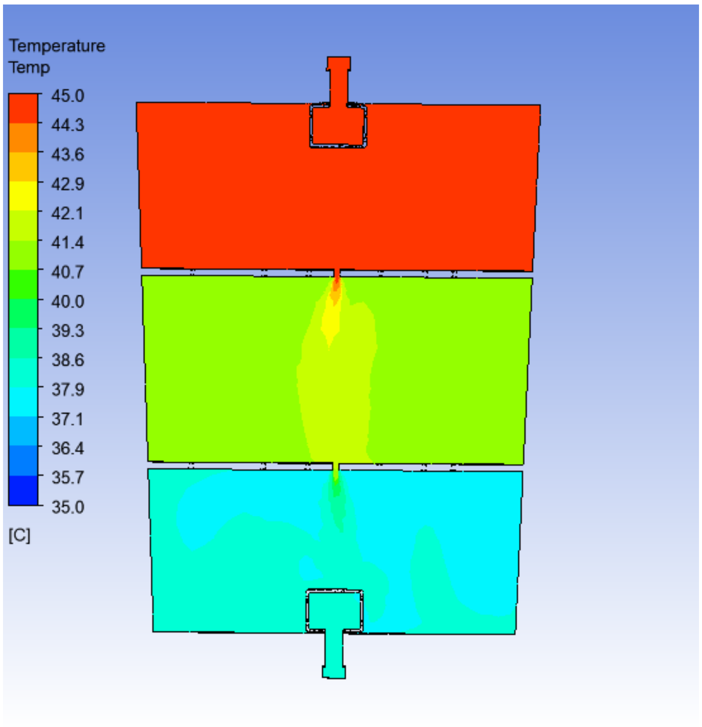

Figure 4.56: 8th Minute Temperature Profile of the Charging Cycle Simulation For Configuration C

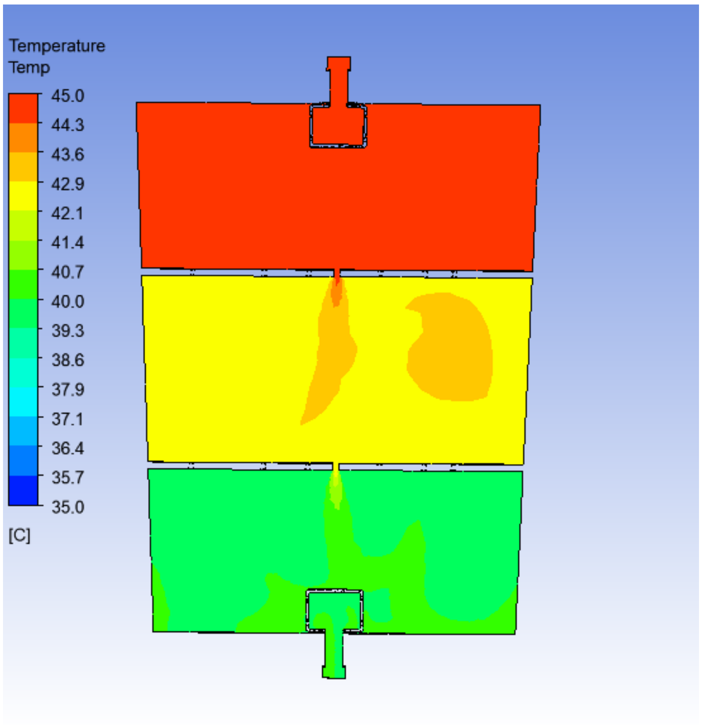

Figure 4.57: 10th Minute Temperature Profile of the Charging Cycle Simulation For Configuration C

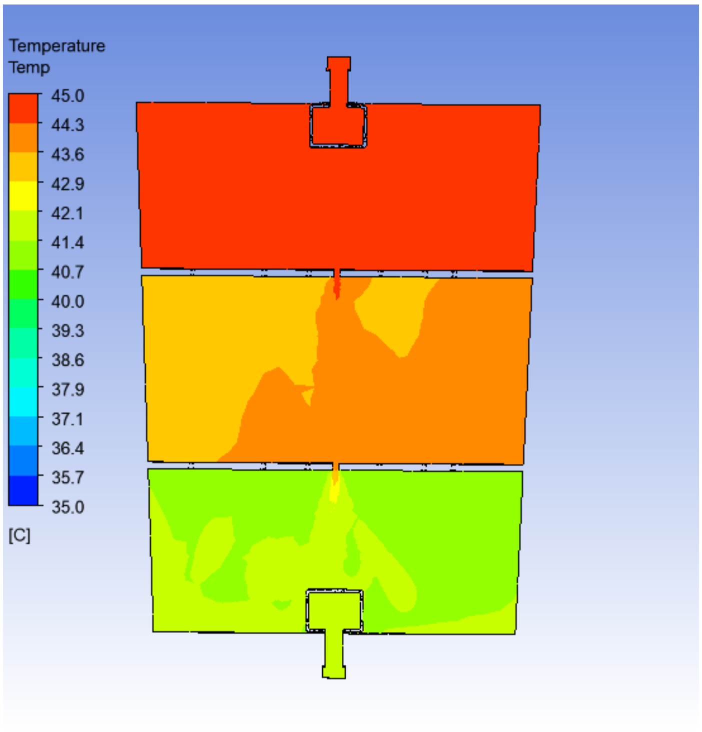

Figure 4.58: 12th Minute Temperature Profile of the Charging Cycle Simulation For Configuration C

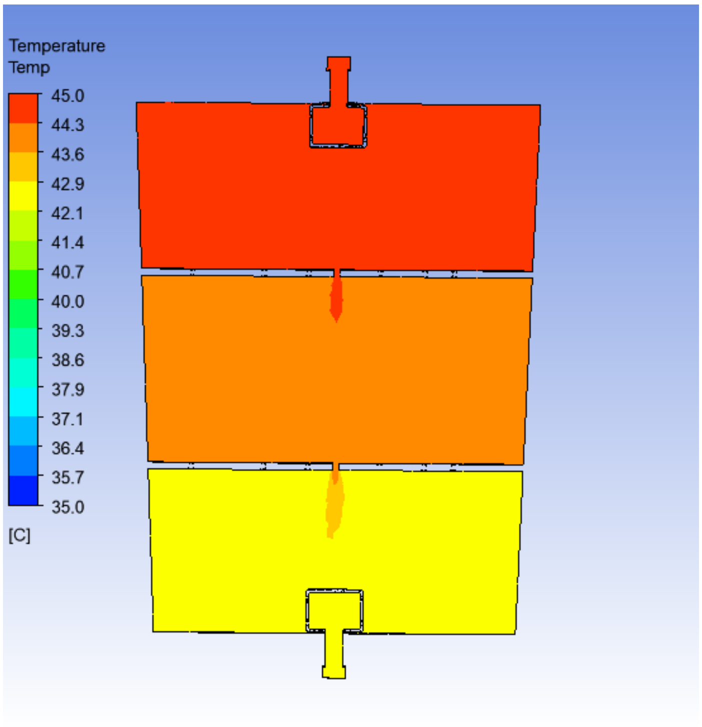

Figure 4.59: 14th Minute Temperature Profile of the Charging Cycle Simulation For Configuration C

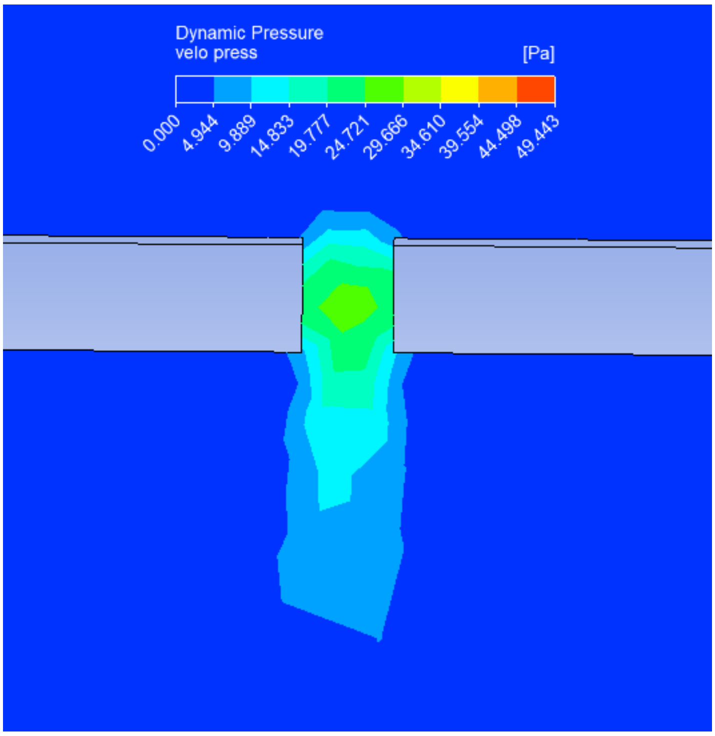

Figure 4.60: Dynamic Pressure Profile of the Charging Cycle Simulation For Configuration C

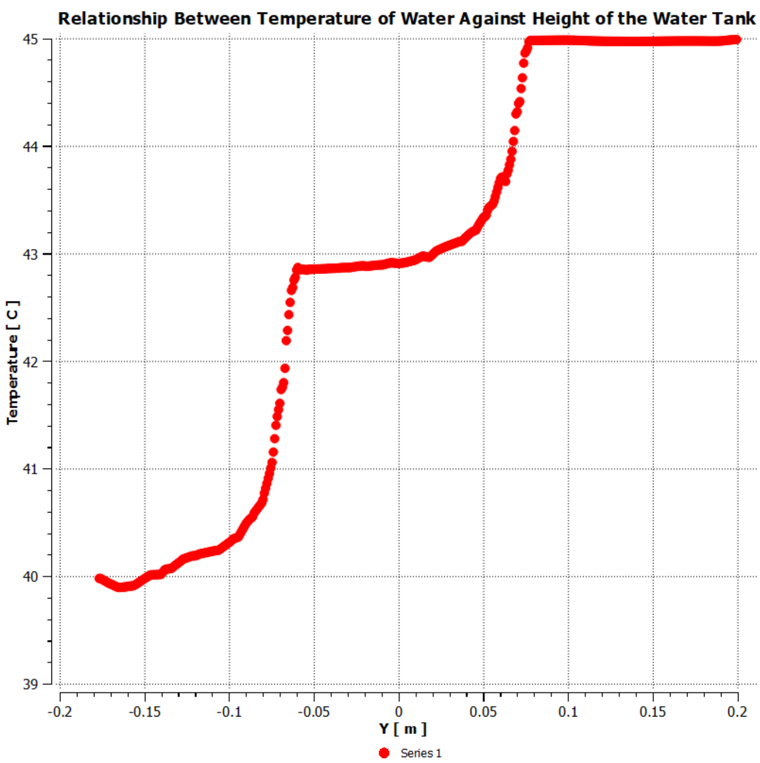

Figure 4.61: 10th Minute Temperature Distribution Plot of the Charging Cycle Simulation for Configuration C

Table 4.14: Position of Performance Indicators at 10th Minute of Charging Cycle CFD Simulation for Configuration C

Performance Indicator, θ	Height of Tank, X (m)	Temperature, Y (K)	Thermocline Layer (m)
0.1	-0.176	309.15	**0.244**
0.9	0.068	317.15	

4.4.4 Experimental Results For Configuration C

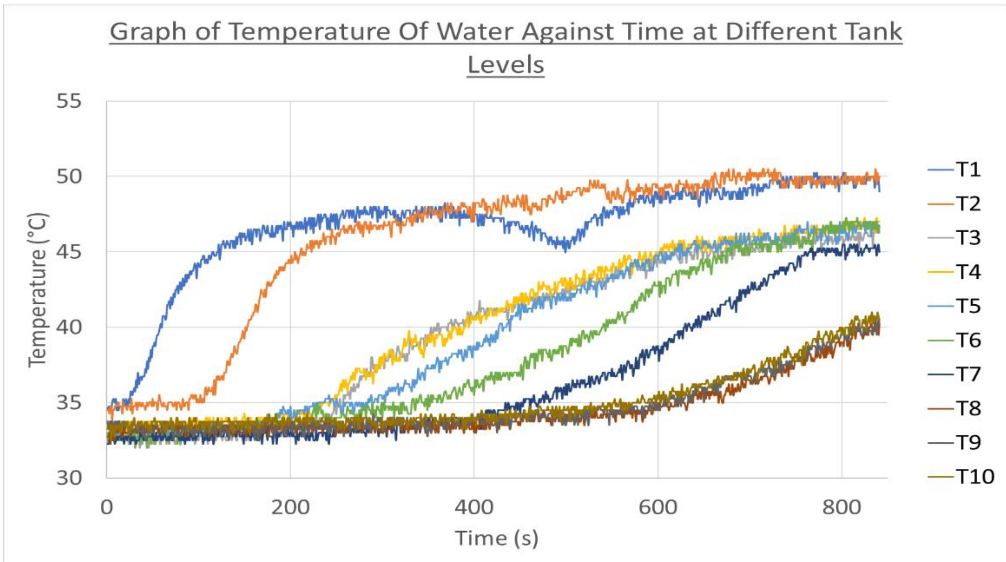

Figure 4.62: Full Charging Cycle Testing Results For Configuration C

4.5 Analysis Of Results Obtained

4.5.1 Analysis Of CFD Results

The temperature distribution plots at the 4th and 8th hour of CFD simulation for all three configurations of perforated plate diffusers in the commercial TES tank for both charging and discharging cycles allow for a better comparison between their performances as shown in Table 4.15.

Table 4.15: Thermocline Layer Thickness for Both Charging and Discharging Cycles at the 4th and 8th hour for Configurations 'A', 'B' and 'C'

Configuration	**Charging Cycle Thickness (m)**		**Discharging Cycle Thickness (m)**	
	4th Hour	**8th Hour**	**4th Hour**	**8th Hour**
A	1.464	1.645	1.628	1.352
B	1.727	1.383	1.770	1.053
C	1.873	0.992	2.195	0.549

Now turning our attention to the prototype tank CFD simulation and physical testing results, focusing first on the CFD simulations, the thermocline layer thickness results when using the two different perforated plate configurations can be compared in Table 4.16.

Table 4.16: Thermocline Layer Thickness for Charging Cycle at the 10th Minute for Configurations 'A' and 'C' Using the Prototype Tank

Configuration	**Thermocline Layer (m)**
A	0.031
C	0.244

Configuration 'A' has the least deviation between thermocline layer thickness readings during both charging and discharging cycle followed by Configuration 'B' and finally Configuration 'C'. However, Configuration 'C' produces the best performance once the charging or discharging cycle is almost completed at the 8th hour. Best performance here refers to the thinnest thermocline layer present in the TES tank. Figure 4.63 and 4.64 compares all three configurations side-by-side for charging and discharging cycles at the 8th hour respectively.

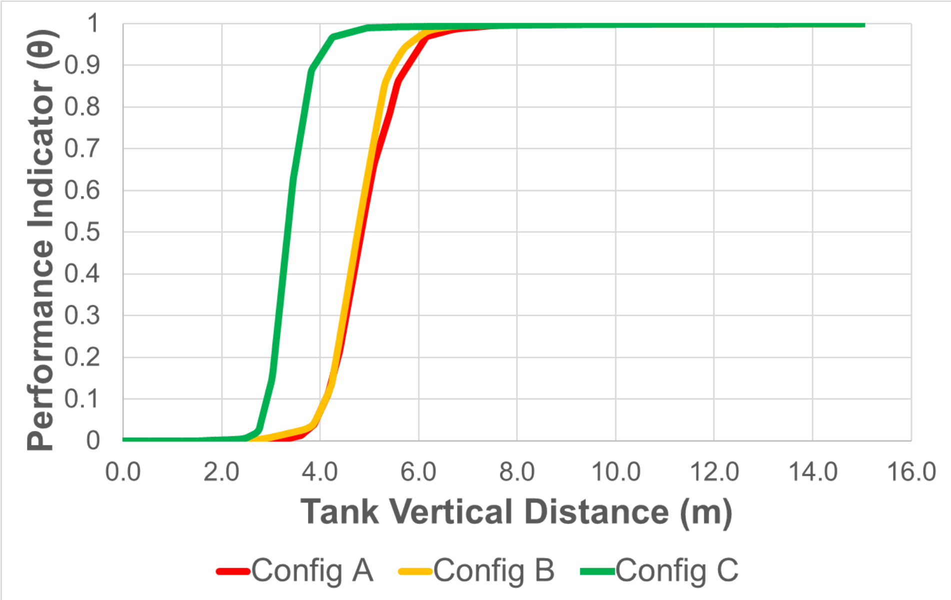

Figure 4.63: Graph Comparison Between the Performance Indicator Curves of the Three Configurations of Perforated Plate Diffusers And The Vertical Tank Distance During the Charging Cycle at the 8th Hour

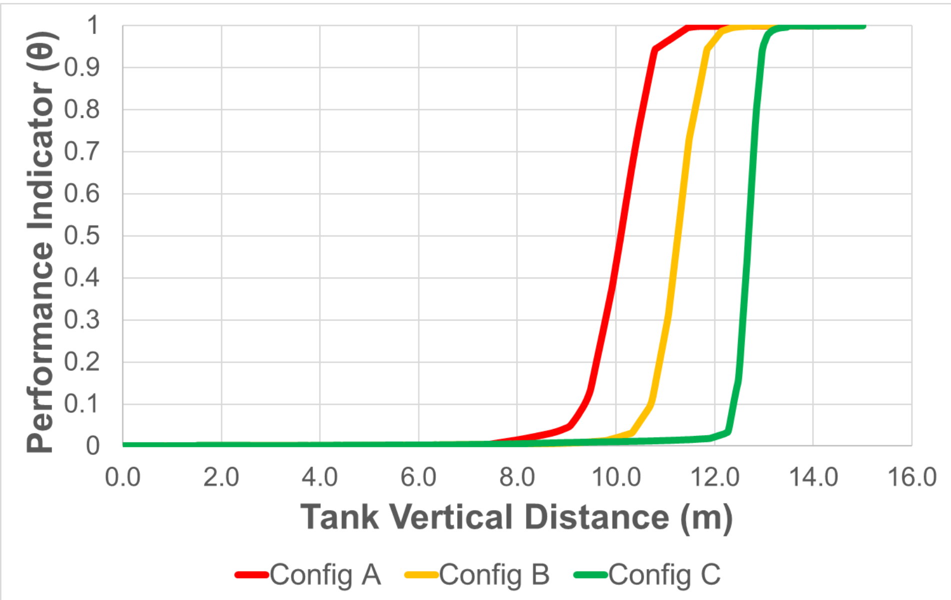

Figure 4.64: Graph Comparison Between the Performance Indicator Curves of the Three Configurations of Perforated Plate Diffusers And The Vertical Tank Distance During the Discharging Cycle at the 8th Hour

From both Figure 4.63 and 4.64, the thermocline layer when using Configuration ‘C’ is further developed down or up the tank during charging or discharging cycles followed by Configuration ‘B’ and Configuration ‘A’ despite having the same inlet flow rate. The increase in velocity and momentum of water flow through the perforation is the main contributor to this effect. As the area of perforation decreases, the velocity and momentum of the water flowing through the perforation will increase with the assumption of negligible change in density of water from the formula of mass flow rate below;

$$\dot{m} = \rho A v$$

where,

$\dot{m}$ – Mass flow rate (kg/s)

ρ – Density of water (kg/m^3)

A – Total perforation area (m^2)

v – Velocity of water flow (m/s)

The increase in momentum of water jet flow will not only push the existing water in the effective storage volume further down the tank, but also induce a greater mixing effect by jetting the hotter / cooler water deeper into the opposite temperature water in the effective storage volume, making it harder for it to stratify according to temperature. This effect can be seen in the CFD simulations for both the large TES commercial tank and the prototype tank well as in the physical testing results for the prototype tank when the thermocline layer initially passes through the first perforated plate diffuser.

For the large TES commercial tank, Configuration ‘A’ produced the thinnest thermocline layer initially during the 2nd and 4th hour of the CFD simulation for both charging and discharging cycles followed by Configuration ‘B’ and finally Configuration ‘C’ due to the effect of the velocity and momentum change from the total perforation area. However, it is worth examining close as the thermocline layer approaches the second perforated plate, the layer compresses and reduces in thickness for all three different configurations used but most significantly for Configuration ‘C’. This is due to the perforated plate diffusers essentially acting as a choke for the flow of water that will reduce the local velocity water flow within the storage volume close to the second perforated plate diffuser. This effect can also be seen in the 10th hour result for Configuration ‘A’ and ‘B’ for both charging and discharging, where the thermocline layer significantly decreases to a similar amount as of the 8th hour results for Configuration ‘C’. The reduction in perforated area will further enhance this effect by eliminating any backflow of water which reduces the mixing effect within the perforated area as found by Chen et al. (2023).

The CFD simulations and physical testing results of the prototype tank also corroborate with the results of the large TES commercial tank at the 2nd and 4th hour when the thermocline layer initially passes through the first perforated plate diffuser. Configuration ‘A’ maintained a thin and stratified thermocline layer past the first perforated plate unlike for Configuration ‘C’ where the water jet through the perforated plate produced an incredibly large mixing effect due to the velocity of water jet produced. Table 4.17 shows the difference in peak dynamic pressure between the two configurations of perforated plates used in the prototype tank.

Table 4.17: Peak Dynamic Pressure Through Perforation of Different Plates

Configuration	**Peak Dynamic Pressure (Pa)**
A	≈ 0.3
C	≈ 29

The large difference in peak dynamic pressure between perforated plate configurations in Table 4.17 shows that the difference in water jet velocity through the perforation is also large between configurations from the dynamic pressure formula below;

$$P_D = \frac{1}{2}\rho v^2$$

where,

P_D – Dynamic pressure (Pa)

ρ – Density of water (kg/m^3)

v – Velocity of water jet flow (m/s)

4.5.2 Analysis Of Prototype Experimental Results

Figure 4.65 and 4.66 shows the converted physical testing results from temperature to the performance indicator.

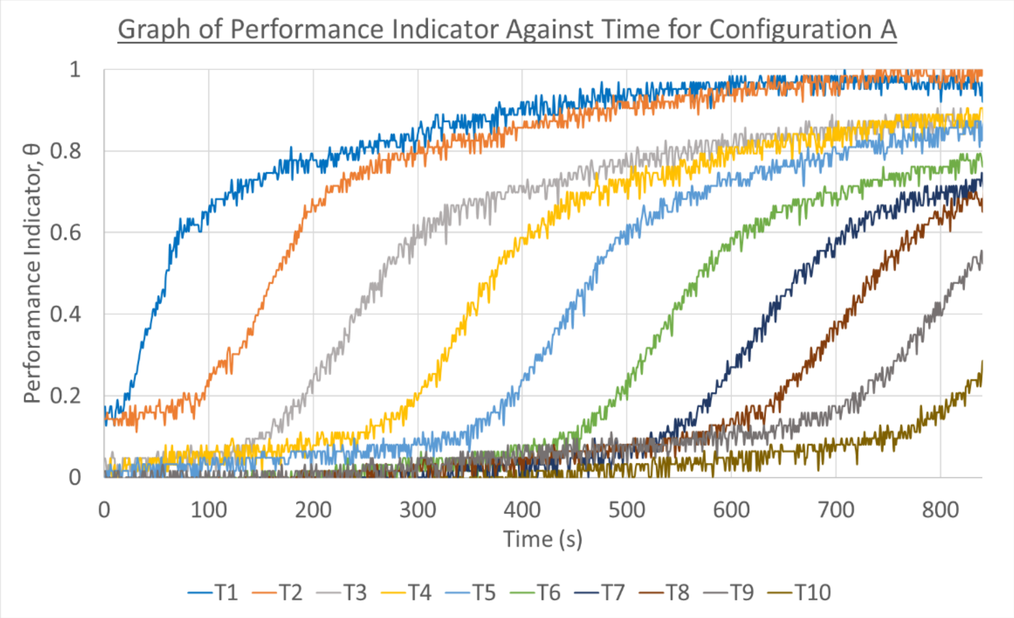

Figure 4.65: Full 14-Minute Charging Cycle Experimental Testing Results Converted Into Performance Indicator For Configuration A

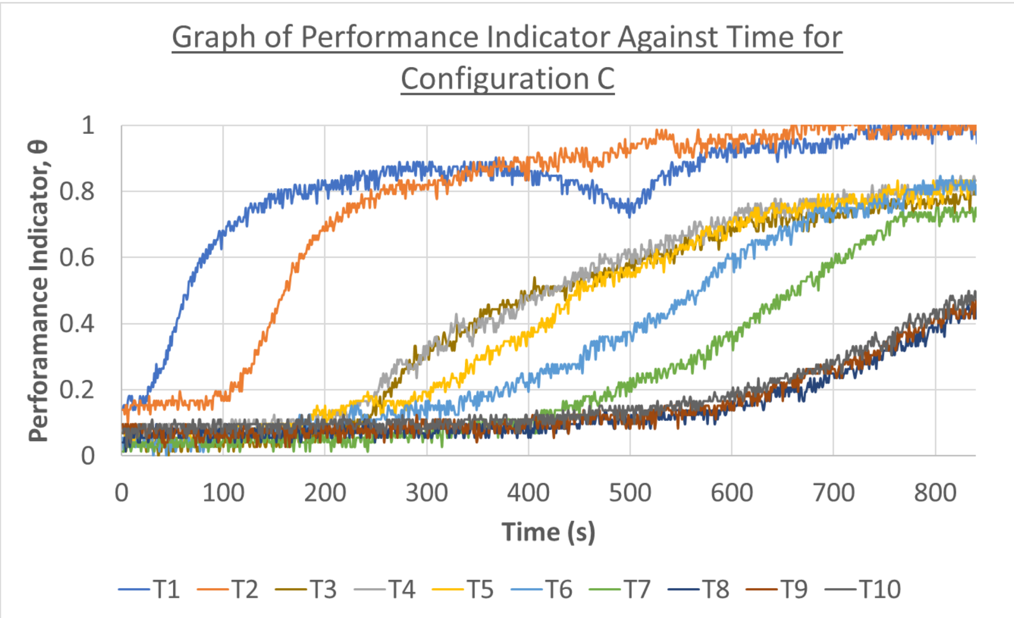

Figure 4.66: Full 14-Minute Charging Cycle Experimental Testing Results Converted Into Performance Indicator For Configuration C

Figure 4.67 shows the interpretation method of the graph of performance indicator against time.

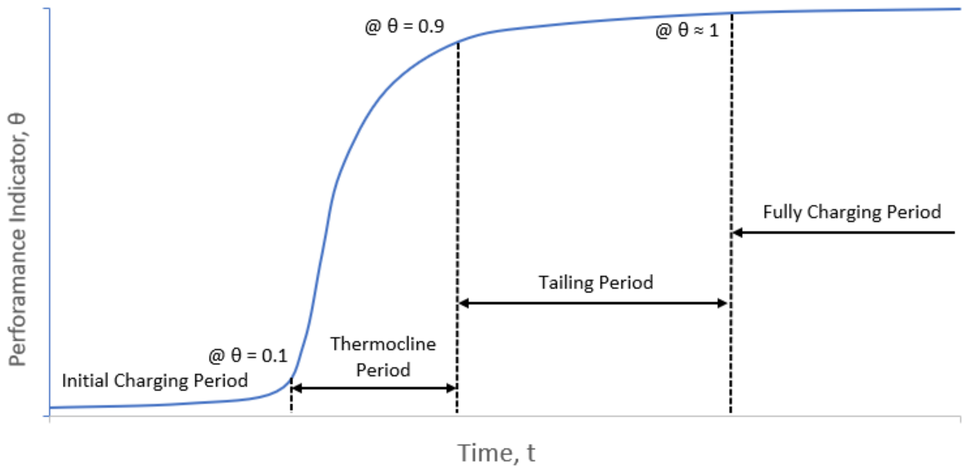

Figure 4.67: Interpretation of Graph of Performance Indicator Against Time

The physical testing results also matches with the CFD simulation results of the prototype tank. For Configuration 'A', the thermocline progresses constantly with a clear indication of a thin and stratified thermocline layer with the curves of each thermocouple reading not overlapping with one another until it only reaches the tailing period. The thermocline period for thermocouples after T3 to T7 also increases as the thermocline layer progresses lower into the tank which indicates that the thermocline layer slows down as it approaches the second perforated plate. On the other hand, in Configuration 'C', there is a clear mixing effect as the thermocline layer passes through the first perforated plate with the temperature profiles of the thermocouples at T3 to T5 climbing up simultaneously together. Temperature profiles at T6 and T7 follow suit with a quick increase to a similar performance indicator as T3, T4 and T5 which indicates that the mixing of different temperature water has reached an equilibrium. T8 to T10 also increase simultaneously which indicate the same mixing effect when the heated water passes through the second perforated plate. All three chambers of the prototype tank have different temperature water due to the large mixing effect caused by the great velocity of water jet flow that has caused the water in each chamber to reach thermal equilibrium.

CHAPTER 5

CONCLUSIONS AND RECOMMENDATIONS

5.1 Conclusion

This study involves the optimization of perforated plate diffusers in a large TES commercial tank. Three different configurations of perforated plate diffusers were tested with varying number of perforation and total perforation surface area in ANSYS CFX simulation, while two configurations were physically tested with a prototype tank. All three configurations were simulated for both charging and discharging cycles, while the two configurations for the prototype tank were tested in a charging cycle.

Configuration ‘C’ produced the best performance in the large TES commercial tank after 8 hours of 0.992 m and 0.549 m thermocline thickness for charging and discharging respectively and pushed the thermocline layer furthest through the tank compared to the other two perforated plate configurations. However, it is worth noting that the deviation in performance for Configuration ‘C’ from initially to fully charging or discharging the tank is the largest by some way with a difference of 0.881 m and 1.646 m for charging and discharging cycles respectively followed by Configuration ‘B’ with 0.344 m and 0.717 m for charging and discharging cycles respectively and Configuration ‘A’ with the least deviation with 0.181 m and 0.276 m for charging and discharging cycles respectively which can reduce its practically, where it needs to be charged to full to be more energy efficient compared to the other configurations.

The physical testing done has offered greater insight into the effect of varying the total perforation area with the results aligning with the CFD simulation results. In conclusion, Configuration ‘A’ is the most ideal for commercial use as it provides a reliable performance under any condition of partial or full charging or discharging with a thermocline layer thickness of 1.464 m and 1.628 m for partial charging and discharging after four hours respectively and 1.645 m and 1.352 m for full charging and discharging after hours respectively.

5.2 Recommendations for future work

One of the limitations experienced in this study is the computational resource and infrastructure available to be utilized for the CFD simulations. Despite having reasonably strong computational power available to carry out the CFD simulations, the simulation for each individual setup will still require plenty of days, if not weeks, to only complete a single simulation depending on the complexity and size of the model to be simulated. This will be compounded when using smaller timestep values, which are important in calculating an accurate result but will further increase the computational time required due to the increase in calculations required. Not to mention, the increase in storage space required to store more transient results that can range in the hundreds of gigabytes in total. Thus, proper scheduling of tasks along with optimization of the solver settings is required to ensure the simulations can be completed within the time frame.

Certain parameters set for the CFD simulations are also based on assumptions such as adiabatic conditions and laminar flow to simplify calculations which may not be the case in the actual operation. The parameters can be optimized further to fully match real world conditions.

Despite identifying the effects of varying the perforation area on a perforated plate diffuser, there are a few other parameters of the perforation plate diffuser that were not fully explored such as the diameter of each perforation on the plate, the distance between the perforated plates and the slotted pipe diffusers and potentially the number of perforated plates used in a TES tank. These parameters could be studied further to not only produce a clearer picture on how all of these parameters interact with one another and what would the performance difference be, but also to potentially increase its commercial viability by improving the TES tank energy efficiency.

The physical prototype tank could also be further improved by adding additional insulation through potentially wrapping the entire tank with a heat insulant material like aluminium foil. Discharge cycle testing can also be done to provide a better understanding on the flow of water through the perforated plates that may be able to also further optimize the large TES commercial tank. A custom prototype tank could be fabricated to fully match the height to diameter ratio of the actual large TES tank to get a better representation of the results.

REFERENCES

Ansys, 2024. *What is Computational Fluid Dynamics (CFD)? | Ansys*. [online] www.ansys.com. Available at: <https://www.ansys.com/simulation-topics/what-is-computational-fluid-dynamics>.

Al-Maraffie, A., Al-Kandari, A. and Ghaddar, N., 1991. Diffuser design influence on the performance of solar thermal storage tanks. *International Journal of Energy Research*, 15(7), pp.525–534. https://doi.org/10.1002/er.4440150702.

Bejan, A., 2013. *Convection Heat Transfer*. John Wiley & Sons.

Cao, L., Yu, J., Liu, X. and Wang, Z., 2024. Evaluation Method and Analysis on Performance of Diffuser in Heat Storage Tank. *Energies*, [online] 17(3), pp.1–15. https://doi.org/10.3390/en17030618.

Chen, J., Zhang, Y., Zou, C., Yulong, X. and Ouyang Yuming, 2023. Thermal performance analysis of a thermocline storage tank with integrated annular distributors. *Frontiers in Energy Research*, 11. https://doi.org/10.3389/fenrg.2023.1190760.

Chung, J.D., Cho, S.H., Tae, C.S. and Yoo, H., 2008. The effect of diffuser configuration on thermal stratification in a rectangular storage tank. *Renewable Energy*, 33(10), pp.2236–2245. https://doi.org/10.1016/j.renene.2007.12.013.

Davidson, J.H., Adams, D.A. and Miller, J.A., 1994. A Coefficient to Characterize Mixing in Solar Water Storage Tanks. *Journal of Solar Energy Engineering*, 116(2), pp.94–99. https://doi.org/10.1115/1.2930504.

Deng, Y., Sun, D., Niu, M., Yu, B. and Bian, R., 2021. Performance assessment of a novel diffuser for stratified thermal energy storage tanks – The nonequal-diameter radial diffuser. *Journal of Energy Storage*, 35, pp.102276–102276. https://doi.org/10.1016/j.est.2021.102276.

Donnelly, C. (2025) *Is The Number of Natural Disasters Increasing?*, *GreenMatch.co.uk*. Available at: https://www.greenmatch.co.uk/blog/are-natural-disasters-increasing. [Accessed 10 July 2025].

Dorgan, C.E. and Elleson, J.S. (1993) *Design Guide for Cool Thermal Storage*. Atlanta, Ga: Ashrae, pp. 4–44–7.

Erdemir, D. and Altuntop, N., 2016. Improved thermal stratification with obstacles placed inside the vertical mantled hot water tanks. *Applied Thermal Engineering*, 100, pp.20–29. https://doi.org/10.1016/j.applthermaleng.2016.01.069.

Ghajar, A.J. and Zurigat, Y.H., 1991. NUMERICAL STUDY OF THE EFFECT OF INLET GEOMETRY ON STRATIFICATION IN THERMAL ENERGY STORAGE. *Numerical Heat Transfer, Part A: Applications*, 19(1), pp.65–83. https://doi.org/10.1080/10407789108944838.

Gutierrez, G., Hincapie, F., Duffie, J.A. and Beckman, W.A., 1974. Simulation of forced circulation water heaters; effects of auxiliary energy supply, load type and storage capacity. *Solar Energy*, 15(4), pp.287–298. https://doi.org/10.1016/0038-092x(74)90018-8.

Han, S.M., Wu, S.T. and Christensen, D.L., 1978. Effects of thermal stratification in water storage tank for the performance of a solar hot water system. *OSTI OAI (U.S. Department of Energy Office of Scientific and Technical Information)*. [online] Available at: <https://www.osti.gov/servlets/purl/6742900> [Accessed 21 August 2025].

Hegazy, A.A., 2007. Effect of inlet design on the performance of storage-type domestic electrical water heaters. *Applied Energy*, 84(12), pp.1338–1355. https://doi.org/10.1016/j.apenergy.2006.09.014.

Ibrahim Dinçer and Rosen, M. (2011) *Thermal Energy Storage : Systems and Applications*. 2nd edn. [e-book] Chichester, Uk: Wiley, pp. 59–90. Available through: ProQuest Ebook Central. [Accessed 16 July 2025].

Ibrahim Dincer and Rosen, M.A., 2012. Exergy Analysis of Thermal Energy Storage Systems. *Elsevier eBooks*, pp.133–166. https://doi.org/10.1016/b978-0-08-097089-9.00009-7.

International Energy Agency (2023) *Buildings - Energy System*, *IEA*. Available at: https://www.iea.org/energy-system/buildings#tracking. [Accessed 10 July 2025].

International Energy Agency (2024) *Overview and key findings – World Energy Investment 2024 – Analysis*, *IEA*. Available at: https://www.iea.org/reports/world-energy-investment-2024/overview-and-key-findings. [Accessed 10 July 2025].

IPCC (2023) ‘Climate Change 2023: Synthesis Report. Contribution of Working Groups I, II and III to the Sixth Assessment Report of the Intergovernmental Panel on Climate Change [Core Writing Team, H. Lee and J. Romero (eds.)]. IPCC, Geneva, Switzerland.’, *Climate Change 2023 Synthesis Report*, p. 43. Available at: https://doi.org/10.59327/ipcc/ar6-9789291691647. [Accessed 10 July 2025].

Krafcik, M. and Perackova, J., 2019. Experimental Measurements of Hot Water Stratification in a Heat Storage Tank. *IOP Conference Series: Materials Science and Engineering*, 471, p.022014. https://doi.org/10.1088/1757-899x/471/2/022014.

Lavan, Z. and Thompson, J., 1977. Experimental study of thermally stratified hot water storage tanks. *Solar Energy*, 19(5), pp.519–524. https://doi.org/10.1016/0038-092x(77)90108-6.

Li, S., Zhang, Y., Li, Y. and Zhang, X., 2014. Experimental study of inlet structure on the discharging performance of a solar water storage tank. *Energy and Buildings*, 70, pp.490–496. https://doi.org/10.1016/j.enbuild.2013.11.086.

Li, Z. and Deusen, D. (2025) 'Role of energy storage technologies in enhancing grid stability and reducing fossil fuel dependency', *International Journal of Hydrogen Energy*, 102, pp. 1055–1074. Available at: https://doi.org/10.1016/j.ijhydene.2024.12.489. [Accessed 10 July 2025].

Lou, W., Fan, Y. and Luo, L., 2020. Single-tank thermal energy storage systems for concentrated solar power: Flow distribution optimization for thermocline evolution management. *Journal of Energy Storage*, 32, p.101749. https://doi.org/10.1016/j.est.2020.101749.

Lou, W., Xie, B., Aubril, J., Fan, Y., Luo, L. and Arrivé, A., 2023. Optimized flow distributor for stabilized thermal stratification in a single-medium thermocline storage tank: A numerical and experimental study. *Energy*, 263, p.125709. https://doi.org/10.1016/j.energy.2022.125709.

McCarthy, D.E. and Wood, B.D., 1990. Experimental Investigation of Solar Storage Tank Stratification Coefficients. *1990 Annual Conference American Solar Energy Society*, pp.95–100.

National Centers for Environmental Information (2024) *Annual 2024 Global Climate Report | National Centers for Environmental Information (NCEI)*, *Noaa.gov*. Available at: https://www.ncei.noaa.gov/access/monitoring/monthly-report/global/202413. [Accessed 10 July 2025].

Nelson, J.E.B., Balakrishnan, A.R. and Murthy, S.S., 1999. Experiments on stratified chilled-water tanks. *International Journal of Refrigeration*, [online] 22(3), pp.216–234. https://doi.org/10.1016/s0140-7007(98)00055-3.

Nicolae Lobontiu (2018) *System dynamics for engineering students : concepts and applications*. London: Academic Press, p. 242.

Parida, D.R., Advaith, S., Dani, N. and Basu, S., 2022. Assessing the impact of a novel hemispherical diffuser on a single-tank sensible thermal energy storage system. *Renewable Energy*, 183, pp.202–218. https://doi.org/10.1016/j.renene.2021.10.099.

Patil, P., Prabhu P.A and Shinde N.N (2012) 'Review of Phase Change Materials For Thermal Energy Storage Applications', *International Journal of Engineering Research and Applications (IJERA)*, Vol. 2(Issue 3), pp. pp.871-875. Available at: https://www.researchgate.net/publication/258521079_Review_of_Phase_Change_Materials_For_Thermal_Energy_Storage_Applications. [Accessed 10 July 2025].

Prakash, E.R. *et al.* (2022) *Materials for Sustainable Energy*. Edited by S. Adhikari. India: Bhabha Atomic Research Centre, p. 37. Available at: https://www.barc.gov.in/barc_nl/2022/20220910.pdf [Accessed 10 July 2025].

Rapp, B.E., 2017. Chapter 9 - Fluids. *Microfluidics: Modelling, Mechanics and Mathematics*, [online] pp.243–263. https://doi.org/10.1016/b978-1-4557-3141-1.50009-5.

S Kalaiselvam and R Parameshwaran, 2014. *Thermal energy storage technologies for sustainability : systems design, assessment and applications*. Amsterdam Etc.: Elsevier ; London . pp.57–62.

Shah, L.J. and Furbo, S., 2003. Entrance effects in solar storage tanks. *Solar Energy*, 75(4), pp.337–348. https://doi.org/10.1016/j.solener.2003.04.002.

Shyu, R.-J., Lin, J.-Y. and Fang, L.-J., 1989. Thermal Analysis of Stratified Storage Tanks. *Journal of Solar Energy Engineering*, 111(1), pp.54–61. https://doi.org/10.1115/1.3268287.

Simpson, J.E., 1999. *Gravity currents : in the environment and the laboratory*. Cambridge: Cambridge University Press.

Tang, J., Shi, Y. and OuYang, Z., 2021. Optimization design of the octagonal water diffuser with uniform flow orifice plate. *Journal of Energy Storage*, 44, pp.103374–103374. https://doi.org/10.1016/j.est.2021.103374.

Tenaga Nasional Berhad (2023) *Green Energy - Tenaga Nasional Berhad*, *TNB Better. Brighter.* Available at: https://www.tnb.com.my/smart-grid/green-energy/. [Accessed 10 July 2025].

Tipasri, W. and Wongwuttanasatian, T., 2019. Effect of height to diameter ratio of chilled water storage tank on temperature gradient during discharging. *Energy Procedia*, 156, pp.254–258. https://doi.org/10.1016/j.egypro.2018.11.138.

Tongsopit, S. *et al.* (2016) 'Energy security in ASEAN: A quantitative approach for sustainable energy policy', *Energy Policy*, 90, p. 70. Available at: https://doi.org/10.1016/j.enpol.2015.11.019. [Accessed 10 July 2025].

United Nations (no date) *Causes and Effects of Climate Change*, *United Nations*. United Nations. Available at: https://www.un.org/en/climatechange/science/causes-effects-climate-change. [Accessed 10 July 2025].

Wang, Z. (2019) 'Thermal Storage Systems', *Design of Solar Thermal Power Plants*, pp. 387–415. Available at: https://doi.org/10.1016/b978-0-12-815613-1.00006-7. [Accessed 10 July 2025].

Wildin, M. and Sohn, C., 1993. *Flow and Temperature Distribution in a Naturally Stratified Thermal Storage Tank*. [online] Available at: <https://apps.dtic.mil/sti/tr/pdf/ADA273511.pdf> [Accessed 1 September 2025].

Wu, L. and Bannerot, B.R., 1987. An experimental study of the effect of water extraction on thermal stratification in storage. pp.445–451.

Wuestling, M.D., Klein, S.A. and Duffie, J.A., 1985. Promising Control Alternatives for Solar Water Heating Systems. *Journal of Solar Energy Engineering*, 107(3), pp.215–221. https://doi.org/10.1115/1.3267681.

Yaïci, W., Ghorab, M., Entchev, E. and Hayden, S., 2013. Three-dimensional unsteady CFD simulations of a thermal storage tank performance for optimum design. *Applied Thermal Engineering*, 60(1-2), pp.152–163. https://doi.org/10.1016/j.applthermaleng.2013.07.001.

Zhang, S. *et al.* (2025) 'A review of design considerations and performance enhancement techniques for thermocline thermal energy storage systems', *Renewable and Sustainable Energy Reviews*, 212, pp. 1–5. Available at: https://doi.org/10.1016/j.rser.2025.115388. [Accessed 10 July 2025].

Zurigat, Y.H., Maloney, K.J. and Ghajar, A.J., 1989. A Comparison Study of One-Dimensional Models for Stratified Thermal Storage Tanks. *J. Sol. Energy Eng.*, 111(3), pp.204–210. https://doi.org/doi.org/10.1115/1.3268308.